UNIVERSITÄT ZU LÜBECK

From the Institute for Nutritional Medicine

of the University of Lübeck

Director: Prof. Dr. med. Christian Sina

Effect of different vaccine adjuvants and checkpoint inhibitors on antibody responses and tumor growth

---

Dissertation

for Fulfillment of

Requirements

for the Doctoral Degree

of the University of Lübeck

from the Department of Natural Sciences

Submitted by

Selina Lehrian

from Bensheim

Lübeck 2024

First referee: Prof. Dr. Marc Ehlers

Second referee: Prof. Dr. Lars Redecke

Date of oral examination: 06th February 2025

Approved for printing: 18th February 2025

Table of contents

I. Figures

II. Tables

III. Abbreviations

ADCC	antibody-dependent cellular cytotoxicity
ADCP	antibody-dependent cellular phagocytosis
ADNP	antibody-dependent neutrophil phagocytosis
AFP	α-fetoprotein
AID	activation-induced deaminase
APC	antigen-presenting cells
B4galT1	beta-1,4-galactosyltransferase 1
BCR	B cell receptor
CD	cluster of differentiation
CDC	cellular dependent cytotoxicity
CDR	complementary determining regions
CFA	complete Freund's adjuvant
CLR	C-type lectin receptor
CSR	class-switch recombination
CTL	cytotoxic T cells
CTLA-4	cytotoxic T-lymphocyte-associated protein 4
DAMP	damage-associated molecular pattern
DC	dendritic cell
DCIR	dendritic cell immunoreceptor
DC-SIGN	dendritic cell-specific ICAM-3-grabbing nonintegrin
DZ	dark zone
eCFA	enhanced complete Freund's adjuvant
ER	endoplasmic reticulum
FA	Freund's adjuvant
Fab	fragment antigen binding
FAO	Food and Agriculture Organization of the United Nations
Fc	fragment crystallizable
FcγR	Fcγ-receptor
FDC	follicular dendritic cell
fuc	fucose/fucosylated
FUT-8	fucosyltranferase-8
Gal	galactose/galactosylated
GC	germinal centers
GlcNAc	N-acetylglucosamine
HBV	hepatitis B virus
HLA	human leukocyte antigen
HPV	human papilloma virus
IFA	incomplete Freund's adjuvant
IFN	interferon
Ig	immunoglobulins
IL	interleukin
ITAM	immunoreceptor tyrosine-based activation motif
ITIM	immunoreceptor tyrosine-based inhibition motif
IVIG	intravenous immunoglobulin
LNPs	lipid nanoparticles

LZ	light zone
MDA5	melanoma differentiation associated gene 5
MGAT3	beta-1,4-mannosyl-glycoproteinm4-beta-N-acetylglucosaminyltransferase
MHC	major histocompatibility complex
MINCLE	macrophage inducible Ca^{2+}-dependent lectin receptor
MPLA	monophophoryl lipid A
NK cells	natural Killer cell
NLR	NOD-like-receptors
NLRP3	NOD-like receptor thermal protein domain associated protein 3
NOD1	nucleotide-binding oligomerization domain 1
PAMP	pathogen-associated molecular patterns
PC	plasma cells
PD-1	programmed cell death protein 1
PD-L1	programmed cell death ligand 1
PRR	pattern recognition receptors
PSA	prostate-specific antigen
RA	rheumatoid arthritis
RIG-1	retinoic acid-induced gene I
SARS-CoV-2	severe acute respiratory syndrome coronavirus 2
SHM	somatic hypermutation
Sial	Sialic acid/sialylated
SIGN-R1	specific ICAM-3 grabbing non-integrin-related 1
St6gal1	alpha-2,6-sialyltransferase 1
TAA	tumor-associated antigens
TCR	T cell receptor
TFH	T follicular helper cells
TFR	T follicular regulatory cells
TGF	transforming growth factor
TH	T helper cells
TLR	toll-like receptors
TME	tumor microenvironment
TNF	tumor-necrosis factor
Treg	regulatory T cells
TSA	tumor-specific antigens
WHO	World health organization

IV. Summary

Immunotherapies such as passive and active vaccinations are not only used to prevent infections caused by bacteria or viruses, but also to treat cancer. In addition to cancer immunotherapies with blocking antibodies against immune checkpoints, tumor antigen-specific monoclonal antibodies, usually of the IgG1 isotype, are used for passive vaccination. These act via mechanisms such as ADCC (antibody-dependent cellular cytotoxicity) through NK cells, but also neutrophils. Active vaccinations with tumor cells or tumor antigens in combination with various adjuvants induce different "qualities" of $CD4^+$ T helper cells depending on the adjuvant, which in turn influence the qualities of $CD8^+$ cytotoxic T cells and antibody-producing B cells.

Subsequently, the effector function of antibodies is influenced by their generated "quantity" and "quality". In the case of IgG antibodies, the latter is influenced by their subclass composition and their type of Fc-N glycosylation. The determination and functional investigation of the "quantity" and "quality" of an IgG antibody response induced by an active vaccination with a defined adjuvant could therefore provide information about its anti-tumor potential and in future be used as a biomarker for the induced T and B cell response to assess the efficacy of a vaccination and to predict the course of the disease.

The aim of this work was to identify suitable adjuvants or adjuvant types for tumor vaccination and to characterize the underlying IgG antibody response. In addition, it should be investigated which induced IgG subclass with which Fc-N glycosylation pattern correlates with reduced tumor growth. Furthermore, the influence of the blockade of the immune checkpoints PD-1 and CTLA-4 on the IgG subclass distribution and Fc glycosylation was to be investigated.

To answer these questions, a murine melanoma tumor model was established in this study. In order to investigate active vaccinations, the mice were immunized prophylactically before or therapeutically after tumor cell injection with soluble "tumor antigen" plus various adjuvants. Subsequently, the influence of the different vaccinations on tumor growth was correlated with the induced IgG subclass and Fc glycosylation response.

Furthermore, the effect of checkpoint inhibitors (anti PD-1, anti-CTLA-4) on IgG-Fc glycosylation was investigated in an immunization model and subsequently compared with the immune response in a melanoma tumor model.

The experiments showed that different adjuvants had different effects on tumor growth. While the adjuvants Poly(I:C) and CFA/eCFA protected against tumor growth in the prophylactic model, the adjuvants Alum and Montanide did not lead to any tumor reduction. In addition, the different adjuvants induced different T cell and antibody responses, which was reflected in the amount and composition of the IgG subclass distribution and the type of Fc-N glycosylation. Differential induced IgG immune responses by Poly(I:C) and CFA/eCFA suggest that both adjuvants induced different protective IgG antibody-induced immune cell responses.

The results show that the type of adjuvant has a major impact on tumor reduction and correlates with different IgG subclasses and Fc glycosylation patterns, which could be used as biomarkers and for the development of new vaccination strategies in the future. In addition, the experiments showed that anti-PD-1 treatment led to a pro-inflammatory immune response, which could explain the reduction in tumor growth and potential inflammatory side effects.

V. Zusammenfassung

Immuntherapien wie passive und aktive Impfungen werden nicht nur zur Vorbeugung von Infektionen durch Bakterien oder Viren, sondern auch zur Behandlung von Krebserkrankungen eingesetzt. Neben Krebsimmuntherapien mit blockierenden Antikörpern gegen Immuncheckpoints werden zur passiven Impfung Tumorantigen-spezifische monoklonale Antikörper, meist vom Isotyp IgG1, eingesetzt. Diese wirken über Mechanismen wie ADCC (antibody-dependent cellular cytotoxicity) durch NK-Zellen, aber auch durch Neutrophile. Aktive Impfungen mit Tumorzellen oder Tumorantigenen in Kombination mit verschiedenen Adjuvantien induzieren je nach Adjuvans unterschiedliche „Qualitäten“ von $CD4^+$ T-Helferzellen, die wiederum die „Qualitäten“ von $CD8^+$ zytotoxischen T-Zellen und Antikörper-produzierenden B-Zellen beeinflussen.

Folglich wird die Effektorfunktion von Antikörpern dabei durch deren generierte „Quantität“ und „Qualität“ beeinflusst. Letztere wird bei IgG-Antikörpern durch deren Subklassen-Zusammensetzung und deren Art der Fc-N-Glykosylierung beeinflusst. Die Bestimmung und funktionelle Untersuchung der „Quantität“ und „Qualität“ einer durch eine aktive Impfung mit definiertem Adjuvans induzierten IgG-Antikörperantwort könnte daher Aufschluss über deren anti-Tumor Potential geben und in Zukunft als Biomarker für die induzierte T- und B-Zell-Antwort zur Beurteilung der Wirksamkeit einer Impfung und zur Vorhersage des Krankheitsverlaufs herangezogen werden.

Ziel dieser Arbeit war es, geeignete Adjuvantien bzw. Adjuvanstypen für die Tumorvakzinierung zu identifizieren und die zugrunde liegende IgG-Antikörperantwort zu charakterisieren. Dabei sollte untersucht werden, welche induzierte IgG-Subklasse mit welchem Fc-N-Glykosylierungsmuster mit einem verminderten Tumorwachstum korreliert. Weiterhin sollte der Einfluss der Blockade der Immun-Checkpoints PD-1 und CTLA-4 auf die IgG-Subklassenverteilung und die Fc-Glykosylierung untersucht werden.

Zur Beantwortung der Fragestellungen wurde in dieser Arbeit ein murines Melanom-Tumormodell etabliert. Die Mäuse wurden prophylaktisch vor oder therapeutisch nach einer Tumorzellinjektion mit löslichem „Tumorantigen“ plus verschiedenen Adjuvantien immunisiert und der Einfluss der verschiedenen Vakzinen auf das Tumorwachstum sowie die Korrelation mit einer spezifischen induzierten IgG-Subklassen- und Fc-Glykosylierungsantwort untersucht. Darüber hinaus wurde die Wirkung von Checkpoint-

Inhibitoren (anti-PD-1, anti-CTLA-4) auf die IgG-Fc-Glykosylierung in einem Immunisierungsmodell untersucht und anschließend mit der Immunantwort in einem Melanom-Tumormodell verglichen.

Die Experimente zeigen, dass verschiedene Adjuvantien unterschiedliche Einflüsse auf das Tumorwachstum hatten. Während im prophylaktischen Modell die Adjuvantien Poly(I:C) und CFA/eCFA vor Tumorwachstum schützten, führten die Adjuvantien Alum und Montanide zu keiner Tumorreduktion. Dabei induzierten die verschiedenen Adjuvantien unterschiedliche T-Zell- und Antikörperantworten, was sich in der Menge und der Zusammensetzung der IgG-Subklassenverteilung und der Art der Fc-N-Glykosylierung zeigte. Unterschiedlich induzierte IgG-Immunantworten durch Poly(I:C) und CFA/eCFA lassen vermuten, dass beide Adjuvantien unterschiedliche schützende IgG Antikörper-induzierte Immunzellantworten induzierten.

Die Ergebnisse zeigen, dass die Art des Adjuvans einen großen Einfluss auf die Tumorreduktion hat und mit verschiedenen IgG-Subklassen und Fc-Glykosylierungsmustern korreliert, die in Zukunft als Biomarker und für die Entwicklung neuer Impfstrategien genutzt werden könnten. Darüber hinaus zeigten die Experimente, dass die Anti-PD-1 Behandlung zu einer pro-inflammatorischen Immunantwort führt, was einerseits die Reduktion des Tumorwachstums und andererseits mögliche entzündliche Nebenwirkungen erklären könnte.

1. Introduction

Since the 19th century, vaccinations have been developed to protect against infectious diseases (Murphy and Weaver 2018). To date, prophylactic vaccinations have been used to protect against diseases such as pertussis (whooping cough), diphtheria, polio, tetanus, influenza, and severe acute respiratory syndrome coronavirus 2 (SARS-CoV-2), as well as from cancer-causing viruses such as human papillomavirus (HPV; which causes cervical cancer) and hepatitis B virus (HBV; which causes hepatocellular cancer) (Ada 2005; Wagner and Hildt 2019; J. Liu et al. 2022; Marriott, Post, and Chablani 2023). Until now, therapeutic cancer treatment with tumor or tumor-antigen containing vaccines is still rare and under development (Baxter 2014; Gouttefangeas and Rammensee 2018; Rammensee et al. 2019; Peng et al. 2019; Zahavi and Weiner 2020; Cuzzubbo et al. 2021; J. Liu et al. 2022).

Active antigen immunizations are often supplemented with adjuvants to enhance the induced antigen-specific T cell and B cell responses that can attack tumor cells. In addition to active immunization, passive immunization can be performed using polyclonal or monoclonal antigen-specific antibodies.

Treatment efficacy of the various therapies is monitored by the reduction in tumor size/cell count and tumor markers such as prostate-specific antigen (PSA) or carcino-embryonic antigen (CEA) (J. Liu et al. 2022). Furthermore, the efficacy of tumor vaccination is characterized by the activation, differentiation and proliferation of tumor antigen-specific $CD8^+$ cytotoxic T cells and $CD4^+$ helper T cells as well as by the induced antibody titers (Taranger et al. 2000; Coudeville et al. 2010), where antibodies can recognize extracellular tumor antigens, but also, as recently proposed, also intracellular antigens (Lu et al. 2016).

However, there may be people who have had a (severe) outbreak of the disease despite a high antibody titer (Taranger et al. 2000; Coudeville et al. 2010). Importantly, it is known that in addition to the antibody titer (amount/ “quantity”) the type and characteristics of an antibody (“quality”) play a role in the efficiency of the immune response. The “quality” of an antibody response is influenced by the antibody isotype and subclass composition as well as their Fc-N glycosylation patterns, inducing different effector functions and affecting vaccination efficiency (Vidarsson, Dekkers, and Rispens 2014; Cobb 2019; Bartsch et al. 2020). The “quality” of the antibody composition thus also reflects also the “quality” of the $CD4^+$ T cell response.

Accordingly, not only the "quantity" but also the "quality" of the T and B cell immune response is influenced by the adjuvant selected during vaccination (Bartsch et al. 2020).

Thus, the different antibody "quantities" and "qualities" could be used as biomarkers of induced T and B cell immune responses and potential vaccine efficacy (Vidarsson, Dekkers, and Rispens 2014; Cobb 2019; Bartsch et al. 2020).

1.1 Antigen recognition by the innate and adaptive immune system

After vaccination, cells of the innate immune system, like dendritic cells or macrophages recognize the foreign antigens, phagocyte and process them to present specific antigens to cells of the adaptive immune system, leading to the induction of a T and B cell immune response. In addition, defined co-stimulatory molecules can be used in adjuvants to co-stimulate these innate antigen-presenting cells (APCs) recognize for instance distinct molecular patterns of pathogens (pathogen-associated molecular patterns (PAMPs)) to stimulate pattern recognition receptors (PRRs). These PAMPs are for instance mannose-rich oligosaccharides, peptide glycans, lipopolysaccharides of bacterial cell walls, or unmethylated CpG DNA. Besides to pathogen-derived PAMPs and fragments of dying cells, so-called damage-associated molecular patterns (DAMPs) can activate APCs (Iwasaki and Omer 2020; Facciolà et al. 2022; Zhao et al. 2023). PPRs are transmembrane receptors like toll-like receptors (TLR), but also NOD-like receptors (NLRs) that recognize intracellular invasive bacteria antigens and receptors that recognize viral DNA/RNA. Activation of these receptors leads to the activation of intracellular signaling cascades that trigger effector mechanisms such as recruitment of adaptive immune cells and secretion of cytokines, leading to quantitatively and qualitatively distinct immune responses (Murphy and Weaver 2018; Zhao et al. 2023).

After receiving danger signals from PPRs (**signal 0**), the APC enhances the presentation of the processed antigenic peptide epitopes on MHC-molecules (major histocompatibility complex) that form peptide:MHC-complexes on the surface (**signal 1**), which leads together with co-stimulatory signals like cytokines (IL-6, IL-12, IL-10, TNFα) and CD80/CD86 **(signal 2),** to the attraction of naïve T cells that recognize the presented antigen via their TCR receptor (Figure 1.1). Epitopes presented on MHC-II molecules recruit $CD4^+$ T cells, whereas epitopes presented on MHC-I molecules recruit $CD8^+$ T cells (Klein, Templeton, and Schwenk 2014; Murphy and Weaver 2018; Zhao et al. 2023). Activated naïve T cells proliferate and differentiate into effector T cells (priming), which have different characteristics and act

differently. $CD8^+$ T cells differentiate into cytotoxic T cells, directly killing target cells, while $CD4^+$ T cells have a broader effector function and can differentiate into different T cell subsets with different functions. These are activating T helper cells (T_H1, T_H17, T_H2, T_{FH}) cells, but also inhibitory regulatory T cells (T_{regs}), responsible for immune suppression (Murphy and Weaver 2018). Effector T cells migrate to different sides of inflammation to perform their effector function or migrate in secondary lymphoid tissue such as spleen, lymph nodes, and Peyer´s patches to activate T cell dependent humoral immunity (Stebegg et al. 2018; Malkiel et al. 2018; Cyster and Allen 2019). In parallel, B cells can be directly activated by antigen epitopes through cross-linking of antigen-specific B cell receptors (BCR) (Klein, Templeton, and Schwenk 2014; Malkiel et al. 2018). Subsequently, $CD4^+$ T helper cells co-activate $CD8^+$ cytotoxic T cells as well as B cells that can differentiate into antibody-producing plasma cells.

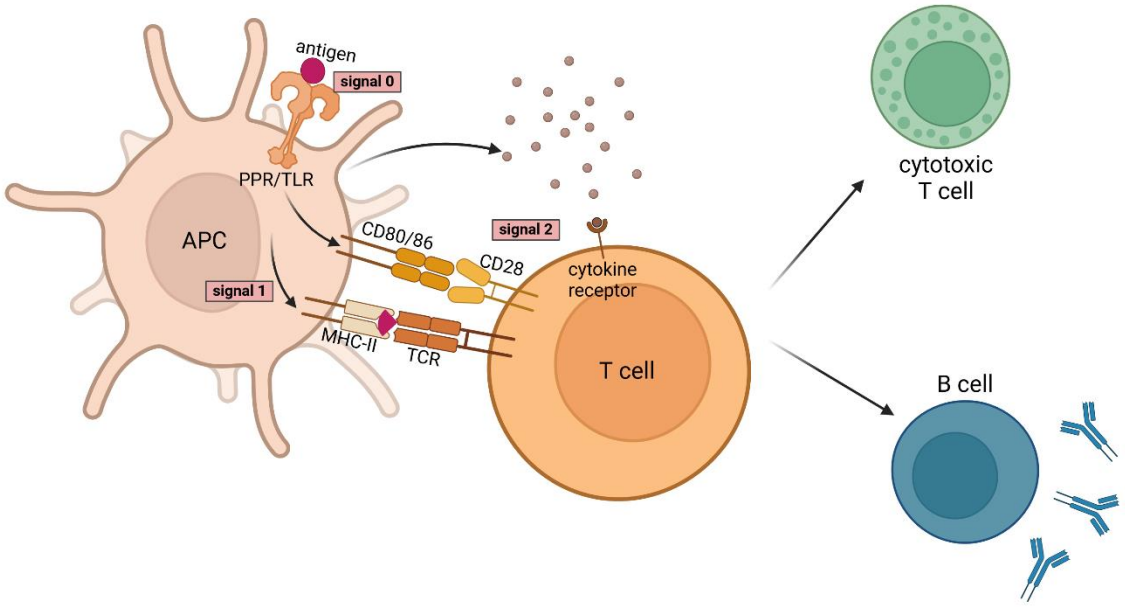

Figure 1.1: APC mediated activation of the innate and adaptive immune response.
APCs like DCs receive danger signals from PPRs (like TLRs) (signal 0) and enhance the presentation of the processed antigen epitopes on MHC-molecules (major histocompatibility complex) building peptide:MHC-complexes on the surface (signal 1). Together with co-stimulatory signals like cytokines (IL-6, IL-12, IL-10, TNFα) and CD80/CD86 (signal 2) naïve $CD4^+$ T cells are recruited, which recognize the presented antigen via their TCR receptor. Afterwards, activates $CD4^+$ T cells lead to the activation of cytotoxic $CD8^+$ T cells and/or B cell dependent humoral immune response.

1.1.1 B cell immune response

The B cell immune response is responsible for the development of antibodies and the development of immunological memory that can be rapidly re-activated by subsequent antigen-contact, leading to a fast immune response (Murphy and Weaver 2018; Zahavi and Weiner 2020).

Initial antibody responses are generated by extrafollicular short-lived plasma cells, whereas long-term antibody responses are generated mainly in germinal centers (GCs).

The GCs are specialized microanatomical structures in secondary lymphoid organs (Nieuwenhuis and Opstelten 1984; Victora and Nussenzweig 2012; Stebegg et al. 2018; Cyster and Allen 2019). GCs are responsible for affinity maturation and the production of long-lived antibody-secreting plasma cells (PCs) and memory B cells (Stebegg et al. 2018). GC formation occurs within approximately 6 days after infection or immunization due to the appearance of foci of rapidly dividing B cells within the B cell follicles of secondary lymphoid organs (Victora and Nussenzweig 2012). Based on their visibility under the microscope, GCs can be anatomically divided into a dark zone (DZ) and a light zone (LZ): dense dividing B cells in the DZ and a follicular dendritic cell (FDC) network in the LZ (Victora and Nussenzweig 2012; Stebegg et al. 2018; Cyster and Allen 2019). After B cell activation on the T:B border of the follicle, B cells either (1) differentiate into short-lived extrafollicular plasma cells, (2) differentiate into extrafollicular memory B cells, or (3) enter the GC to initiate GC responses (Figure 1.2) (Kurosaki 2010; Victora and Nussenzweig 2012; Stebegg et al. 2018). The initiation of (1) short-lived (also class-switched) extrafollicular plasma cells (PCs) leads to the generation of the first wave of antibodies, which die within a few days (Kurosaki 2010). If the antigen affinity of antigen-specific B cells does not reach a certain threshold required to differentiate into extrafollicular PCs, they (3) enter the GC to undergo affinity maturation induced by somatic hypermutations and class-switching (S. Paul et al. 2016).

After entering the GC, GC B cell precursors divide rapidly in the DZ and undergo clonal expansion. GC B cells express the enzyme activation-induced deaminase (AID), which induces somatic hypermutation (SHM) and class-switch recombination (CSR), by deaminating cytidine residues in the VDJ and switch region of the immunoglobulin gene, inducing DNA mutations (LeBien and Tedder 2008; Victora and Nussenzweig 2012; Stebegg et al. 2018). During SHM in the DZ, autoreactive antibodies can also be generated, which in most cases are negatively selected in the LZ or by checkpoints, thus preventing autoimmunity (Victora and Nussenzweig

2012). Afterwards, GC B cells migrate to the LZ of the follicle, where cytokine-dependent CSR takes place and FDCs and T_{FH} cells (T follicular helper cells) are responsible for the positive selection of high affinity BCRs through presentation of antigen epitopes by FDCs and positive signals from T_{FH} cells to GC B cells. B cells that do not receive a positive signal undergo apoptosis. Selected GC B cells can then (4) eighter re-enter the DZ to undergo further rounds of proliferation, maturation, and affinity selection (diversification, affinity maturation) or (5) exit the GC as long-lived PCs, secreting antibodies into the blood or (6) as memory B cells, migrating to the bone marrow, where they rest until a new antigen contact. Upon new antigen contact memory B cells differentiate into PCs and rapidly secret antibodies or re-enter the GC (Manz, Thiel, and Radbruch 1997; Victora and Nussenzweig 2012; De Silva and Klein 2015). T_{FR} cells (T follicular regulatory cells) regulate the output of the GC response, by suppressing T_{FH} and B cells. Therefore, altered T_{FH}/T_{FR} ratios indicate altered GC responses (Sage and Sharpe 2015; Stebegg et al. 2018).

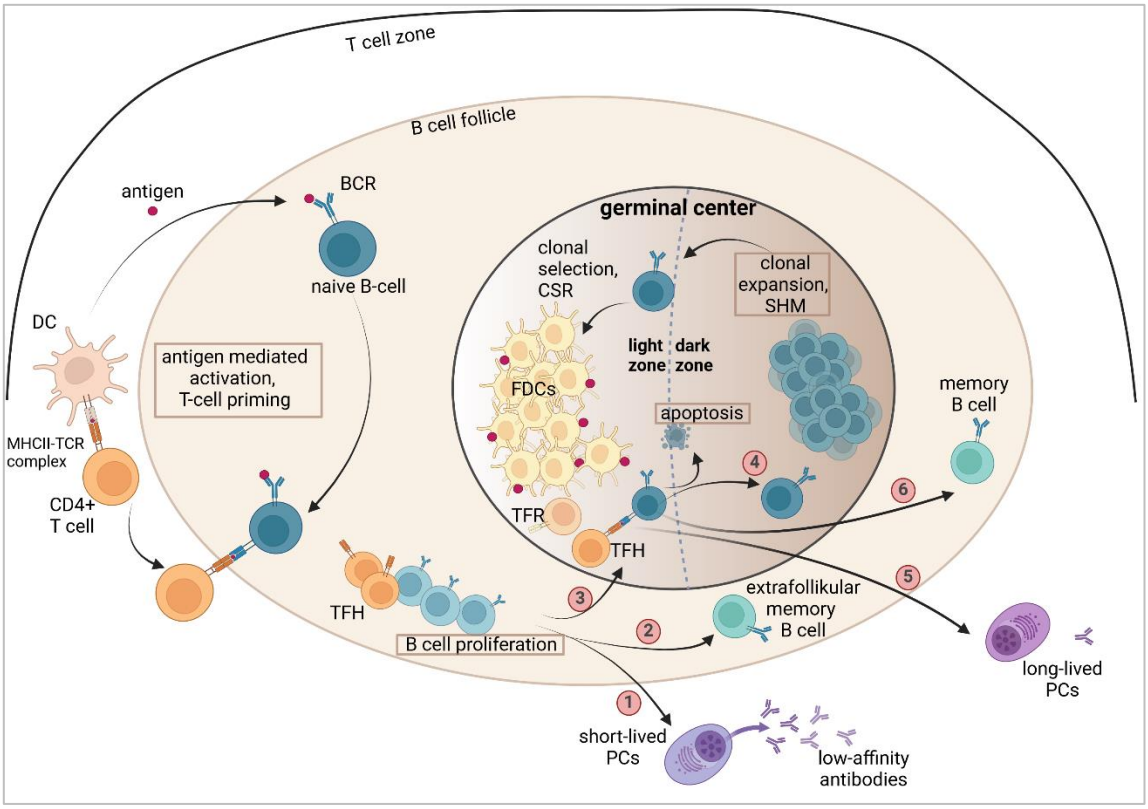

Figure 1.2: Germinal center reaction.
GCs are responsible for affinity maturation as well as the generation of long-lived PCs and memory B cells. For more details see text. Briefly, naïve $CD4^+$ T cells activate naïve B cells on the T:B border by antigen presentation, leading to B cell proliferation and differentiation of naïve T cells to T_{FH} cells. B cells either differentiate into (1) short-lived extrafollicular (also class switched) PCs, (2) extrafollicular memory B cells or (3) enter the GC. Within the GC, B cells undergo clonal expansion, SHM, selection of high affinity B cell clones and CSR. B cells receiving no positive signal from T_{FH} cells undergo apoptosis, while B cells receiving a positive signal can (4) re-enter the DZ or exit the GC as (5) long-lived PCs or (6) memory B cells. (created with Biorender.com)

1.1.2 Antibody isotypes and subclasses

An important component of the adaptive immune response are antibodies, which recognize antigens and induce multiple effector functions, leading to the killing of pathogens, infected cells, or cancer cells (Baxter 2014; J. Liu et al. 2022). B cells express antibodies in membrane-bound form, representing the BCR and in secreted form, as antibody. Antibodies are immunoglobulins (Ig) and there are 5 different Ig classes in human and mice: IgM, IgD, IgG, IgA, and IgE, which differ in the structure and characteristics of the constant region (Vidarsson, Dekkers, and Rispens 2014; Murphy and Weaver 2018). Antibodies are heterodimeric proteins consisting of two heavy (H) and two light (L) chains linked by disulfide bonds in the hinge region (Figure 1.3). The N-terminal region contains hypervariable regions of the heavy and light chains (V_H, V_L) building the variable region and are responsible for specific antigen binding. This part is therefore called the Fab-part (fragment antigen binding). These hypervariable regions are composed of three complementary determining regions (CDRs) in each arm, which multiple combinations determining the specificity of the antibody (Murphy and Weaver 2018). The highly variable antibody repertoire has evolved through recombination of different heavy and light chain gene segments, encoded by V-D-J gene segments, generating at least 10^{11} different Ig-molecules (Murphy and Weaver 2018). The constant region of IgG consists of four distinct domains C_H1, C_H2, and C_H3 of the heavy chain and C_L of the light chain, which builds the Fc-part (fragment crystallizable) of the antibody, which is responsible for effector functions (Vidarsson, Dekkers, and Rispens 2014; de Haan et al. 2017; Murphy and Weaver 2018). IgG molecules make up 10-20% of human plasma protein and are the most dominant isotype. IgG has a molecular mass of 150 kDa and can be further subdivided into four different subclasses. According to their occurrence in human serum, they are divided into IgG1, IgG2, IgG3, and IgG4, which are ~90% homologous in their amino acid sequence, but show some variation in half-life, antigen binding, Fab arm exchange, hinge region and Fc-part, affecting their effector function (Vidarsson, Dekkers, and Rispens 2014; de Taeye et al. 2020). Different IgG subclass switching depend on the type of antigen and co-stimulus (Vidarsson, Dekkers, and Rispens 2014). In mice they are divided into IgG1, IgG2a, IgG2b and IgG3, which are functionally homologous to human IgGs as follows: muIgG1-hu IgG4, muIgG2a-huIgG1, muIgG2b-huIgG3, muIgG3-huIgG2. In C57BL/6 mice IgG2c exists as an allelic variant instead of IgG2a (Zhang, Goldschmidt, and Salter 2012; de Haan et al. 2017).

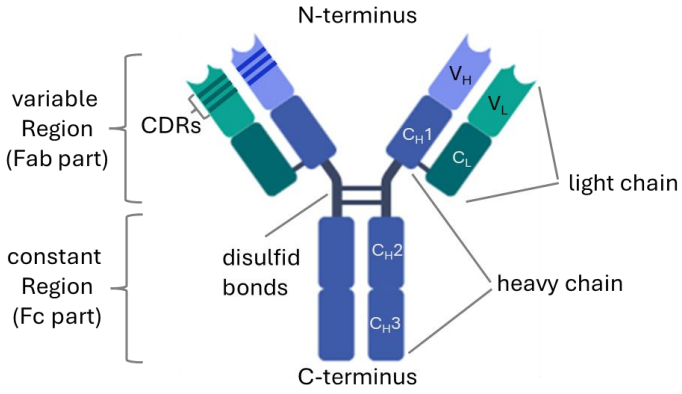

Figure 1.3: Schematic illustration of the IgG antibody structure.
An IgG molecule consists of two heavy and two light chains which are connected by disulfide bonds in the hinge region. In the N-terminal Fab part region is the variable region with the complementary determining regions (CDRs), determining the antigen binding. The Fc part of the heavy chains is responsible for effector functions.

As the first response to an immune stimulus, B cells express IgD and IgM, which are characterized by their heavy chain genes called Cμ (IgM) and Cδ (IgD). The expression of the different heavy chains is determined by the specific heavy chain gene segments, which are located in the Ig locus. After DNA rearrangement they undergo isotype switching by expressing the heavy chain genes Cγ (IgG1-4), Cα (IgA1-2), or ε (IgE) (Murphy and Weaver 2018).

The differences in the Fc part of the different subclasses, as well as the length and flexibility of the hinge region influence the effector function of the different antibody subclasses, which differs between the different IgG subclasses in the number of disulfide bonds and the length of the amino acid sequence (Figure 1.4). This also influences the binding to different Fcγ-receptors (Vidarsson, Dekkers, and Rispens 2014).

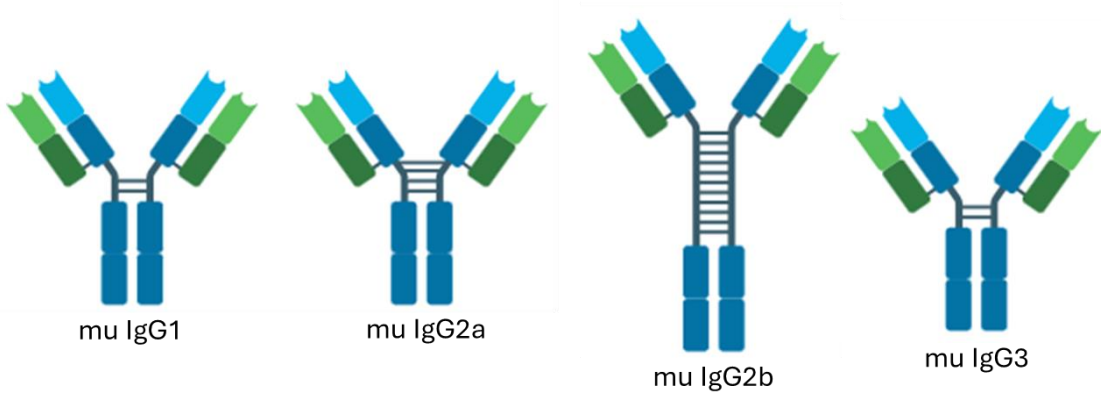

Figure 1.4: Schematic representation of the different murine IgG subclasses.
Murine IgG subclasses are divided into IgG1, IgG2a, IgG2b and IgG3. They differ in their length and flexibility of their hinge region as well as in the Fc part.

1.1.3 Antibody effector functions

Depending on the IgG subclass bound to an antigen, certain innate immune functions are induced, leading to effector mechanisms like antibody-dependent complement deposition (ADCD), antibody-dependent cellular cytotoxicity (ADCC), and antibody-dependent cellular phagocytosis (ADCP), (Nimmerjahn and Ravetch 2005; Nimmerjahn et al. 2010; Vidarsson, Dekkers, and Rispens 2014; de Taeye et al. 2020). Which mechanism is activated depends on the IgG subclass and the Fcγ-receptor (FcγR) expressed on target immune cells. Human IgG1 (murine IgG2a) and human IgG3 (murine IgG2b) show a strong interaction with activating Fcγ-receptors and C1q. Human IgG4 (murine IgG1), on the other hand, is induced after prolonged or repeated exposure to antigens (like in allergen-specific immunotherapy), and show less interaction with certain activating Fcγ-receptors and C1q (Nimmerjahn and Ravetch 2005; Nimmerjahn et al. 2010; Vidarsson, Dekkers, and Rispens 2014; Buhre et al. 2023; Irrgang et al. 2022). IgG2 (murine IgG3) also show less interaction with activation Fcγ-receptors (Bruhns 2012).

In humans and mice, there are different **FcγR** with different expression profiles on immune cells. There are several activating FcγRs (human FcγRI, FcγRIIA, FcγRIIC, FcγRIIIA and mouse FcγRI, FcγRIII, FcγRIV) containing the immunoreceptor tyrosine-based activation motif (ITAM), required for activation, but only one inhibiting FcγRIIB, containing an immunoreceptor tyrosine-based inhibition motif (ITIM), negatively regulates cell activation, degranulation, cell proliferation, endocytosis, and phagocytosis (Figure 1.5) (Bruhns 2012; Vidarsson, Dekkers, and Rispens 2014). Mouse FcγRIV is a functional homologue of human FcγRIIIA, which plays a major role in virus infections and tumor control by activating of ADCC mechanisms (Nimmerjahn and Ravetch 2005; Nimmerjahn et al. 2010; de Taeye et al. 2020).

Mouse FcγRIV is expressed on neutrophils, macrophages, and monocytes and has a high affinity for mouse IgG2a and IgG2b, but no affinity for IgG1 and IgG3. Mouse FcγRI, expressed on monocyte-derived DCs, has a high affinity for IgG2a and IgG2b. Mouse FcγRIII, which is expressed on NK cells, neutrophils, macrophages, monocytes, DCs, basophils, mast cells, and eosinophils has a lower affinity for IgG1, IgG2a, and IgG2b. In addition, the inhibitory mouse FcγRIIB, which is expressed on the same immune cells as mouse FcγRIII, but on B cells instead of NK cells, also binds IgG1, IgG2a, and IgG2b with low affinity, too (Nimmerjahn and Ravetch 2005; Nimmerjahn et al. 2010; Bruhns 2012).

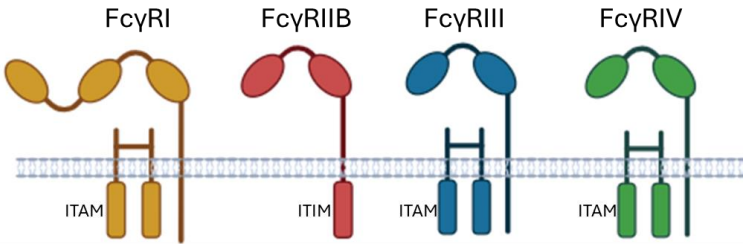

activation	inhibition	activation	activation
-	IgG1	IgG1	-
IgG2a,b	IgG2a,b	IgG2a,b	**IgG2a,b**
IgG3	-	-	-
DCs	B cells, Monocytes/ Macrophages, Neutrophils, DCs, Basophils, Mastcells, Eosinophils	NK cells, Monocytes/ Macrophages, Neutrophils, DCs, Basophils, Mastcells, Eosinophils	Monocytes/ Macrophages, Neutrophils

Figure 1.5: Murine Fcγ receptors and their expression pattern on immune cells.
The Fcγ receptors I, III and IV contain activating ITAM motifs, while Fcγ receptor IIB contains an inhibitory ITIM motif. The different receptors also differ in their affinity to different IgG subclasses (bold indicates higher affinity to the receptor) and are expressed on different immune cells. (created by Biorender.com; adapted from Bruhns et al.2012)

Human NK cell mediated ADCC via FcγRIIIA is the most important Fc-mediated effector function to kill cancer cells (Figure 1.6) (Nigro et al. 2019; de Taeye et al. 2020). In this mechanism, NK cells secrete cytolytic enzymes like perforin or granzymes, resulting in the killing of target cells. This mechanism is also used by therapeutic monoclonal IgG antibodies used in cancer therapy (Nimmerjahn and Ravetch 2005; Nimmerjahn et al. 2010; Nigro et al. 2019; de Taeye et al. 2020). Studies in murine melanoma models have shown a strong anti-tumor activity of IgG2a and IgG2b and FcγRIV (Nimmerjahn et al, 2005). Others reported that FcγRI and FcγRIII are also important for the anti-tumor activity of IgG2a antibodies (Albanesi et al. 2012). Interestingly, although human FcγRIIIA (the functional homolog of murine FcγRIV) is expressed on NK cells, FcγRIV is not. Instead, FcγRIV is expressed e.g. on neutrophils, suggesting that FcγRIV expression e.g. on murine neutrophils may also play an important role in ADCC (Albanesi et al. 2013). Accordingly, murine neutrophils have been described to be involved in antibody-induced antitumor effects (Albanesi et al, 2013). Interestingly, also human neutrophils have been described to be involved in tumor cell attack (Xiong, Dong, and Cheng 2021).

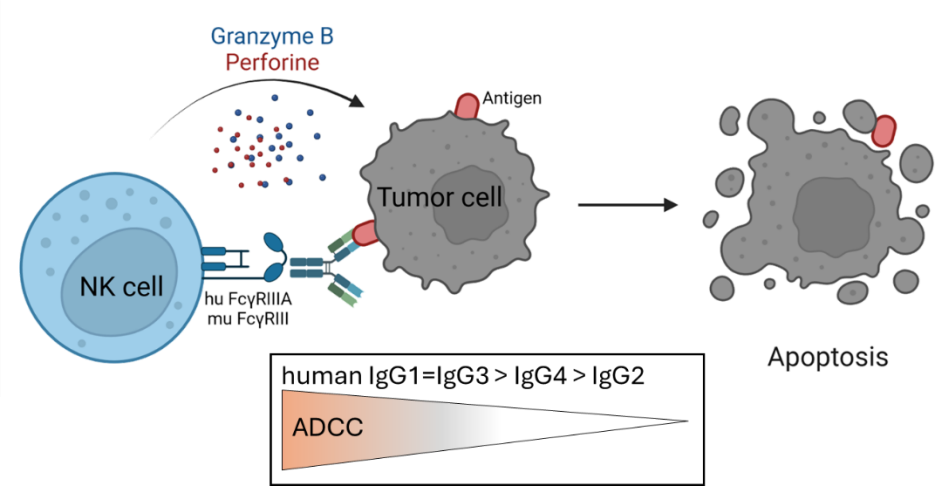

Figure 1.6 Mechanism of antibody-dependent cellular cytotoxicity (ADCC) via NK cells.
Human antibodies can bind tumor antigens via their Fab portion, while their Fc portion leads to the recruitment of effector cells, such as NK cells, by binding to their Fcγ receptor. NK cells are then activated, leading to the secretion of cytotoxic cytokines and the killing of tumor cells. The efficiency of ADCC activation depends on the IgG subclass.

1.1.3.1 Antibody Fc-N glycosylation impacts antibody effector function

Besides the different IgG subclasses, the effector function of IgG is also influenced by the Fc-N glycosylation, which further affects the interaction with different FcγRs and glycan binding C-type lectin receptors (Vidarsson, Dekkers, and Rispens 2014; de Haan et al. 2017). Glycosylation is a post-translational modification of proteins that affects their stability, conformation, biological activity, and antigenicity and was first reported in 1976 by F.Ciccimarra (Ciccimarra et al. 1976; Alter, Ottenhoff, and Joosten 2018; Cobb 2019). The IgG molecule has one glycosylation side at asparagine-297 (Asn-297) at each heavy chain in the Fc-part (Figure 1.7). The IgG N-glycan consists of a biantennary core structure of 4 N-acetylglucosamines (GlcNAc) and 3 mannoses (Man), which can be further extended with a core fucose (fuc), a bisecting GlcNAc, 1-2 galactose (gal), and 1-2 sialic acid (sial).

In humans, over 90% of total IgGs are fucosylated, 15-35% are galactosylated, approximately 10% are sialylated and approximately 10% have a bisecting GlcNAc (Irvine and Alter 2020; Vattepu, Sneed, and Anthony 2022).

Removal of fucose alters the conformation of the glycan, which increases the interaction with activating human FcγRIIIA and mouse FcγRIV and thus the induction of ADCC. The removal of fucose from IgG results in a 50-fold increase in affinity for the receptor in humans

(Vidarsson, Dekkers, and Rispens 2014; de Haan et al. 2017; Alter, Ottenhoff, and Joosten 2018; Irvine and Alter 2020; Larsen et al. 2021; W. Wang et al. 2021).

Induction of antigen-specific afucosylated IgG has been found when the antigen is expressed membrane-associated like alloantibodies to red blood cells and platelets (blood transfusions), and after certain infections and vaccinations (Vidarsson, Dekkers, and Rispens 2014; de Haan et al. 2017; Alter, Ottenhoff, and Joosten 2018; Irvine and Alter 2020; Larsen et al. 2021). Accordingly, clinical studies are currently running to investigate the potential of non(a)-fucosylated tumor-antigen-specific therapeutic monoclonal antibodies (Pereira et al. 2018; Caracciolo et al. 2021; Cohen Saban et al. 2023). However, the target induction of afucosylated IgG antibodies by vaccination needs further investigation.

Reduced galactosylation and sialylation of total and autoantigen-specific IgG are associated with inflammatory (auto) immune conditions such as in autoimmune diseases like rheumatoid arthritis (RA), systemic lupus erythematosus (SLE), multiple sclerosis (MS), diabetes and inflammatory bowel disease (IBD) (Collin and Ehlers 2013; de Haan et al. 2017; Alter, Ottenhoff, and Joosten 2018). However, during pregnancy or anti-TNF treatment both leading to disease remission the glycosylation shifts to higher galactosylation and sialylation levels in RA patients, associated with disease improvement (de Haan et al. 2017; Bartsch et al. 2020). Accordingly, the anti-inflammatory effects of IVIG (pooled serum IgG from healthy donors) for the treatment of inflammatory autoimmune diseases are associated with a re-enhancement of the sialylated IgG sub-fraction binding to murine SignR1 leading to the upregulation of FcγRIIB (Anthony et al. 2011; Collin and Ehlers 2013; Hess et al. 2013; Vattepu, Sneed, and Anthony 2022).

The role of vaccination-induced IgG galactosylation, sialylation, and bisection is less clear. Recent murine and human studies have shown that short-term IgG responses after vaccination are highly galactosylated and sialylated and low bisected, whereas long-term IgG is less galactosylated and sialylated and higher bisected (Bartsch et al. 2020; Buhre et al. 2023; 2024). The kind of adjuvant used during vaccination seems to influence in particular the long-term IgG galactosylation and sialylation levels (Bartsch et al. 2020). More inflammatory adjuvants seem to induce more reduced long-term IgG galactosylation and sialylation than less inflammatory adjuvants (Bartsch et al. 2020).

Presumably, differently glycosylated short-term and long-term IgG antibodies may have different roles.

Galactosylation of IgG modestly increases binding to C1q, which is responsible for ADCD induction (Dekkers et al. 2017), and increases NK cell activation *in vitro* (Murphy and Weaver 2018; Alter, Ottenhoff, and Joosten 2018) as well as binding to FcγRIIB and Dectin-1 on neutrophils in mice, thereby inhibiting inflammatory responses (Karsten et al. 2012; Irvine and Alter 2020). Terminal sialylation decreases the binding affinity to activating murine FcγRs (Collin and Ehlers 2013; Alter, Ottenhoff, and Joosten 2018; Irvine and Alter 2020; Bartsch et al. 2020). In contrast, de-galactosylated IgG seems to enhance the activation of neutrophils (Epp et al. 2018; Clauder et al. 2021). De-galactosylated IgG antibodies may attack cancer cells via the activation of neutrophils. The role of the bisecting glycan structures is still unclear and needs further investigation (Vidarsson, Dekkers, and Rispens 2014; Alter, Ottenhoff, and Joosten 2018; Irvine and Alter 2020).

Reports on more or less total IgG(1) galactosylation and sialylation levels of certain cancer patients (W. Wang et al. 2021) may reflect more the inflammatory status of the patients with unclear influence on the anti-tumor fighting potential. Total IgG(1) galactosylation levels were reduced in most of the cancer patients examined (W. Wang et al. 2021). Most cancer patients also showed an increased total IgG(1) fucosylation (Bastian et al. 2021; J. Wang et al. 2021). However, the role of anti-tumor IgG glycosylation has to be further investigated.

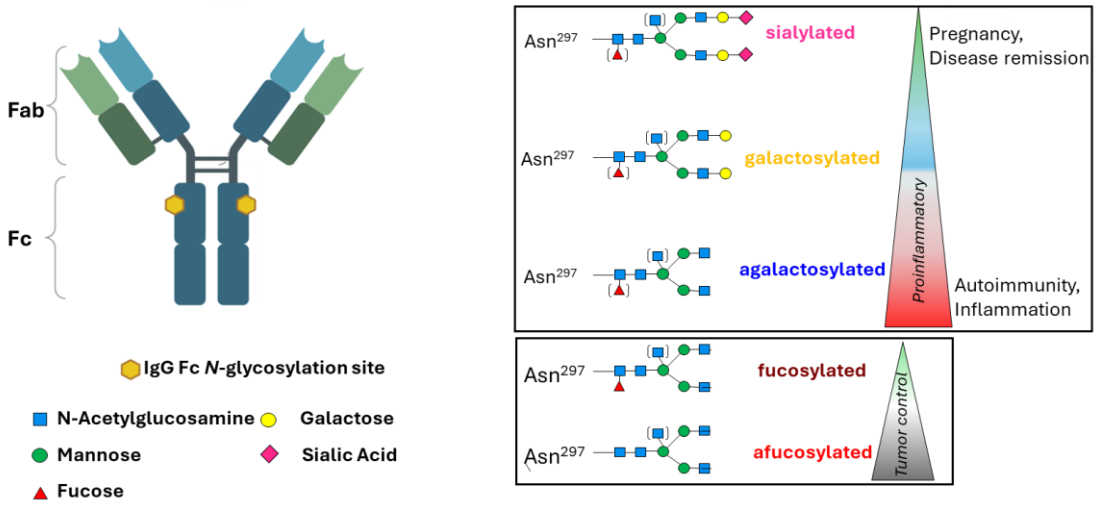

Figure 1.7: Schematic representation of Fc-N glycosylation of an IgG antibody.
IgG antibodies have a conserved glycosylation side on Asn-297 of the Fc-part. The biantennary core structure consists of 4 N-acetylglucosamines (GlcNAc) and 3 mannoses, which can be further elongated with a core fucose (fuc), bisecting GlcNAc, 1-2 galactoses (gal), and 1-2 sialic acids (sial). Agalactosylated (de-galactosylated) forms characterize inflammatory (auto) immune conditions. Fucosylation impacts the tumor control capacity.

1.1.3.2 Fc-N glycosylation is regulated by certain enzymes

The IgG Fc-N glycosylation is a post-translational process that occurs mainly in antibody-producing B cells. A biantennary high mannose structure is added to Asn-297 by mannosidase I in the endoplasmic reticulum (ER). The antibody is then transferred to the cis-Golgi apparatus, where further trimming and remodeling of the glycan occurs with glycosidases and glycotransferases, producing the core glycan (Figure 1.7) (Dekkers, Rispens, and Vidarsson 2018; Irvine and Alter 2020). Subsequently, the core structure is modified by certain enzymes and substrates. As an early process, MGAT3 can add bisecting GlcNAc to the core structure. Fucosyltranferase-8 (FUT-8) adds core fucose to the glycan in the medial Golgi. In the trans-Golgi, beta-1,4-galactosyltransferase 1 (B4galT1) and the substrate UDP-galactose can add one or two galactoses, which can be further elongated by the addition of one sialic acid to each galactose by alpha-2,6-sialyltransferase 1 (St6gal1) and CMP-activated sialic acid (Dekkers, Rispens, and Vidarsson 2018; Cobb 2019; Irvine and Alter 2020). Noteworthy, the sialic acid Neu5Ac (N-acetylneuraminic acid) is expressed in humans and Neu5Gc (N-glycolylneuraminic acid) in mice (de Haan et al. 2017).

Different stimuli seem to regulate the expression of these enzymes in B cells (Bartsch et al. 2018; Coillie et al. 2023). The inflammatory immune status of each individual characterized by the IgG galactosylation, sialylation, and bisection levels (natural or influenced by adjuvants) seems to influence antigen-specific responses in B cells (Bartsch et al. 2018). The regulation of fucosylation seems to be independent of the immune status (Coillie et al. 2023).

1.2 Antibodies in cancer therapy

Monoclonal antibodies are widely used in the treatment of cancer. Tumor antigen-specific antibodies have been developed and can be genetically engineered to improve therapeutic efficacy (Zahavi and Weiner 2020; Delgado and Garcia-Sanz 2023; Zinn et al. 2023). In addition, monoclonal antibodies are used to block for instance immune checkpoints such as PD-1 and CTLA-4.

In 1980, the first trial to treat cancer with monoclonal antibodies was made in a lymphoma patient (Koprowski et al. 1978; Lm et al. 1980; Ortho Multicenter Transplant Study Group 1985; Zahavi and Weiner 2020). However, this was still challenging, because the monoclonal antibodies were produced in murine hybridoma cells and were therefore immunogenic in humans. In the late 1080s, humanized monoclonal antibodies were generated using transgenic

mice or *in vitro* phage/yeast display technology (Zahavi and Weiner 2020). To date, 197 antibodies have been approved by the FDA/EMA, of which 91 are antibodies for cancer treatment (Delgado and Garcia-Sanz 2023). There are different mechanisms by which anti-cancer antibodies act: (1) Most antibodies target cancer cell surface molecules/receptors that are overexpressed or mutated, resulting in increased cancer cell proliferation, migration, or growth. For example, these antibodies target/block EGFR (Epidermal Growth Factor Receptor) (*Cetuximab*), which is overexpressed in many solid tumors and involved in proliferation, migration, and invasion, or targets HER2 (human epidermal growth factor receptor 2) (*Pertuzumab, Trastuzumab*), a tyrosine kinase receptor overexpressed in ovarian and breast cancer, for example (Zahavi and Weiner 2020; Delgado and Garcia-Sanz 2023; Zinn et al. 2023). (2) In addition, antibodies can target surface antigens or receptor ligands, involved in neovascularization, migration, metalloprotease secretion, or cell invasion. Blocking of VEGF or VEGFR (vascular endothelial growth factor or vascular endothelial growth factor receptor) prevents angiogenesis and the formation of new blood vessels (Zahavi and Weiner 2020; Delgado and Garcia-Sanz 2023; Zinn et al. 2023). (3) In addition, surface antigens on immune cells can be targeted by agonists that enhance the activation of an immune response. Binding to receptors on APCs or T cells of the TNF family like CD40, OX40, and 4-1BB enhances the effector function of these cells while suppressing the function of T_{regs}. Other targets include checkpoint inhibitors such as CTLA-4 and PD-1 or their ligands such as PD-L1, which can be blocked to prevent receptor/ligand binding, thereby increasing the efficiency of the T cell response (Zahavi and Weiner 2020; Delgado and Garcia-Sanz 2023; Zinn et al. 2023).

Rituximab, for instance, is a monoclonal antibody used in B cell malignancies (e.g. Non-Hodkin lymphoma) that targets CD20 on B cells (Zahavi and Weiner 2020; Zinn et al. 2023). Obinutuzumab was the first glycoengineered (removal of core fucose) antibody of rituximab, additionally being fully humanized. The antibody showed higher direct killing activity by ADCC efficiency (Zahavi and Weiner 2020; Zinn et al. 2023; Hernandez et al., n.d.). Furthermore, antibodies without fucose and sialic acid are engineered to enhance their therapeutic efficiency (Ollila, Sahin, and Olszewski 2019; Beck and Reichert 2012).

1.2.1 Immune checkpoint inhibition

Immune checkpoints are inhibitory receptors and pathways, that control the immune response, preventing excessive immune responses and the induction of autoimmune responses to maintain self-tolerance (Zahavi and Weiner 2020). Immune checkpoint receptors are mainly expressed on exhausted T cells, which are upregulated during chronic infections to downregulate the immune response (Seidel, Otsuka, and Kabashima 2018).

Noteworthy, tumors can take advantage of these receptors to evade the immune system. Blocking of these receptors in cancer therapy can enhance the immune response against cancer cells. Immune checkpoint blockade mainly with monoclonal antibodies has already been shown to increase survival in melanoma patient (Seidel, Otsuka, and Kabashima 2018).

Programmed cell death protein 1 (PD-1) is an inhibitory receptor, constitutively expressed on some T cells such as T follicular helper cells, $CD8^+$ T cells, and T_{regs}. It is also expressed by activated B cells, myeloid DCs, mast cells, NK cells, or Langerhans cells and the expression is further induced by TCR activation and cytokines such as IL-2, IL-15, IL-21, or TGFβ (Seidel, Otsuka, and Kabashima 2018; Zahavi and Weiner 2020). PD-1 is an important regulator of effector T cell function (Zahavi and Weiner 2020). Upon binding of its ligands PD-L1 or PD-L2, which are expressed on APCs, tyrosine residues of PD-1 are phosphorylated, inducing intracellular signaling cascades that dephosphorylate TCR signaling components, leading to reduced cytokine production (IL-2, IFNγ, TNF-α), cell cycle progression and reduced expression of genes involved in effector function (T-bet, Eomes) (Figure 1.8) (Seidel, Otsuka, and Kabashima 2018). However, PD-L1 is also expressed by cancer cells and tumor-infiltrating lymphocytes such as macrophages. In addition, it is upregulated by IFNγ stimulation, which represents an anti-tumor immune response but also leads to immunosuppression (Seidel, Otsuka, and Kabashima 2018; Chae et al. 2018; Zahavi and Weiner 2020). Accordingly, the expression level of PD-L1 on tumor cells correlates with cancer prognosis, with high expression levels correlating with poor prognosis in melanoma, renal cancer, esophageal, gastric, and ovarian cancers (Seidel, Otsuka, and Kabashima 2018). In addition, the response to therapy is higher in patients with high tumor PD-L1 expression than in patients with low PD-L1 expression and in tumors with a higher mutational burden prior to therapy (Juneja et al. 2017; Seidel, Otsuka, and Kabashima 2018).

Cytotoxic T-lymphocyte-associated protein 4 (CTLA-4) is another immune checkpoint receptor that belongs to the B7/CD28 family and is constitutively expressed on T_{regs}, but can be

upregulated on $CD4^+$ T cells after activation (Seidel, Otsuka, and Kabashima 2018). CTLA-4 competes with CD80/CD86 for binding to CD28 on T cells and is also able to remove CD80/CD86 from the cell surface due to its higher affinity for CD28. This inhibits CD28-mediated signaling, resulting in dampened T cell effector function. This represents the T_{reg}-mediated immune suppression (Figure 1.8) (Seidel, Otsuka, and Kabashima 2018).

In addition, CTLA-4 is expressed in tumor lesions on infiltrating T cells, T_{regs}, and tumor cells, where it exerts its immunosuppressive function. Blocking of CTLA-4 prevents its inhibitory function and enhances T cell functions and cytotoxic signals, resulting in improved tumor clearance (Seidel, Otsuka, and Kabashima 2018; Zahavi and Weiner 2020). This effect was first reported with *ipilimumab* (anti-CTLA-4 antibody) (Seidel, Otsuka, and Kabashima 2018).

Other immune checkpoints under investigation include LAG-3 (lymphocyte activation gene 3), TIM3 (T cell immunoglobulin and mucin domain-containing 3), TIGIT (T cell immunoglobulin and immunoreceptor tyrosine-based inhibitory motif domain), or VISTA (V-domain Ig suppressor of T cell activation) (Zahavi and Weiner 2020).

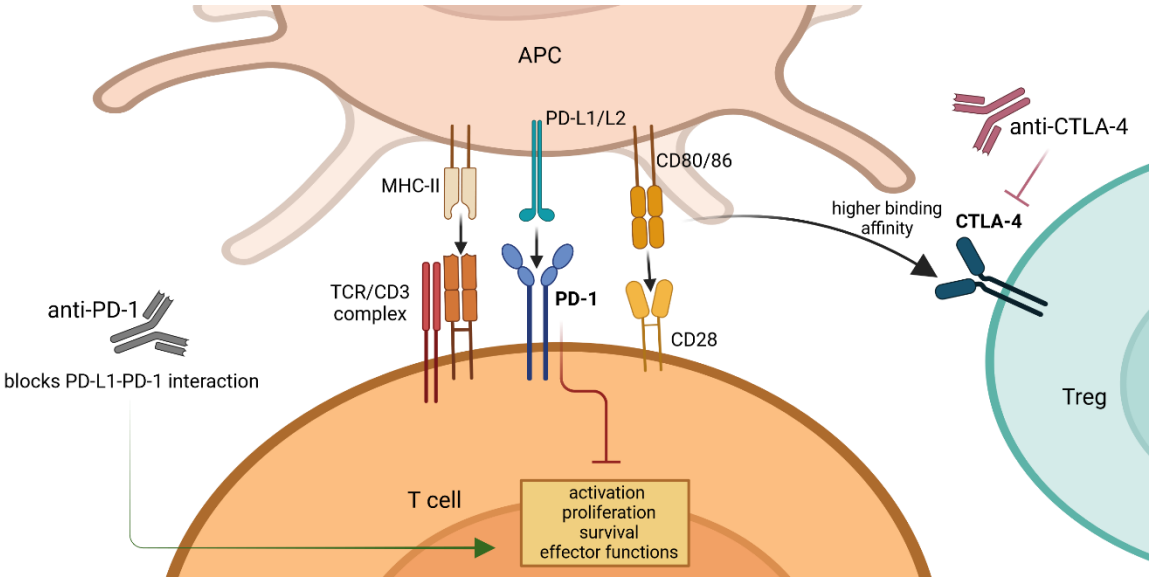

Figure 1.8: Representation of immune checkpoint mediated immune inhibition.
Binding of PD-1 to its ligand PD-L1 or PD-L2 blocks T cell functions and survival, while binding of CTLA-4 to its ligand CD80/CD86 activates T_{reg}, which further dampens the immune response. Blockade of both immune checkpoint receptors by antibodies increases the T cell function and survival and inhibits T_{reg} function, resulting in an enhanced immune response. (created by Biorender.com)

1.2.2 Challenges in antibody therapy

Immune checkpoint inhibitors have revolutionized cancer treatment. However, the treatment activates the whole immune system, and many (auto)inflammatory side effects have been observed. Furthermore, only a small subset of patients benefits from these therapies (Lei et al. 2020; Ma, Pham, and Li 2022; Dai, Gao, and Wei 2022). Development of monoclonal antibodies against specific tumor antigens is still rare. Furthermore, many patients develop resistance to the antibodies, which can be innate or acquired over time. Innate resistance includes mutations in target molecules that are required prior to therapy, whereas acquired resistance occurs due to immune selection pressure and immunoediting during therapy. This can include mutations in target molecules, induction of alternative signaling pathways, epithelial-to-mesenchymal transition (EMT), or impaired effector cell response. This affects the efficacy of the therapy as it depends on the expression and function of the target molecule (Juneja et al. 2017; Zahavi and Weiner 2020). Therefore, immune checkpoint blockade is combined with other therapeutic options such as chemotherapy, radiation, molecular target drugs (e.g. tyrosine kinase inhibitors), antibodies against the same target, other immune checkpoint blockade (e.g. LAG-3 or TIM-3), cellular therapies or vaccines (Zahavi and Weiner 2020; Lorentzen et al. 2023).

1.3 Active immunization

Since the eradication of smallpox in 1980, vaccination has received considerable attention. The most commonly used vaccine formats have been live attenuated, whole killed pathogens or subunit vaccines, containing natural or recombinant antigens such as proteins, or polysaccharides. The use of killed pathogen- and live-attenuated pathogen-containing vaccines has often induced a robust, long-lasting immunity, whereas purified or recombinant antigens have induced only a weak and short-term antibody response (Iwasaki and Omer 2020). It has been shown that antigen vaccination without adjuvant may rather induce tolerogenic conditions (Oefner et al. 2012). Gaston Ramon observed in 1925 that inflammation on the side of the vaccine injection enhanced the immune response. The addition of tapioca, lecithin, agar, starch oil, saponin, or breadcrumbs increased the immune responses to the diphtheria vaccine (Christensen 2016; Iwasaki and Omer 2020). In 1926, Alexander Glenny discovered that the addition of aluminum salts to the diphtheria toxoid resulted in precipitation and increased immune responses (Christensen 2016; Iwasaki and Omer 2020; Zhao et al. 2023). Later, in the 1930s, aluminum salts were used as adjuvants in pertussis and tetanus vaccines. Nowadays,

aluminum salts are also used in vaccines against hepatitis A and B (HBV A, B), *Haemophilus influenzae* type b, *pneumococcus,* and human papillomavirus (HBV) (Christensen 2016; Iwasaki and Omer 2020). Since then, particles or molecules known as adjuvants (Latin *adjuvare* = "to help") have been added to the vaccines to enhance the immune response (Murphy and Weaver 2018). While antigens in vaccines stimulate the adaptive immune system, adjuvants stimulate the innate immune system, for example through PPRs (Iwasaki and Omer 2020), thereby enhancing the adaptive immune response.

In 1940, Freund and colleagues developed a water-in-oil emulsion as strong adjuvant (FA: Freund's adjuvant), but it was toxic in humans. Lipopolysaccharides (LPS) from bacterial cell walls as adjuvant also showed local systemic side effects in humans. Therefore, since 1997, Aluminum hydroxide has long been the only adjuvant approved for human use in Europe. Later in 1997, the oil-in-water emulsion MF59 was approved for use in influenza vaccines. (Zhao et al. 2023). To date, several more adjuvants have been licensed for human vaccines (AS04, AS03, AS01, CpG ODN 1018) (Zhao et al. 2023).

In addition, it has been figured out that vaccines should contain pathogen-specific or at least carrier proteins to involve T cell activation.

1.3.1 Impact of different adjuvants on the innate and adaptive immune response

Today, adjuvants are used as delivery systems and co-stimulants in vaccines to enhance the adaptive immune response against an antigen (Facciolà et al. 2022). Other compounds, that have been evaluated for use as adjuvants include mineral salts, microbial products, emulsions, saponins, synthetic small molecule agonists, polymers, nanoparticles, and liposomes (Zhao et al. 2023). In general, adjuvants often stimulate the innate immune system, by mimicking defined structures of pathogens. These are for example PAMPS, which activate PPRs, mainly stimulating APCs (e.g. DCs) and facilitating antigen uptake, processing, and epitope presentation by MHC molecules (signal 1). They also recruit other immune cells such as $CD4^+$ T cells. Further costimulatory signals such as CD40, CD80, and CD86 on APCs or cytokines such as IL-6, IL-10, IL-12, and TNFα (signal 2) support the stimulation of T cells (Zhao et al. 2023). In addition, delivery systems facilitate the antigen presentation to APCs and prolong their bioavailability. Examples include lipid nanoparticles (LNPs), poly(lactide-*co*-glycolide)

(PLGA), and caged protein nanoparticles. Certain nanoparticles are also able to directly co-activate B cells (Zhao et al. 2023).

Whereas adjuvants have long been used to enhance the "quantity" of an antigen-specific IgG response, it now becomes clear that different adjuvants induce different "qualities" of T and B cell and the resulting IgG antibody responses (Bartsch et al. 2020).

Following the activation of the innate immune response, adjuvants influence the adaptive immune response and activate different IgG subclasses and glycosylation patterns (Oefner et al. 2012; Bartsch et al. 2020).

1.3.1.1 Adjuvant types

Aluminum-based adjuvants such as aluminum hydroxide (Alum) and aluminum phosphate (Adju-Phos®) precipitate with antigens in solutions (Coffman, Sher, and Seder 2010). They act as delivery systems, increasing the antigen bioavailability and thus antigen uptake and presentation by APCs (Coffman, Sher, and Seder 2010; Facciolà et al. 2022; Zhao et al. 2023). Alum also induces necrotic cell death at the injection site, resulting in danger signals such as uric acid or DNA being released from dying cells and acting as DAMPs to activate PPRs (Coffman, Sher, and Seder 2010; Zhao et al. 2023). In humans, Alum-antigen mixtures induce T_H1 and T_H2 immune responses, whereas in mice a profound T_H2 response is induced with appropriate antibody subclasses (murine IgG1) (Coffman, Sher, and Seder 2010). Besides this, Alum has been reported to activate the NLRP3 inflammasome and induce a T_H2 response (Coffman, Sher, and Seder 2010; Facciolà et al. 2022; Zhao et al. 2023).

Water-in-oil emulsions, such as complete and incomplete Freund's adjuvants (**CFA, IFA**) and **eCFA** (enriched CFA) are mixtures of paraffin oil and surfactants with heat-killed Mycobacterium tuberculosis (M.tb.) in which aqueous antigen solutions are emulsified (Coffman, Sher, and Seder 2010; Facciolà et al. 2022). These adjuvants induce necrotic cell death at the injection site, leading to danger signals and NOD1/2-mediated signaling, which triggers T_H2 immune responses. In addition, a component of M.tb., namely the cord factor contained in CFA and eCFA, binds to MINCLE, triggering appropriate signaling pathways and initiating T_H1 and T_H2 immune responses (Coffman, Sher, and Seder 2010; Zhao et al. 2023). eCFA additionally induces T_H17 cells. However, Freund's adjuvants have severe side effects and are therefore not used in human vaccines (Facciolà et al. 2022). **CAF01**, a synthetic ligand

for MINCLE, formulated in liposomes, has been used in tuberculosis vaccines (Coffman, Sher, and Seder 2010; Knudsen et al. 2016). **Montanide ISA51** and **ISA720** are novel water-in-oil emulsions used in clinical trials (influenza, malaria, melanoma), primarily as delivery systems. Montanide ISA51 is emulsified with mineral oil and mannide monooleate, while ISA720 is emulsified with non-mineral oil and mannide monooleate. The immunomodulatory mechanisms are similar to those of IFA (Coffman, Sher, and Seder 2010; Zhao et al. 2023). Furthermore, water-in-oil adjuvants strongly affect the GC response by strongly enhancing the plasma cell response and strongly reducing the long-term level of IgG galactosylation and sialylation. These effects were further enhanced with eCFA containing elevated concentrations of M.tb. (5 mg/mL (CFA: 1 mg/mL)) (Bartsch et al. 2020).

Oil-in-water emulsions such as **MF59** (Novartis) and **AS03** (GlaxoSmithKline) consist of the oil squalene, Tween80, and Span85, which are more easily metabolized than the paraffin oil used in Freund's adjuvants (Coffman, Sher, and Seder 2010; Facciolà et al. 2022). In 1997, MF59 was the first non-aluminum-based adjuvant licensed for influenza vaccines. It can act as a delivery system and immunostimulant, by prolonging the antigen delivery and slowing antigen release in the lymph nodes. This enhances the antigen presentation by APCs and thus leads to a strong immune (mixed T_H1 and T_H2) and antibody response (Coffman, Sher, and Seder 2010; Zhao et al. 2023). AS03 consists of alpha-tocopherol, squalene, and Tween80 and has similar immunological effects as MF59. It acts as a delivery system and immunostimulant, mediating mainly a T_H2 immune response and a weak T_H1 response. AS03 is licensed primarily for influenza vaccines (Zhao et al. 2023).

AS04 consists of **Alum** and **MPLA** (monophosphoryl lipid A) and induces a stronger antibody response compared to Alum, because of MPLA. MPLA is a detoxified form of LPS, binds to TLR4 and induces a T_H1 immune response. AS04 is used in an HPV vaccine (*Cervarix*) and an HBV vaccine (*Fendrix*) (Zhao et al. 2023).

Synthetic dsRNA targets TLR3 and MDA5 on APCs, inducing cytokines such as IL-12 and type I interferons, which induce T_H1 and CTL responses. Poly(I:C) and Poly(ICLC) activate DCs via TLR3, resulting in cross-presentation of exogenous antigens to $CD8^+$ T cells, inducing T_H1 and antibody responses. The use of Poly(I:C) and Poly(ICLC) in cancer vaccines has demonstrated tumor-specific T cell and NK cell responses leading to tumor regression (Zhao et al. 2023). Due to dose-dependent side effects such as fever and coagulation abnormalities, both adjuvants need to be improved before they can be approved for human use. Poly(ICLC)

contains poly-L-lysine and carboxymethyl cellulose, which prolongs the adjuvant effect compared to Poly(I:C) (Coffman, Sher, and Seder 2010; Zhao et al. 2023).

Imidazoquinolines can activate TLR7 and TLR8, inducing type I interferons and T_H1/CTL immune responses. Imiquimod (R837) and Resiquimod (R848) are used in preclinical/clinical studies. Imiquimod has been used in vaccines against melanoma, HPV, breast cancer, and T cell lymphoma, while Resiquimod has been used in cancer and antiviral vaccines and has shown strong antibody and T cell responses (Coffman, Sher, and Seder 2010; Zhao et al. 2023).

Lipid nanoparticles (LNPs) are nanoscale particles composed of ionizable lipids, phospholipids, cholesterol, and polyethylene glycol-modified lipids. LNPs act as delivery systems, prolonging the bioavailability of antigens and increasing the particle size to promote antigen uptake by APCs. In addition, they promote $CD8^+$ T cell responses by preventing antigen release from endosomes through membrane fusion. As adjuvants, LNPs induce strong humoral and cellular immune responses and have been used in vaccines against COVID-19 and in a murine melanoma model (Oberli et al. 2017; Zhao et al. 2023).

Other adjuvant systems include **polymer particles** or **virus-like particles** (**VLPs**) (Facciolà et al. 2022; Zhao et al. 2023).

Noteworthy, the different adjuvant groups induce different innate immune responses leading to qualitatively distinct T and B cell responses and the resulting IgG subclass and Fc-glycosylation responses with yet unclear effects on tumor clearance.

The different adjuvants may thereby distinctly influence the extrafollicular and the germinal center-derived plasma cell and antibody response.

1.3.1.2 Impact of different adjuvants on the GC-derived antibody response

As published in Bartsch et al. 2020 and in the dissertations of Y. Bartsch and H. Lunding, immunizations with the soluble foreign model antigen ovalbumin (Ova; the albumin of chicken) together with different adjuvants influence the antigen-specific germinal center response and thus the antigen-specific IgG antibody subclass composition and glycosylation pattern in mice (Figure 1.9) (Bartsch 2019; Bartsch et al. 2020; Lunding 2021).

The water-in-oil adjuvants eCFA, CFA, IFA, and Montanide ISA51 induced strong antigen-specific IgG antibody titers, which were progressively less after vaccination with Alum, Adju-Phos, MPLA, Poly(I:C), Addavax (MF59) and R848.

However, further differences between the adjuvants were observed with respect to IgG subclasses. IgG1 antibody titers showed a similar trend as total IgG, whereas IgG2c (analogous to IgG2a in C57BL/6 mice) was additionally induced after eCFA, CFA, IFA, and Poly(I:C), and MPLA vaccination. The latter two increased further after a booster vaccination with Ova without adjuvant. It is noteworthy that Montanide also induced quite low IgG2c antibody titers, comparable to those induced by Alum immunization. IgG2b antibody titers were also increased with eCFA, CFA, and IFA, but rather lower with Montanide, MPLA and Poly(I:C), which however also increased after booster vaccination. The overall levels of IgG3 were overall quite low.

In addition, the short-term (day 7) IgG1 and IgG2 (IgG2c+IgG2b) antibodies induced by the different adjuvants were highly galactosylated and sialylated. Subsequently, upon day 14, most likely when the GC-derived IgG antibodies became visible, IgG1 and IgG2 galactosylation and sialylation were reduced. However, upon day 14, differences between the different adjuvant groups became visible. The water-in-oil adjuvants induced a sharper down-regulation of IgG1 and IgG2 galactosylation compared to the other adjuvant groups. Noteworthy, after boosting with Ova without adjuvant on day 28 all IgG galactosylation and sialylation levels increased again to fall down after a few days again in the mentioned differences.

The IgG subclass antibody titers also correlate with corresponding IgG subclass GC B cell and PC frequencies and the IgG subclass sialylation with the expression level of St6gal1 in the GC B cells and plasma cells on day 12, which is responsible for the sialylation of the IgG Fc-N glycan (Bartsch et al. 2020). The data suggest that the GC response is responsible for different long-term IgG antibody responses after vaccination and is dependent on the kind of adjuvant (Bartsch et al. 2020; Lunding 2021).

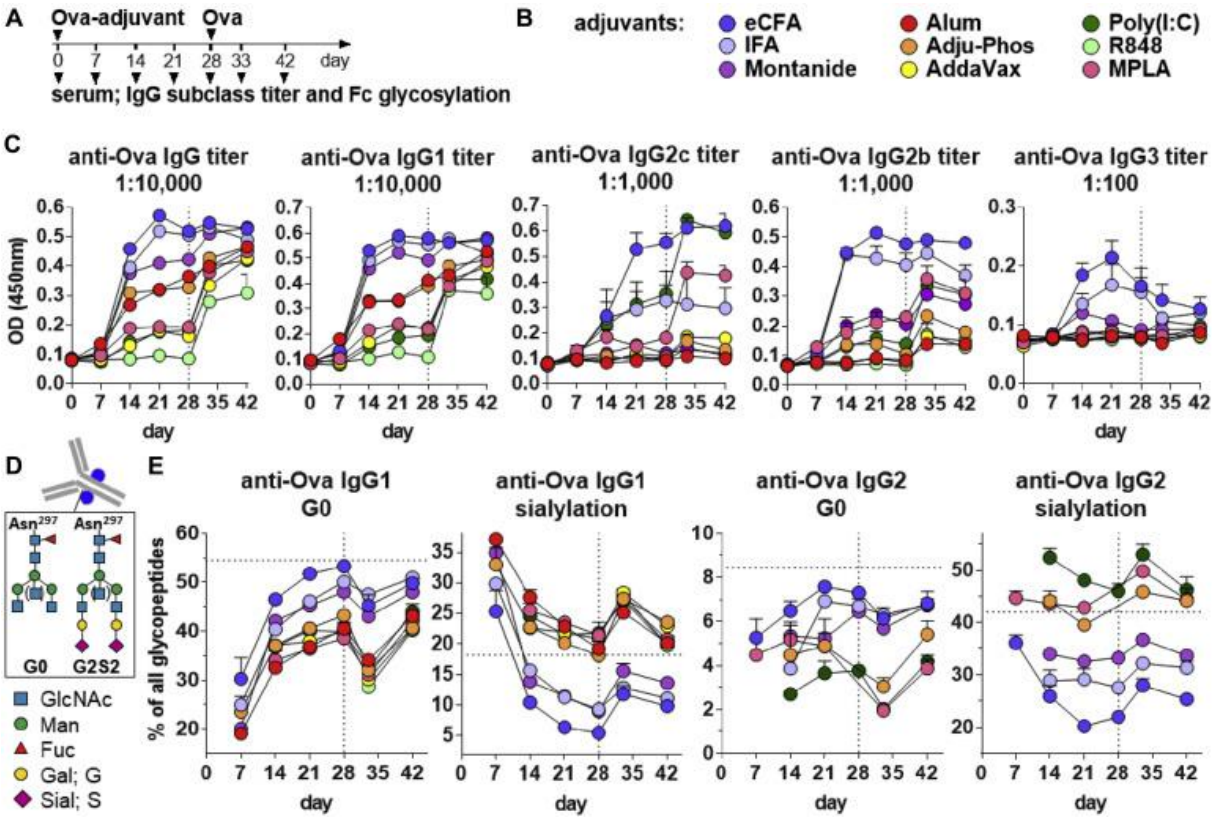

Figure 1.9: Impact of different adjuvants on the IgG subclass titers and glycosylation patterns over time.
The Figure was published in **(Bartsch et al. 2020)**. (A) Experimental design: C57BL/6 WT mice were immunized with Ova plus different adjuvants on day 0 and boosted with Ova without adjuvants on day 28 (vertical dashed line). On day 7, 14, 21, 28, 33 and 42 after first immunization, blood was collected, and serum was analyzed for IgG subclass titer by ELISA and IgG glycosylation patterns by LC-MS. (B) Color code of the investigated adjuvants. (C) Serum anti-Ova IgG titers of different subclasses on indicated days after immunization. (D) Serum anti-Ova IgG1 and IgG2 (c+b) subclass glycosylation patterns on indicated days after immunization. Percentages of de-galactosylated and sialylated IgG subclass glycopeptides are shown.

1.3.2 Vaccination platforms in cancer therapy

Most licensed vaccines are for infectious diseases caused by viruses or bacteria. Some vaccines have been developed against viruses that induce cancers, such as cervical cancer caused by HPV and hepatocellular carcinoma caused by HBV. Vaccination with tumor cells or tumor antigens is still under development. However, vaccination for cancer treatment has become more attractive again because it can trigger immune cells to target cancer cells, prevent immune escape, and generate immunological memory (Gouttefangeas and Rammensee 2018; Zahavi and Weiner 2020).

The first cancer vaccine was used in 1980, which was based on tumor cells and tumor lysates to treat colorectal cancer (Hoover et al. 1985; J. Liu et al. 2022). In 1990, the first melanoma antigen was identified (J. Liu et al. 2022), and in 2010, a dendritic cell-based vaccine to treat

prostate cancer (Sipuleucel-T) made a further step in cancer vaccination. It's still challenging to develop applicable cancer vaccines, because the vaccine must target tumor-specific antigens, which in most cases are also difficult to select or to identify due to their similarities to healthy cells. Cancer vaccines should also induce cellular and humoral immune responses and have low side effects. There are two different types of tumor antigens that can be selected for cancer vaccines: tumor-associated antigens (**TAAs**) and tumor-specific antigens (**TSAs**) (Gouttefangeas and Rammensee 2018; J. Liu et al. 2022).

TAAs are differentiated and overexpressed "self-antigens" on tumor cells but are also expressed at some level on normal cells. They also include cancer-testicular antigens and "non-self-antigens" of viral origin (Gouttefangeas and Rammensee 2018; J. Liu et al. 2022). Overexpressed antigens include human epidermal growth factor receptor 2 (HER2) and human telomerase reverse transcriptase. Tissue differentiation antigens include prostate-specific antigen (PSA), expressed by the prostate gland and prostate cancer, and melanoma antigen tyrosinase, expressed by normal melanocytes and melanoma cells (J. Liu et al. 2022). However, TAAs have had limited success as vaccines. This is due to the low affinity of T cells for these antigens due to their expression on normal tissue cells, resulting in a weak T cell response and poor anti-tumor activity. Furthermore, the expression level is not validated in each individual patient, but the expression levels reported for the tumor entity were used instead (Gouttefangeas and Rammensee 2018). In addition, TAAs can be considered as autoantigens by the central immune tolerance of the thymus, and T cells recognizing these TAAs can be eliminated. The fact that TAAs are expressed on normal cells also increases the risk of "vaccine-induced autoimmune toxicity" (J. Liu et al. 2022). Therefore, tumor antigens that "break the tolerance" need to be identified (J. Liu et al. 2022).

Instead, **TSAs** are expressed only on tumor cells and arise through mutations such as point or frameshift mutations, fusion proteins, or spliced peptides. They are individual- and tumor-specific and are non-autogenous proteins, which is why they are called **"neoantigens"** (Gouttefangeas and Rammensee 2018; J. Liu et al. 2022). Therefore, TSAs or neoantigens are not affected by immune tolerance mechanisms and are more immunogenic, leading to a higher T cell response, resulting in an enhanced anti-tumor response and eradication (Gouttefangeas and Rammensee 2018; J. Liu et al. 2022). To identify neoantigen peptides, algorithms have been established to predict peptide epitopes that bind to MHC molecules. To do this, whole tumor genomes are sequenced by next-generation sequencing, followed by *in silico* MHC-binding prediction (Gouttefangeas and Rammensee 2018; J. Liu et al. 2022). As a result, the

first personalized cancer vaccine consisting of patient-specific, predicted neoantigens (as peptides or RNA) was administered to melanoma patients in 2008 (clinical trial NCT00683670, BB-IND 13590) (Carreno et al. 2015). Vaccine-induced T cell infiltration and neoantigen-specific killing of autologous tumor cells resulted in reduced metastatic event and prolonged progression-free survival. The combination with checkpoint blockade further enhanced the anti-tumor effects (Carreno et al. 2015; Ott et al. 2017; Gouttefangeas and Rammensee 2018; Sahin et al. 2020; J. Liu et al. 2022). Furthermore, neoantigens can be loaded onto DCs, which also leads to promising T cell response and antigenic spreading in melanoma patients (Carreno et al. 2015; J. Liu et al. 2022). Notably, neoantigen vaccine efficacy depends on the tumor entity and its mutational burden. For example, melanoma and lung cancer, carry nearly 200 mutations, whereas leukemia and childhood cancer carry less than 10 mutations (Gouttefangeas and Rammensee 2018). Nevertheless, HLA (human leukocyte antigen) ligandomes from certain tumors have already been analyzed in order to use this information, together with their genomic expression, to identify HLA ligands for vaccines (Gouttefangeas and Rammensee 2018).

Cancer vaccines can be further divided into different categories based on their composition: cell-based, virus- and virus-like-particle (VLP)-based, peptide-based, and nucleic acid vaccines (J. Liu et al. 2022). **Cell-based vaccines** contain whole cells or cell fragments containing neoantigens that are loaded onto DCs. These vaccines generally elicit a broad immune response (J. Liu et al. 2022). **Virus- and VLP-based vaccines** are inherently immunogenic and contain genetic material modified to encode tumor antigen sequences. For example, adenoviruses are used as vectors (J. Liu et al. 2022). **Peptide-based vaccines** should activate $CD8^+$ and $CD4^+$ T cell (J. Liu et al. 2022). In addition, antigenicity can be enhanced by fusion to carrier proteins such as heat shock proteins (HSP) and keyhole limpet hemocyanin (KLH) to increase their size and immunogenicity, with enhanced antigen presentation. These peptide- and protein-based vaccines have to be combined with adjuvants to enhance and guide the immune response. However, the choice of the best adjuvant is still unclear. Besides this, peptide-based vaccines are combined with adjuvants to enhance their immunogenicity (J. Liu et al. 2022). **Nucleic acid-based vaccines** contain RNA or DNA sequences that encode for the target antigen. In addition, sequences encoding e.g. CpG motifs act via TLR9 to further enhance the immune response (J. Liu et al. 2022) or the nucleic acids are placed in LNPs, which also can have an adjuvant effect as the LNPs in the new mRNA-based COVID-19 vaccines inducing an T_H1 response.

1.3.3 Status in cancer vaccine therapies

Despite these findings, cancer therapies remain challenging. Chemotherapies weaken the immune system by destroying rapidly dividing cells, including cancer cells and healthy cells, which affects healthy immune cells and leaves the body vulnerable to infection (Marriott, Post, and Chablani 2023). In many cases, chemotherapy is combined with immune checkpoint inhibitors, which increases the effectiveness of the therapy (Marriott, Post, and Chablani 2023). However, alterations in the TME (tumor microenvironment) render tumors resistant to this therapy, necessitating alternative therapeutic options such as therapeutic vaccination. To date, prophylactic pathogen vaccination has been approved against cancers caused by HPV and HBV. These include adjuvants, that target PPRs by acting as DAMPs or PAMPs, such as MPLA (TLR4 agonist) and CpG (TLR9 agonist) in *Cervarix*^{TM} and *Heplisav*^{TM} (J. Liu et al. 2022; Marriott, Post, and Chablani 2023), respectively. However, it is not clear whether other adjuvants would further increase their effectivity.

Current therapeutic vaccines include *sipuleucel-T* (*Provenge*™), *BCG Theracys*™ (*TICE*), and *Talimogene Laherparepvec* (*T-vec*™), which are also combined with co-stimulatory molecules. *Sipuleucel-T* is a vaccine for prostate cancer, currently in Phase III clinical trials, consisting of PBMCs previously isolated from the patient and activated *ex vivo* with an antigen and GM-CSF, which stimulates the patient's APCs and stimulates the anti-tumor immune response after vaccination. *T-vec*™ is a melanoma vaccine consisting of a modified oncolytic herpes virus encoding GM-CSF, which enhances the recruitment of APCs (Marriott, Post, and Chablani 2023). In addition, the vaccines are combined with adjuvants or adjuvant combinations, such as GM-CSF, Poly(I:C), imiquimod, CpG ODNs, and saponins (e.g., Montanide ISA51+Poly(I:C), which increase $CD8^+$ T cell activity (Marriott, Post, and Chablani 2023).

In addition, neoantigen vaccinations are under development to induce an antigen-specific immune response (Löffler et al. 2016; Gouttefangeas and Rammensee 2018; Rammensee et al. 2019; Peng et al. 2019; Nelde, Rammensee, and Walz 2021). Adjuvants are added to the neoantigens to improve the immune reaction.

Newer mRNA vaccine trials for melanoma are being considered by BioNTech and Moderna. BioNTech has generated the BNT111 vaccine, which encodes for four known conserved melanoma antigens that are considered as tumor-associated antigens: NY-ESO-1, MAGE-A3, tyrosinase, and TPTE. The vaccine is combined with immune checkpoint inhibitors (NCT04526899). Another clinical trial (NCT03289962), now in Phase II, involves BioNTech's

mRNA vaccine BNT122, which encodes up to 20 patient-specific neoantigens. The Phase IA/IB trial of the BNT122 vaccine evaluated efficacy as monotherapy or in combination with immune checkpoint inhibitors (anti-PD-L1 antibody Atezolizumab) (NCT03289962) and demonstrated neoantigen-specific T cell and clinical responses (J. Liu et al. 2022). Moderna generated the mRNA-4157 vaccine, which encodes up to 34 personalized neoantigens encapsulated in LNPs. They also evaluated the efficacy of the vaccine as a monotherapy or in combination with immune checkpoint inhibitors (anti-PD-L1, pembrolizumab), which showed good results in Phase I and is now in Phase II (J. Liu et al. 2022).

However, currently, it is unclear which adjuvant would best improve the potential of neoantigen and mRNA vaccines.

1.4 Aim of the thesis

Immunotherapies with checkpoint inhibitors such as anti-PD-1 and anti-CTLA-4 for the treatment of cancer have received a lot of attention in recent years. In addition to standard chemotherapy, radiation, or surgery, immunotherapy stimulates the immune system more strongly to kill tumor cells itself. Immune checkpoint inhibitor therapies are already considered standard of care for certain solid tumors, including melanoma, but also have a low long-term response rate in patients and strong inflammatory side effects.

Recent approaches target cancer and patient-specific tumor neoantigens by vaccination, which are identified by immunopeptidome and sequencing techniques. In parallel, several new kinds of adjuvants have been developed or are under development. An open question is, which would be the best possible adjuvant for specific vaccination to induce quantitatively and qualitatively very effective tumor neoantigen-specific T and B cell immune responses. $CD4^+$ helper T cells support important $CD8^+$ cytotoxic T cells as well as B cells that generate antibodies, which are not only suitable biomarker for proper immune responses but also can attack tumor cells by inducing for instance antibody-dependent cellular cytotoxicity (ADCC) like in passive tumor vaccination.

Therefore, the first aim of this work was to identify suitable adjuvants or adjuvant types for tumor antigen vaccination to reduce tumor growth of a murine melanoma cell line expressing an extracellular “tumor antigen” in mice. This should be done in prophylactic and therapeutic settings.

Secondly, the characteristic immune responses of the different adjuvant groups should be characterized, thereby I should in particular focus on the “quantity” and “quality” of the IgG antibody response including the IgG subclass composition and IgG Fc-N glycosylation patterns, which may be used as biomarkers as well as may have tumor fighting potential.

The third aim was to determine the effects of checkpoint inhibitor therapy on antigen-specific immune responses and tumor eradication to identify characteristic IgG subclasses and glycosylation patterns that can be used as biomarkers.

Overall, the work aims to predict the efficacy of vaccination or checkpoint inhibitor therapy by identifying specific IgG subclass compositions or glycosylation patterns. Further use of these biomarkers could improve early cancer screening based on changes in bulk- or antigen-specific IgG subclasses and/or glycosylation patterns and help to improve tumor vaccination strategies.

2. Material and Methods

2.1 Material

2.1.1 Mice

C57BL/6 wildtype mice were originally purchased from the Jackson Laboratories, bred and maintained in the internal facility of the University to Lübeck, according to the institutional guidelines. In addition, mice were purchased from Janvier Labs (Le Genest-Saint-Isle, France) and maintained in the internal facility until they were used for experiments. Male and female mice between 8-12 weeks old (at the beginning of the experiment) were used. All experiments were approved by the Federal Ministry of Energy, Agriculture, the Environment and Rural Areas Schleswig-Holstein (License numbers: 34-4-20, 48-6-18).

2.1.1 Cell lines

For the tumor vaccination experiments, the C57BL/6 melanoma cell line B16-mOVA was used, provided by Mikael Karlsson, Professor of Immunology, Karolinska Institute, Stockholm, stably expressing membrane-bound Ova (Hiltbrunner et al. 2016). The B16-mOVA cells were previously produced elsewhere by stable transfection of B16-F10 cells with an expression plasmid (pIRES2-EGFP) containing cDNA encoding full-length OVA protein linked to the transmembrane region of H-2Db (DiLillo, Yanaba, and Tedder 2010; Ehst, Ingulli, and Jenkins 2003).

For the anti-PD-1 experiments the C57BL/6 melanoma cell line B16-F10 were used, purchased from the American Type Culture Collection (ATCC).

2.1.2 Media and Supplements

Table 1: List of media

Media	Supplements	Concentration
B16-F10 media	FCS Penicillin Streptomycin β-Mercaptoethanol L-Glutamine in DMEM	10% (v/v) 100 u/mL 50 µM 4 mM
B16-mOVA media	Geneticin in B16-F10 media	1.5 mg/mL
Cell freezing media	DMSO in FCS	5%
T cell culture media	FCS β-Mercaptoethanol HEPES Penicillin Streptomycin in RPMI1640 (L-Glutamine)	10% (v/v) 100 µM 1 mM 100 u/mL
T cell pre-stimulation media	Brefeldin A Monensin PMA Ionomycin in T cell media	1x 1x 0.5 µg/mL 1 µg/mL
Neutrophil chemiluminescence media (NCL)	HEPES Penicillin Streptomycin in RPMI (without phenol red)	10 mM 1%

2.1.3 Buffer

Table 2: List of buffers

Buffer	Components	Concentration
Coating buffer (ELISA)	Carbonate-Bicarbonate in pure H_2O	50 mM
Blocking buffer (ELISA)	Milk-powder in D-PBS	2.5% (w/v)
Red blood cell lysis buffer	EDTA Ammonium chloride (NH_4Cl) Sodium bicarbonate ($NaHCO_3$) in pure H_2O, adjusted to pH 7.2	100 µM 155 mM 10 mM
FACS buffer	BSA in D-PBS	0.5% (w/v)
PBS-T	Tween-20 in D-PBS	0.05% (v/v)
PermWash buffer	BSA Saponin Sodium azide (NaN_3) D-PBS in pure H_2O	0.1% (w/v) 0.05% (w/v) 0.01% (w/v) 0.05x
Fecete´s solution	95% ethanol H_2O 37% formaldehyde solution glacial acetic acid	For 1 liter 580 mL 200 mL 80 mL 40 mL
Murine neutrophil buffer (MNB)	BSA glucose in HBSS-/-	0.1% 0.02%

2.1.4 Kits

Table 3: List of kits

Kit	Manufacturer /Vendor
True-Nuclear™ Transcription Factor Buffer Set	Biolegend, (San Diego, CA, USA)
AlexaFluor 488 Abs labeling kit	Thermo Fisher (Waltham, MA, USA)

2.1.5 Antibodies

Table 4: List of antibodies

Specificity	Clone	Isotype	Conjugate	Manufacturer/ Vendor
mouse IgG Fc	polyclonal	goat IgG	HRP	Bethyl Laboratories (Montgomery, TX, USA)
mouse IgG1	polyclonal	goat IgG	HRP	Bethyl Laboratories
mouse IgG2b	polyclonal	goat IgG	HRP	Bethyl Laboratories
mouse IgG2c	polyclonal	goat IgG	HRP	Bethyl Laboratories
mouse IgG3	polyclonal	goat IgG	HRP	SouthernBiotech (Birmingham, USA)
mouse/human B220 (CD45R)	RA3-6B2	rat IgG2a	BV786, AF488	Biolegend (San Diego, CA, USA)
mouse CD4	RM4-5	rat IgG2a	BV785	
mouse CD8α	53-6.7	rat IgG2a	AF700	
mouse CD44	IM7	rat IgG2b	BV510	
mouse CXCR5 (CD185)	L138D7	rat IgG2b	Biotin	
mouse/human GL7	GL7	rat IgM	PerCP/ Cy5.5	
mouse IFNγ	XMG1.2	rat IgG1	AF647	
mouse IgG1	RMG1-1	rat IgG	BV421	
mouse IgG1	polyclonal	goat IgG	AF647	Thermo Fisher (Waltham, MA, USA)
mouse CD138	281-2	rat IgG2a	BV711	BD Bioscience (San Diego, CA, USA)
mouse Fas (CD95)	Jo2	hamster IgG2	BV510	
mouse Foxp3	MF-23	rat IgG2b	AF647	
human and mouse St6gal1	polyclonal	goat IgG	self-labeled with AF488	R&D Systems (Minneapolis, MN, USA)
Isotype control to human and mouse St6gal1	polyclonal	goat IgG	self-labeled with AF488	R&D Systems (Minneapolis, MN, USA)
mouse/rat IL-17A	eBio17B7	rat IgG2a	PE	Thermo Fisher (Waltham, MA, USA)
mouse Ly-6G/Ly-6C (Gr-1)	RB6-8C5	rat IgG2b	BV605	Biolegend (San Diego, CA, USA)
mouse/human CD11b	M1/70	rat IgG2b	BV421	Biolegend (San Diego, CA, USA)
mouse FcγRIII (CD16)	275003	rat IgG2a	PE	R&D Systems (Minneapolis, MN, USA)

mouse FcγRIV (CD16.2)	9R9	armenian hamster IgG	FITC	Biolegend (San Diego, CA, USA)
mouse TNP	H5	IgG1	unconjugated	InvivoGen (Toulouse, France)
mouse TNP	HA	IgG2a ,b (switch variants)	unconjugated	prepared in laboratory
mouse PD-1 (CD279, inVivoMab)	RMP1-14	rat IgG2a	unconjugated	BioXcell (Lebanon, NH, USA)
mouse CTLA-4 (CD152)	UC10-4F10-11	armenian hamster IgG	unconjugated	provided by M. Brunner,Universitätsklinikum Magdeburg
Streptavidin BV605 or BV421 conjugated				Biolegend (San Diego, CA, USA)

2.1.6 Used Adjuvants

Table 5: List of adjuvants

Adjuvant	**Manufacturer / Vendor**
Incomplete Freund's Adjuvant (IFA)	Sigma-Aldrich (St, Louis, MO, USA)
Complete Freund's Adjuvant (CFA, 1 mg/mL M. tb.)	Sigma-Aldrich (St, Louis, MO, USA)
M. Tuberculosis Des. H37 Ra (non-viable)	BD Bioscience (San Diego, CA, USA)
eCFA (enriched CFA; 5 mg/mL M. tb. in IFA)	self prepared/mixed
Montanide ISA 51 VG 10ST	AIR LIQUIDE Medical
AddaVax™	InvivoGen (Toulouse, France)
Adju-Phos adjuvant	
Alhydrogel adjuvant 2% (Alum)	
Monophosphoryl Lipid A (MPLA) –SM VacciGrade™	
Poly(I:C) HMW VacciGrade™	
R848 VacciGrade™	
TDB VacciGrade™	
TDB-HS15	
Alum – Poly(I:C) (Alum + Poly (I:C))	self prepared/mixed

2.1.7 Chemicals

Table 6: List of chemicals

Chemical compound	Manufacturer / Vendor
Ammonium chloride (NH_4Cl)	Merck KGaA (Darmstadt, Germany)
Atipamezol (Alzane, Atipamezol-hydrochlorid) (5 mg/mL)	Zoetis (New Jersey, USA)
BD OptEIA (TMB substrate)	BD Bioscience (San Diego, CA, USA)
Brefeldin A (1000x)	Biolegend (San Diego, CA, USA)
BSA (bovine serum albumin)	GE Healthcare (Little Chalfont, UK)
Carbonate-bicarbonate buffer	Sigma-Aldrich (St, Louis, MO, USA)
Cytofix/Cytoperm	BD Bioscience (San Diego, CA, USA)
DMEM	Thermo Fisher (Waltham, MA, USA)
DMSO	Roth (Karlsruhe, Germany)
Dulbecco´s Phosphate-buffered saline	Thermo Fisher (Waltham, MA, USA)
EDTA	Sigma-Aldrich (St, Louis, MO, USA)
Glacial acetic acid	Carl Roth (Karlsruhe, Germany)
Ethanol	Carl Roth (Karlsruhe, Germany)
FCS (Fetal calf serum)	Thermo Fisher (Waltham, MA, USA)
Fixable viability dye (eFluor780)	Thermo Fisher (Waltham, MA, USA)
Focusing Fluid	Thermo Fisher (Waltham, MA, USA)
Formaldehyde (37%)	Carl Roth (Karlsruhe, Germany)
Geneticin™ Selective Antibiotic (G418 Sulfate) (50 mg/mL)	Thermo Fisher (Waltham, MA, USA)
Glucose	Merck KGaA (Darmstadt, Germany)
HBSS-/-	Thermo Fisher (Waltham, MA, USA)
HEPES (N-(2-Hydroxyethyl) piperazin-N'-(2-ethansulfonacid))	Thermo Fisher (Waltham, MA, USA)
Histopaque 1119	Sigma-Aldrich (St, Louis, MO, USA)
Hydrochloric acid (HCl)	Merck KGaA (Darmstadt, Germany)
Ionomycin	Biolegend (San Diego, CA, USA)
Ketamin 10 mg/mL	WDT (Garbsen, Germany)
Luminol	Sigma-Aldrich (St, Louis, MO, USA)
Nonfat dried milk powder	AppliChem GmbH (Darmstadt, Germany)
Medetomodin (Medetomidinhydrochlorid) (1 mg/mL)	Zoetis (New Jersey, USA)
Monensin (1000x)	Biolegend (San Diego, CA, USA)
Ovalbumin AF647 conjugated	Thermo Fisher (Waltham, MA, USA)
Ovalbumin Grade VI	Sigma-Aldrich (St, Louis, MO, USA)
Penicillin (10,000 IU mL-1)/ Streptomycin (10 mg/mL)	Thermo Fisher (Waltham, MA, USA)
Percoll	Cytiva Life Science (Marlborough, MA, USA)
Permeabilization Buffer 10x	Thermo Fisher (Waltham, MA, USA)
PMA (Phorbol myristate acetate)	InvivoGen (Toulouse, France)
Xylazine (20 mg/mL)	WDT (Garbsen, Germany)
RPMI1640 (L-Glutamine)	Thermo Fisher (Waltham, MA, USA)
Saponin	Sigma-Aldrich (St, Louis, MO, USA)
Sodium azide (NaN_3)	AppliChem (Darmstadt, Germany)
Sodium bicarbonate ($NaHCO_3$)	Merck KGaA (Darmstadt, Germany)
Sodium chloride (NaCl)	Merck KGaA (Darmstadt, Germany)
Sodium hydroxide (NaOH)	Merck KGaA (Darmstadt, Germany)
Streptavidin BV605 conjugated	Biolegend (San Diego, CA, USA)

Streptavidin BV421 conjugated	Biolegend (San Diego, CA, USA)
Sulfuric acid (H_2SO_4)	Sigma-Aldrich (St, Louis, MO, USA)
Tris-HCl	Sigma-Aldrich (St, Louis, MO, USA)
Trizmabase (Tris)	Sigma-Aldrich (St, Louis, MO, USA)
Trypan blue solution	Sigma-Aldrich (St, Louis, MO, USA)
Trypsin 0.25 %/EDTA 0.53 mM in HBSS, w/o: Ca and Mg, w: Phenol red	PAN-Biotech (Aidenbach, Germany)
Tween 20	Sigma-Aldrich (St, Louis, MO, USA)
β-Mercaptoethanol	Sigma-Aldrich (St, Louis, MO, USA)

2.1.8 Consumables

Table 7: List of consumables

Material		**Manufacturer / Vendor**
3-way stopcock, Discofix C		Braun (Melsungen, Germany)
8-well tube strips		Kisker Biotech (Steinfurt, Germany)
96-well PP plate (conical, 450µl/well)		Thermo Fisher (Waltham, MA, USA)
Cell culture flask or adherent cells, PS (50 mL, 25 cm²), (250 mL, 75 cm²), (550 mL, 175 cm²)		Greiner Bio-one GmbH (Kremsmünster, Austria)
Cell strainer EASYstrainer™, 40 µm, green (50 Stück/Pack)		Greiner Bio-one GmbH (Kremsmünster, Austria)
Cell strainer 70 µm (Falcon)		Corning (Kennebunk, ME, USA)
Costar Assay plates (high binding), 96-well		Corning (Kennebunk, ME, USA)
Cryo tubes (CryoPure 1,6mL violet)		Sarstedt (Sarstedt, Germany)
ELISA reagent reservoir		Thermo Fisher (Waltham, MA, USA)
Falcon tubes (15, 50 mL)		Greiner Bio-one (Kremsmünster, Austria)
Filter Stericup 0,22 µm		Merck KGaA (Darmstadt, Germany)
Flow Cytometry tube 5 mL		Sarstedt (Sarstedt, Germany)
Greiner LUMITRAC™ 600 microplate		Greiner Bio-one (Kremsmünster, Austria)
MiniCollect® TUBE 0.5/0.8 mL CAT Serum Sep Clot Activator		Greiner Bio-one (Kremsmünster, Austria)
Needles 26G (0.45x13mm); 26G (0.45x25mm); 30G (0.3x13mm)		Braun (Melsungen, Germany)
Needle (Eclipse)		BD Bioscience (San Diego, CA, USA)
Neubauer chamber		Assistant (Sondheim vor der Rhön, Germany)
Pipette tips with and without filter (10, 100, 200, 1000 µL)		Sarstedt (Nümbrecht, Germany)
Reaction tubes (0.5, 1.5, 2.0 mL)		Sarstedt (Nümbrecht, Germany)
Serological pipettes (5, 10, 25, 50 mL)		Sarstedt (Nümbrecht, Germany)
Single-use syringes (1, 2, 5, 10 mL)		Braun (Melsungen, Germany)
Solofix blood lancets		Braun (Melsungen, Germany)
Tissue culture plates, 6-well and 12-well, suspension		Sarstedt (Nümbrecht, Germany)

2.1.9 Instruments/Equipment

Table 8: List of instruments/equipment

Instrument		Manufacturer / Vendor
Attune NxT Flow Cytometer		Thermo Fisher (Waltham, MA, USA)
Autoclave VX-75		Systec (Linden, Germany)
Barnstead GenePure Pro (Ultrapure water)		Thermo Fisher (Waltham, MA, USA)
BioGARD Hood		The Baker Company, Inc. (Sanford, ME, USA)
Calliper digital		Carl Roth
Centrifuge 5424R		Eppendorf (Hamburg, Germany)
Centrifuge 5810R		Eppendorf (Hamburg, Germany)
Centrifuge Mega Star 3.0R		VWR
Cryo container		Nalgene™/ Thermo Fisher (Waltham, MA, USA)
Electronic balance		Kern & Sohn (Balingen-Frommern, Germany)
ELISA-Reader Spectra Max iD3		Molecular Devices, LLC. (San Jose, CA, USA)
Incubator AutoFlow NU-5510		NuAire (Plymouth, MN, USA)
Microscope Primovert		Zeiss
NanoDropTM One		Thermo Scientific (Waltham, MA, USA)
Neubauer chamber		VWR
pH Meter FiveEasy F20		Mettler-Toledo (Columbus, OH, USA)
Pipetboy Accu 2		IntegraBioscience (Zizers, Switzerland)
Pipettes (multi-channel), (single-channel)		Eppendorf (Hamburg, Germany)
Pipette Multi-channel Eppendorf Xplorer® plus		Eppendorf (Hamburg, Germany)
Tailveine restrainer for mice		Braintree Scientific (Braintree, USA)
Vortex-Genie 2		Scientific Industries (Bohemia, NY, USA)
Vortex ZX3		VELP Scientifica (UsmateVelate, Italy)
Waterbath SW-20C		Julabo

2.1.10 Software

Software	Company
Microsoft Office	Microsoft (Redmond, WA, USA)
FlowJo	BD Bioscience (San Diego, CA, USA)
Prism v. 6.04 and v.10.1.	GraphPad Software (San Diego, CA, USA)
Biorender.com	

2.2 Methods

2.2.1 Cell culture

Culturing Melanoma cells

The C57BL/6 melanoma cell lines B16-F10 and B16-mOVA were cultured in DMEM medium (purchased from Life Technologies) supplemented with 10% fetal bovine serum, 1 % penicillin/ streptomycin, 4 mM L-Glutamine, 50 µM b-mercaptoethanol at 37°C and 5% CO_2. To maintain Ova expression 1.5 mg/ml geneticin was added to B16-mOVA cells as selection marker (DiLillo, Yanaba, and Tedder 2010). B16-mOVA cells were generated by another laboratory, by transfecting of B16-F10 cells with a plasmid, containing an ovalbumin cDNA (Ehst, Ingulli, and Jenkins 2003; DiLillo, Yanaba, and Tedder 2010). The expression vector used was pIRES-GFP, which also encodes for the selection marker neomycin (analog of geneticin). The Ovalbumin cDNA was fused next to the H-2Db (MHC-I) transmembrane coding gene region, resulting in cell surface expression of ovalbumin.

Cells were detached with trypsin/EDTA and split at a ratio of 1:10 to 1:30, depending on the experiment, twice a week. All work was performed under sterile conditions.

2.2.2 *In vitro* generation of IgG subclass glycosylation forms

Murine monoclonal anti-TNP antibodies (IgG1 (clone H5), IgG2a and IgG2b (clone HA, switch variants with identical V(D)J sequences (Strait et al. 2015; Epp et al. 2018)) were previously produced and glycoengineered in our laboratory (collaboration with Janina Petry, detailed procedure not described in this study, for more details see (Epp et al. 2018; Bartsch et al. 2020; Petry et al. 2021; Dühring et al. 2023). Briefly, anti-TNP IgG2a and IgG2b antibodies were produced by hybridoma cells and IgG1 was purchased from *InVivo* (Toulouse, France). The antibodies were modified with sialidase A (*Agilent, Santa Clara, CA, USA*) and b(1-4)-galactosidase (*ProZyme, Hayward, CA, USA*) to generate de-sialylated and de-galactosylated antibodies. In addition, galactosylated and sialylated glycosylation forms were generated, using β-1,4-galactosyltransferase (*Roche, Basel, Switzerland*) together with UDP-galactose (*Merck KGaA, Darmstadt, Germany*) and α-2,6-sialyltransferase (*Roche, Basel, Switzerland*) together with CMP-sialic acid. The different glycosylation forms were purified by size exclusion (100 kDa Amicon Ultra Centrifugal Filters, *Merck KGaA*) or affinity chromatography (Protein G Resin (*Concile GmbH, Freiburg, Germany*)).

2.2.3 Mouse handling

Melanoma mouse model

For each experiment, an aliquot of melanoma cells was freshly thawed, and cells were replicated in cell culture for approximately 10 days. Cells were sub-cultured to reach a confluence of approximately 50-80% for harvesting. Cells were detached with trypsin/EDTA and centrifuged at 200 x g for 5 min at 4°C. The supernatant was discarded, and the cells were washed with D-PBS (centrifugation 200 x g for 5 min at 4°C). To prevent clotting, cells were separated through a 40 µm filter.

For the **lung metastasis model**, the cells were diluted to 25 x 10^5/mL in PBS and divided into aliquots. For tumor cell injection, 200 µl of PBS containing 5 x 10^5 cells were injected into the tail vein (i.v.) of the mice. At the end of the experiment, the lungs of the mice were removed and fixed in Fecete´s solution for 24 hours. The number of visible surface lung metastasis in the whole lung was determined by counting.

For the **subcutaneous tumor model**, the cells were diluted to 10x10^5/mL in PBS and divided into aliquots. For tumor cell injection, 200 µl of PBS containing 2 x 10^5 cells was injected under the skin on the right flank of the mice. Therefore, mice were anesthetized by i.p. injection of 200 µl medetomidine/ketamine (75 mg/kg medetomidine + 1 mg/kg ketamine) and shaved on the right flank. Cells were injected subcutaneously into the flank. 30 min after anesthesia, the mice were injected with atipamezole (5 mg/kg) to counteract the anesthesia and accelerate the wake-up process. Mice were awakened by warming the cages under red light lamps. Subcutaneous tumor growth was monitored 2-3 times per week by measuring the diameter with an electronic caliper. The tumor volume was determined using the formula: TV (mm^3) = a (mm) x b^2 (mm^2) x 0.5 (where "a" is the largest diameter and "b" is the perpendicular diameter of the tumor representing an idealized ellipsoid).

Immunization

For immunization, 100 µg ovalbumin (Ova) dissolved in 100 µl of 1x PBS [1mg/mL] was mixed with 100 µl adjuvant for each mouse. 200 µl of Ova-adjuvant solution was i.p. injected into each mouse. Depending to the type of adjuvant, the preparation was different and performed according to the manufacturer's protocol.

Water based adjuvants

Aluminum-based adjuvant (Alum): Alum (Alhydrogel adjuvant 2%) (Invivogen) is a ready-to-use adjuvant. It was mixed 1:1 (v/v) with the Ova solution by adding Alum dropwise while vortexing and then pipetting the mixture up and down for 5 min to ensure complete absorption of the antigen to Alum.

Poly(I:C): Poly(I:C) HMW VacciGrade™ (Invivogen) was dissolved in endotoxin-free physiological water to obtain a concentration of 1 mg/mL concentration. The solution was heated at 65°C for 1 hour to allow the annealing of the RNA. To prepare an Ova adjuvant solution, 100 µl of 100 µg of Poly(I:C) was mixed 1:1 (w/v) with the Ova solution by pipetting up and down.

Alum-Poly(I:C): Ova-Alum was prepared as described above. Poly(I:C) was then added to the Ova-Alum solution 1:3 (v/v/v) and mixed by pipetting to achieve equal volume distributions.

MPLA: Monophosphoryl Lipid A (MPLA-SM*) VacciGradeTM (Invivogen) was dissolved in sterile DMSO to give a 1 mg/mL solution. For immunization, 10 µg MPLA was dissolved in 1x PBS to a final volume of 100 µl and mixed 1:1 with 100 µl of Ova solution by pipetting.

Water-in-oil adjuvants

Montanide ISA51, **IFA** and **CFA** are ready-to-use adjuvants and 100 µl of adjuvant were mixed 1:1 with 100 µl Ova solution as described below. **eCFA** was prepared by adding 100 mg Mtb.H37 RA to 20 mL IFA to reach a final concentration of 5 mg M.tb./mL (instead of 1 mg/mL in CFA).

Water-in-oil adjuvants were emulsified 1:1 (v:v) with Ova solution using 3-way stopcocks to achieve the required pressure. The adjuvant and Ova were then filled into appropriate syringes and the air bubbles were removed. An emulsion was prepared by transferring Ova through the 3-way stopcock into the adjuvant and then transferring from one syringe to the other for 5 min. After air bubbles were removed, the emulsion was filled into syringes using the 3-way stopcock for injection.

Serum transfer experiments

For the serum transfer experiments, sera from previously immunized mice (experiments from former students) were pooled and diluted 1:1 (v/v) with 1xPBS. 200 µl of the diluted serum was i.p. injected into each mouse, one day before tumor cell injection (i.v.) or one day before and one day after tumor cell injection.

Anti-PD-1 treatment of mouse melanoma model (s.c.)

For checkpoint inhibitor treatments, mice were treated with anti-mouse PD-1 (CD279) (clone RMP1-14) on day 7, 9, 11, 13 ,15 and 17 after s.c. tumor cell injection. Mice were injected i.p. with 200 µg anti-PD-1 in PBS (in 200 µl).

Anti-PD-1 and anti-CTLA-4 treatment during immunization experiments

The effect of checkpoint inhibitors on Ova+adjuvant immunization was investigated by treating mice with anti-PD-1 or anti-CTLA-4 during the immunization experiments. Therefore, mice were i.p. immunized with Ova-Alum on day 0 and injected with anti-PD-1 or anti-CTLA-4 on day -1 and day 1, 3, 5, 7, 9 before/after immunization. As a control, mice were immunized with Ova-eCFA without checkpoint inhibitor treatment. 12 days after immunization, spleens and blood were collected for further analysis.

Blood collection

To analyze IgG titers during the experimental period, blood (2 drops) was collected from the *vena facialis* of the mice and collected in mini collection tubes. For serum collection, the blood was centrifuged at 4000 x g for 5 min at 4°C. Serum was stored at -20°C for further analysis.

Organ sampling

Mice were anesthetized with 200 µl ketamine (80 mg/kg)/xylazine (10 mg/kg) in PBS (i.p.) 21 days after tumor cell injection or 12 days after immunization in the case of immunization trials without tumor cell application. Final bleeding was performed by heart puncture and mice were killed directly by cervical dislocation. Lungs and spleens were then taken for further analysis. Serum was collected from the blood as described previously. Lungs were fixed in Fekete´s solution (Overwijk and Restifo 2000) for 20-24 hours and the number of lung metastasis were determined. Spleens were prepared for flow cytometry analysis (Immune cell analysis by flow cytometry).

2.2.4 Antibody analysis

Anti-Ova IgG ELISA

For the detection of antigen-specific serum IgG, anti-Ova ELISA was performed. For this purpose, 10 µg/mL Ova, diluted in coating buffer (0.05 M Bicarbonate/Carbonate buffer) was coated onto polystyrene 96-well assay plates by adding 50 µl of the Ova-solution to each well. Only coating buffer was used to discriminate non-specific signals. The plate was incubated overnight at 4°C. The next day, the coating solution was removed, and each well was washed three times with 150 µl PBST (0.05% Tween) followed by blocking with 150 µl of 2.5% milk powder in PBS for 1 h at RT on a shaker. Afterward, serum samples were diluted in serial dilutions (1:100, 1:1000, 1:10 000) in ELISA buffer (2.5% milk powder in PBS). 50 µl of the diluted samples were added to the appropriate well and the plate was incubated for 1 h at RT on a shaker. The serum dilutions were removed, and the wells were washed three times with 150 µl PBST (0.05%). For the detection of different IgG subclasses, anti-IgG-HRP (1:10 000), anti-IgG1-HRP (1:10 000), anti-IgG2c-HRP (1:1000), anti-IgG2b-HRP (1:5000) or anti-IgG3-HRP (1:5000) were diluted in ELISA buffer as indicated. 50 µl of the diluted detection antibodies were added to each well. The plate was incubated for 1 hour at RT with shaking. After removal of the detection antibody solution, the wells were washed 3 times with 150 µl PBST (0.05%). To detect bound antibodies, TMB substrates A and B were mixed 1:1 (v/v) and 50 µl were added to each well. The reaction was stopped with 50 µl of sulfuric acid (4.2% H_2SO_4) per well and absorbance was measured at 450 nm using a microplate reader.

Analysis of Fc-N glycosylation by LC-MS

The analysis of the IgG Fc-N glycosylation was performed by a collaborator (Manfred Wuhrer, Leiden University Medical Center, Leiden in the Netherlands) as described elsewhere (de Haan et al. 2017).

Briefly, the analysis of IgG subclass Fc glycopeptides was performed by Liquid Chromatography-Mass Spectrometry (LC-MS). For this purpose, bulk or anti-Ova antibodies were isolated from the serum using protein G sepharose columns or Ova-coupled protein sepharose columns (made in the laboratory) or alternatively Ova-coated wells, respectively, and digested with trypsin, resulting in different glycopeptides, containing different amino acid sequences of the CH2 domain, thus determining the different IgG subclasses (IgG1, IgG2 (b+c), IgG3). The subclasses IgG2c and IgG2b could not be distinguished by the used method because of identical glycopeptide amino acid sequence. The peptides contain the Fc glycopeptides with the different glycans on asparagin-297

were separated by size-dependent elution and m/z. The AUC values of the IgG subclass peaks were summed and the relative fractions of galactosylated, sialylated, bisecting, and fucosylated IgG subclass glycan peaks were calculated for the different IgG subclasses. The following peaks were identified: G0F1, G1F1, G2F1, G3F1, G4F1, G1S1F1, G1S2F1, G2S1F1, G3S1F1, G2S2F1, G0F0, F1F0, G2, F0

2.2.5 Immune cell analysis by flow cytometry

For the analysis of the immune cell response, splenocytes were prepared for subsequent staining of splenic T and B cells. For this purpose, spleens were meshed through 70 µm filters with ice-cold PBS to separate the splenocytes and filled up to 20 mL. The cell suspension was centrifuged at 300 x g for 5 min at 4°C and the supernatant was discarded. The cell pellet was resuspended in 5 mL red blood cell lysis buffer to remove red blood cells and incubated for 5 min at RT. The reaction was stopped by the addition of 20 mL ice-cold PBS. The suspension was centrifuged again at 300 x g for 5 min at 4°C, the supernatant was removed, and the pellet resuspended in 1 mL ice-cold FACS buffer.

Analyzation of splenic T cells

To analyze different T cell subsets, 2.5 x 10^6 prepared spleen cells were used for each flow cytometric staining. Cells were transferred to a conical 96-well plate and the supernatant was removed after centrifugation at 300 x g for 5 min at 4°C. Cell pellets were resuspended in FACS buffer, containing the appropriate antibodies and reagents. For defined antibodies (anti-ICOS, anti-CXCR5, anti-FoxP3), appropriate controls were included that did not contain the respective antibody (FMO = fluorescence minus one) required for correct gating of the cell populations in the analysis procedure. For the staining of cell surface markers, the following antibodies were diluted in FACS buffer as indicated (Table 9).

Table 9: Flow cytometry staining panel for cell surface markers for splenic T cells

cell marker/antibody	cell type/structure	fluorescence dye	dilution	final concentration
Life dead	dead cells	APC-Cy7	1:10 000	
αmouse B220	B cells	AF488	1:200	2.5 µg/mL
αmouse CD4	$CD4^+$ T cells	BV786	1:200	1 µg/mL
αmouse CD8α	$CD8^+$ T cells	AF700	1:200	2.5 µg/mL
αmouse CD44	effector/memory T cells	BV510	1:200	1 µg/mL

αmouse ICOS	follicular T cells	PE-Cy7	1:100	2 µg/mL
αmouse CXCR5	follicular T cells	Biotin	1:100	2 µg/mL

Cells were resuspended in 100 µl of the antibody mixture and incubated for 45 min on ice in the dark. Then, 150 µl FACS buffer was added to the cells and centrifuged. The supernatant was discarded. For CXCR5 detection, cells were subsequently resuspended in 100 µl of 1 µg/mL streptavidin-BV605 (stock [0.1 mg/mL] diluted 1:100) in FACS buffer. After 20 min incubation on ice in the dark, the cells were centrifuged at 300 x g for 5 min at 4°C and the supernatant was discarded. To detect regulatory T cells, intranuclear staining for FoxP3 was additionally performed. Cells and nuclei were permeabilized and fixed with True Nuclear™, diluted 1:4 in the appropriate diluent (eBioscience). Cells were resuspended in 200 µl of the fixative dilution and incubated for 1 hour at RT in the dark. Afterwards, 150 µl of 1x eBioscience™ Foxp3 Perm Buffer was added to the cells and centrifuged at 300 x g for 5 min at 4°C. The supernatant was discarded, and the cells were washed twice with 200 µl of 1x Foxp3 Perm buffer. For the intra-nuclear staining, anti-mouse FoxP3 AF647 was diluted 1:200 in 1x Foxp3 Perm buffer and the cells were resuspended in 100 µl of the antibody dilution. Staining was performed for 45 min on ice in the dark. Finally, the cells were centrifuged at 300 x g for 5 min at 4°C, the supernatant was discarded, and the cells were resuspended in 200 µl of FACS buffer. For flow cytometry measurement, the cells were mixed with 200 µl of focusing fluid and the detection was performed at a flow rate of 200 µl/min. The measurement was performed using the Attune NxT flow cytometer. Analysis was then performed using FlowJo software.

Analyzation of T cell cytokine expression

To measure cytokine expression in T cells, the cells were restimulated with ionomycin, phorbol myristate acetate (PMA), brefeldin A and monensin. PMA and ionomycin stimulate intracellular signaling cascades leading to T cell activation pushing the original cytokine production (Ai et al. 2013). Brefeldin A and monensin inhibit the intracellular cytokine trafficking between Golgi and ER, resulting in cytokine accumulation (O'Neil-Andersen and Lawrence 2002).

For pre-stimulation $1x10^7$ splenocytes were transferred into 3.5 mL pre-warmed pre-stimulation media, containing brefeldin A, monensin, ionomycin, and PMA (Table 1) in a 6-well culture plate. Cells were incubated for 4-5 hours at 37°C and 5% CO_2. After the incubation period, the cells were transferred to 15 mL tubes and centrifuged at 300 x g for 5 min at 4°C. The

supernatant was discarded, and the cells were resuspended in the remaining medium and transferred to a conical 96-well plate for antibody staining. To remove the remaining medium, the cells were centrifuged at 300 x g for 5 min at 4°C and the supernatants were discarded. For staining of cell surface markers, the same protocol as for extracellular T cell staining (described above, Table 9) was used. In this case, the cells were resuspended afterwards in 100 µl of 5 µg/mL streptavidin-BV421(stock [0.5 mg/mL] diluted 1:100) in FACS buffer. After 20 min incubation on ice in the dark, the cells were centrifuged at 300 x g for 5 min at 4°C and the supernatant was removed. For intracellular cytokine staining, the cells were resuspended in 200 µl Cytofix/Cytoperm and incubated for 30 min at RT in the dark. The cells were then resuspended in 150 µl of 1xPermeabilization/Wash buffer and centrifuged at 300 x g for 5 min at 4°C. The supernatant was discarded, and the cells were washed twice with 200 µl Permeabilization/Wash buffer. For cytokine staining, the appropriate antibodies (Table 10) were diluted in 1xPermeabilization/Wash buffer and the cells were resuspended in 100 µl of the antibody mixture. FMOs were prepared for anti-IFNγ and anti-IL17A.

Table 10: Flow cytometry staining panel for intracellular cytokine detection

cell marker/antibody	cell type/structure	fluorescence dye	dilution	final concentration
αmouse IFNγ	T_H1 cells, cytotoxic T cells	AF647	1:200	2.5 µg/mL
αmouse IL-17A	T_H17, Tc17	PE	1:200	2.5 µg/mL

Cells were incubated for 30 min on ice in the dark. Afterwards, 150 µl of Permeabilization/Wash buffer was added and the cells were centrifuged at 300x g for 5 min at 4°C. For flow cytometry measurement, the cells were resuspended in 200 µl FACS buffer and mixed with 200 µl of focusing fluid and the detection was performed at a flow rate of 200 µl/min. The measurement was performed using the Attune NxT flow cytometer. Analysis was then performed using FlowJo software.

Analyzation of splenic B cells

To analyze splenic B cell responses induced by tumor cells or therapy, $5x10^6$ splenocytes were used for flow cytometry staining. CD138 and B220 were used as surface markers to distinguish B cells and plasma cells (PCs) (Table 11). GL7 and Fas (CD95 ligand) were used to characterize germinal center (GC) B cells. Furthermore, antibody production in these cells was determined using anti-IgG1 and anti-IgG2(c,b) antibodies. In addition, the expression of the glycosylation enzyme sialyltransferase (St6gal1) was measured by staining with anti-St6gal1 antibody

(labeled in our laboratory) and analyzation of the mean fluorescence intensity (MFI). An isotype control for this anti-enzyme antibody was included.

The **anti-St6gal1** antibody was labeled using the AlexaFluor 488 labeling kit. A 1 mg/mL antibody solution was prepared, by dissolving 100 µg of lyophilized antibody in 0.1 M ammonium bicarbonate and transferring it to the supplied AF488 fluorescent dye. The mixture was inverted and incubated at RT for 1 h in the dark. To quench the reaction, 50 µl of 1 M Tris (pH8) was added to the mixture, inverted, and incubated for 30 min at RT in the dark. Afterwards, a working solution of 0.2 mg/mL anti-St6gal1 was prepared by adding 350 µl of FACS buffer to get a final volume of 500 µl (containing 100 µg anti-St6gal1 antibody).

Cell surface staining of splenic B cells was performed by transferring $5x10^6$ splenocytes into a conical 96-well plate, centrifuging at 300 x g for 5 min at 4°C, and discarding the supernatant. Cell pellets were resuspended in FACS buffer, containing the appropriate antibodies and reagents. For Ova-AF647, a FMO was included. For cell surface marker staining, following antibodies were diluted as indicated in FACS buffer (Table 11).

Table 11: Flow cytometry staining panel for cell surface markers of splenic B cells

cell marker/antibody	cell type/structure	fluorescence dye	dilution	final concentration
Life dead	dead cells	APC-Cy7	1:10 000	
αmouse B220	B cells	BV786	1:200	1 µg/mL
αmouse CD138	Plasma cells	BV711	1:200	1 µg/mL
αmouse FAS/CD95lig	Germinal center B cells	BV510	1:200	1 µg/mL
αmouse GL7	Germinal center B cells	PerCpCy5.5	1:200	1 µg/mL
αmouse IgG2a	IgG2a/BCR production	PE	1:200	1 µg/mL
αmouse IgG2b	IgG2b/BCR production	PE	1:200	5 µg/mL
αmouse IgG1	IgG1/BCR production	BV421	1:200	0.25 µg/mL
OVA	Ova specific IgG/BCRs	AF647	1:500	4 µg/mL

Cells were resuspended in 100 µl of the antibody mixture and incubated for 45 min on ice in the dark. Afterwards, 150 µl of FACS buffer was added to the cells and centrifuged. The supernatant was discarded, and the cell pellet was resuspended in 200 µl Cytofix/Cytoperm for intracellular staining. After incubation for 30 min at RT in the dark, 150 µl of 1xPermeabilization/Wash buffer was added to the cells and centrifuged at 300 x g for 5 min at 4°C. The supernatant was discarded, and the cells were washed twice with 200 µl of 1xPermeabilization/Wash buffer. Cell pellets were then resuspended in 1xPermeabilization/Wash buffer, containing antibodies as indicated in Table 12.

Table 12: Flow cytometry staining panel for intracellular staining of splenic B cells

cell marker/antibody	cell type/structure	fluorescence dye	dilution	final concentration
αIgG2a	IgG2a production	PE	1:200	1 µg/mL
αIgG2b	IgG2b production	PE	1:200	5 µg/mL
αIgG1	IgG1 production	BV421	1:200	0.25 µg/mL
OVA	Ova specific antibodies	AF647	1:500	4 µg/mL
αSt6gal1	St6gal1 production	AF488	1:50	4 µg/mL
Isotype control αSt6gal1		AF488	1:50	4 µg/mL

Cells were incubated for 30 min on ice in the dark. Afterwards, 150 µl of Permeabilization/Wash buffer was added and the cells were centrifuged at 300 x g for 5 min at 4°C.

For flow cytometry measurement, the cells were resuspended in 200 µl FACS buffer and mixed with 400 µl of focusing fluid and the detection was performed at a flow rate of 200 µl/min. The measurement was performed using the Attune NxT flow cytometer. Analysis was then performed using FlowJo software.

Analyzation of murine bone marrow neutrophils

To analyze FcγR expression by murine neutrophils, 2 x 10^5 isolated neutrophil (isolation described in 2.2.6) were prepared for flow cytometric staining. Remaining neutrophil buffer were removed by centrifugation at 300 x g for 5 min at 4°C. For the staining of cell surface markers, the following antibodies were diluted in FACS buffer as indicated (Table 13).

Table 13: Flow cytometry staining panel for cell surface markers for bone marrow neutrophils

cell marker/antibody	cell type/structure	fluorescence dye	dilution	final concentration
Life dead	dead cells	APC-Cy7	1:10 000	
αmouse Gr-1	myeloid differentiation (Ly-6G/ Ly-6C)	BV605	1:200	1 µg/mL
αmouse CD11b	neutrophils/activation marker	BV421	1:200	1 µg/mL
αmouse FcγRIV		FITC	1:100	5 µg/mL
αmouse FcγRIII		PE	1:50	-

Cells were resuspended in 100 µl of the antibody mixture and incubated for 30 min on ice in the dark. The intracellular staining of the FcγRs was performed as described for B cells using Cytofix/Cytoperm for cell permeabilization and 1xPermeabilization/Wash buffer to dilute the antibodies. Dilutions were prepared as for the extracellular staining.

For flow cytometry measurement, the cells were resuspended in 200 µl FACS buffer and the detection was performed at a flow rate of 200 µl/min. The measurement was performed using the Attune NxT flow cytometer. Analysis was then performed using FlowJo software.

2.2.6 *In vitro* neutrophil ROS release assay

For *in vitro* neutrophil activation, a murine ROS (Reactive Oxygen Species) assay was performed. Neutrophils were isolated from the bone marrow of naïve C57BL/6J mice. Femurs and tibias were harvested, and bone marrow was rinsed with sterile murine neutrophil buffer (MNB) containing 0.1% BSA and 1% glucose and filtered through a 70 µm cell strainer. For density gradient centrifugation, Percoll with five different densities (81%, 62%, 55%, 50%) were stacked to obtain a gradient. Isolated bone marrow cells were washed with MNB, resuspended in Percoll (p = 45%) and layered on top of the prepared Percoll gradient. After centrifugation (1600 x g, 10°C, 30 min, brake off), the cells between the two lower Percoll layers (between 81% and 62%) were collected, washed twice with MNB and centrifuged at 600 x g for 10 min at 10°C. The cells were then resuspended in MNB, loaded onto Histopaque 1119, and centrifuged again (1600 x g, 10°C, 30 min, brake off). Neutrophils accumulated above the Histopaque 1119 and were harvested and washed in MNB. For the ROS release assay, a 96-well plate (Lumitrac) was coated with 10 µg/mL Ova or 10 µg/mL of monoclonal anti-

TNP IgG antibodies (IgG1 (clone H5), IgG2a (clone HA), IgG2b (clone HA)) for 1 h at RT and washed three times with PBST (0.05% Tween). Blocking was performed with 2.5% milk in PBS for 1 hour at RT, followed by three washes. Serum (undiluted) was added to the plate for 1 hour at RT, followed by three washes. 200,000 (for serum) or 300,000 (for monoclonal antibodies) isolated neutrophils in neutrophil chemiluminescence (NCL) media containing 0.2 mg/mL luminol were added to each well and luminescence was measured immediately for 1.5 h at 37°C using a microplate reader. The ROS assay was performed in collaboration with Janina Petry, a former postdoc in our laboratory.

2.2.7 Statistical analysis

Statistical analysis was performed using Graph Pad Prism v.6.02. and v.10.01. Experiments were considered as Gaussian' normal distributions and analyzed by one-way ANOVA (analysis of variance) and Tukey's multiple comparisons among all groups. Where indicated, comparisons between two groups were analyzed by unpaired Students' t-test. Data are presented as means and the standard errors of the mean (SEM). Pearson's correlation and linear regressions were used for correlation analysis. P-values were considered significant as follows: *$p < 0.05$, **$p < 0.01$, ***$p < 0.001$, ****$p < 0.0001$. Otherwise indicated in the graphs. For expression levels, measured by flow cytometry, the mean fluorescence intensity (MFI) was calculated using FlowJo software.

3. Results

3.1 Effect of different adjuvants on vaccine efficiency

Tumor antigen- and neoantigen (mutated antigen)-specific vaccination are promising approaches to target cancer cells (Löffler et al. 2016; Gouttefangeas and Rammensee 2018; Rammensee et al. 2019; Nelde, Rammensee, and Walz 2021; J. Liu et al. 2022; Marriott, Post, and Chablani 2023). To sufficiently activate the immune system, adjuvants must be included in the vaccines (Oefner et al. 2012; Baxter 2014; Gouttefangeas and Rammensee 2018; Bartsch et al. 2020; Facciolà et al. 2022; Marriott, Post, and Chablani 2023). To date, only a few adjuvants are in clinical trials targeting tumor cells or tumor antigens (e.g. Montanide ISA51, Imiquimod (R837), Resiquimod (R848), Poly(I:C), Poly(ICLC)) (Coffman, Sher, and Seder 2010; Zhao et al. 2023). Besides $CD8^+$ and $CD4^+$ T cell responses, antibody titers have generally been used to measure immune system activation and thus vaccine or adjuvant efficacy (Taranger et al. 2000; Coudeville et al. 2010). However, not only the "quantity" (number of antibodies) but also the "quality" of the induced antibodies (isotype and subclass composition and kind of antibody glycosylation) may play a role in the vaccination efficacy, which may also reflect as biomarker the quality of the T cell response. So here it was investigated whether the use of different adjuvants in vaccines leads to different tumor control capacities. And whether this correlates with different antibody or immune cell responses.

To investigate this, the mouse B16 melanoma cell line that expresses the recombinant foreign model protein antigen ovalbumin on its cell membrane (mOva) was used. The B16 melanoma, which is spontaneously derived from C57BL/6 mice, is poorly immunogenic and shares many characteristics with human melanoma (DiLillo, Yanaba, and Tedder 2010; Aranda et al. 2011). In addition, the cells used are highly metastatic and generate lung metastasis upon intravenous injection (DiLillo, Yanaba, and Tedder 2010; Aranda et al. 2011; Seliger et al. 2001). Therefore, in this work, the cells were injected intravenously into C57BL/6 mice, which developed lung metastasis over 21 days. Furthermore, the mice were either prophylactically or therapeutically vaccinated with the "tumor antigen" Ova in combination with different adjuvants, and the immune cell response was analyzed.

3.1.1 Adjuvants and their immunologic function

Different adjuvants are used in the following vaccination experiments, including licensed adjuvants (Alum, MPLA), adjuvants used in clinical research (Montanide ISA51, Poly(I:C)) and adjuvants that are used in animal studies (IFA, CFA, eCFA). Therefore, adjuvants belonging to different groups (aluminum-based, water-in oil, TLR-agonists) were tested (Table 14).

Table 14: Adjuvants and their characteristics used in experiments.

adjuvant	type	Expected immune response; see introduction	clinical stage
Alum	Aluminum-based	T_H2, (in humans also T_H1), antibodies	licensed
Poly(I:C)	TLR3 agonist	T_H1, antibodies	pre-clinical
Alum-Poly(I:C)	Aluminum-based + TLR3 agonist	T_H2, T_H1, antibodies	animal testing
MPLA	TLR4 agonist; MPLA (TLR-4 agonist, detoxified form of LPS	T_H1, antibodies	licensed
Montanide ISA51	water-in-oil	T_H1, T_H2, antibodies	licensed
IFA	water-in-oil	T_H1, T_H2, antibodies	pre-clinical, animal testing
CFA	water-in-oil	T_H1, T_H2, T_H17, antibodies	animal testing
eCFA	water-in-oil	T_H1, T_H2, T_H17, antibodies	animal testing

3.1.2 Prophylactic vaccination with a “tumor antigen” in combination with different adjuvants leads to differences in tumor growth

Most cancer treatments today are therapeutic in nature. However, in order to prevent the development of cancer by vaccination, for example against common tumor antigens or neoantigens, it would be useful to also vaccinate prophylactically.

Therefore, we tested the efficiency of vaccination with different adjuvants prophylactically and therapeutically, also to compare their efficiency.

Accordingly, C57BL/6 wild-type (WT) mice were prophylactically vaccinated with Ova in combination with the different adjuvants. After 12 days, the B16-mOVA cells were injected intravenously (i.v.) into the tail vein of the mice. 21 days after tumor cell injection, the mice were sacrificed, and the lungs were examined for lung metastasis (Figure 3.1).

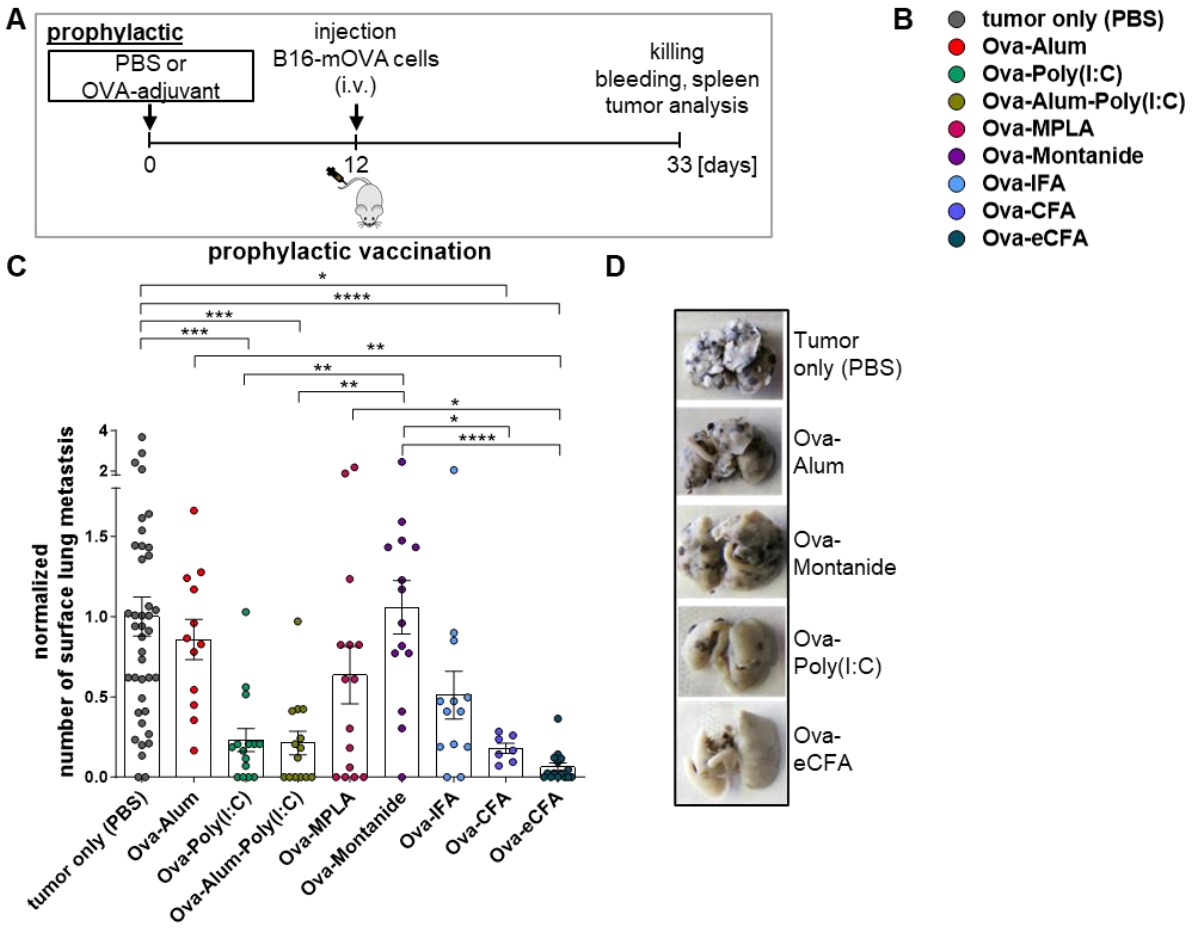

Figure 3.1: Growth of surface lung metastasis in mice after prophylactic vaccination with Ova in different adjuvants.
(A) Experimental design: C57BL/6 WT mice were prophylactically immunized i.p. with Ova in different adjuvants. 12 days later, B16-mOVA cells were injected i.v. 21 days after tumor cell injection, blood and spleens were collected and the number of surface lung metastasis were determined. **(B)** Color code of the adjuvants investigated. **(C)** Normalized number of surface lung metastasis on day 21 after tumor cell injection from different experiments. The number of surface lung metastasis of all immunized mice was normalized to the mean of the number of lung metastasis of the tumor only mice (grey dots) in each individual experiment. The graphs show normalized data from different experiments. Statistics: One-way ANOVA (**** P<0.0001), Tukey's multiple comparison, *p < 0.05, **p < 0.01, ***p < 0.001, ****p < 0.0001. **(D)** Representative images of fixed lungs with metastasis on day 33 after Ova immunization.

The unvaccinated mice (tumor only) and the group vaccinated with Ova-Montanide showed the highest number of metastasis, followed by the group vaccinated with Ova-Alum. Instead, the use of Poly(I:C), Alum-Poly(I:C), CFA and eCFA led to a significant reduction in lung metastasis compared to the unvaccinated group. MPLA and IFA resulted in a moderate reduction of the metastasis. This shows that different adjuvants have different capacities in the tumor control after prophylactic vaccination.

3.1.2.1 Impact of different adjuvants on the IgG subclass induction

As already described, different $CD4^+$ T cell signals lead to different IgG subclasses and the distinct IgG subclasses have different functions by different specificities and affinities to Fcγ receptors (Bruhns 2012). IgG2a/c and IgG2b show strong interactions with activating FcγR and C1q, whereas IgG1 and IgG3 show less interaction with activating FcγR and IgG1 does not bind to C1q (Nimmerjahn and Ravetch 2005; Bruhns 2012).

To investigate the anti-Ova IgG subclass vaccine response after i.p. injection of Ova plus the different adjuvants, blood was collected on day 14 (without tumor cell injection) (Figure 3.2). This experiment was performed before the start of this work and has been already published in Bartsch et al. 2020.

In my work, these IgG subclass titers were processed (Figure 3.2) and subsequently used to compare them with the tumor growth in Figure 3.1. The aim was to analyze which IgG subclass titers/compositions develop after vaccination and occur on the day of tumor challenge (day 12 or in this case day 14 after vaccination). To compare the IgG subclass titers among each other and between the different adjuvant groups, dilution series curves were used to calculate relative IgG subclass titers for each mouse (Figure S 1). For this purpose, a vertex straight line was laid through the dilution curves of the individual mice, intersecting as many curves as possible. If there were no curve intersections, a second straight line was used, and the values were calculated accordingly. The x-axis intersections of the vertex lines were then determined, and the y-axis values or relative OD values of the individual dilution curves were determined using the curve formula. A relative OD value was then assigned to each mouse. The mean of the relative OD values of each adjuvant group was normalized to the mean of the relative OD values of a reference group (anti-Ova IgG1 of the Ova-IFA group). This led to an approximate value for the comparison of the OD values between the different groups and IgG subclasses. In addition, the values for CFA-immunized mice, originate from another experiment, were used and related to eCFA in that other experiment in order to subsequently compare the relative OD values with the other adjuvants from the first mentioned experiment. The relative titers of IgG2c and IgG2b were summed in order to get relative IgG2 titers.

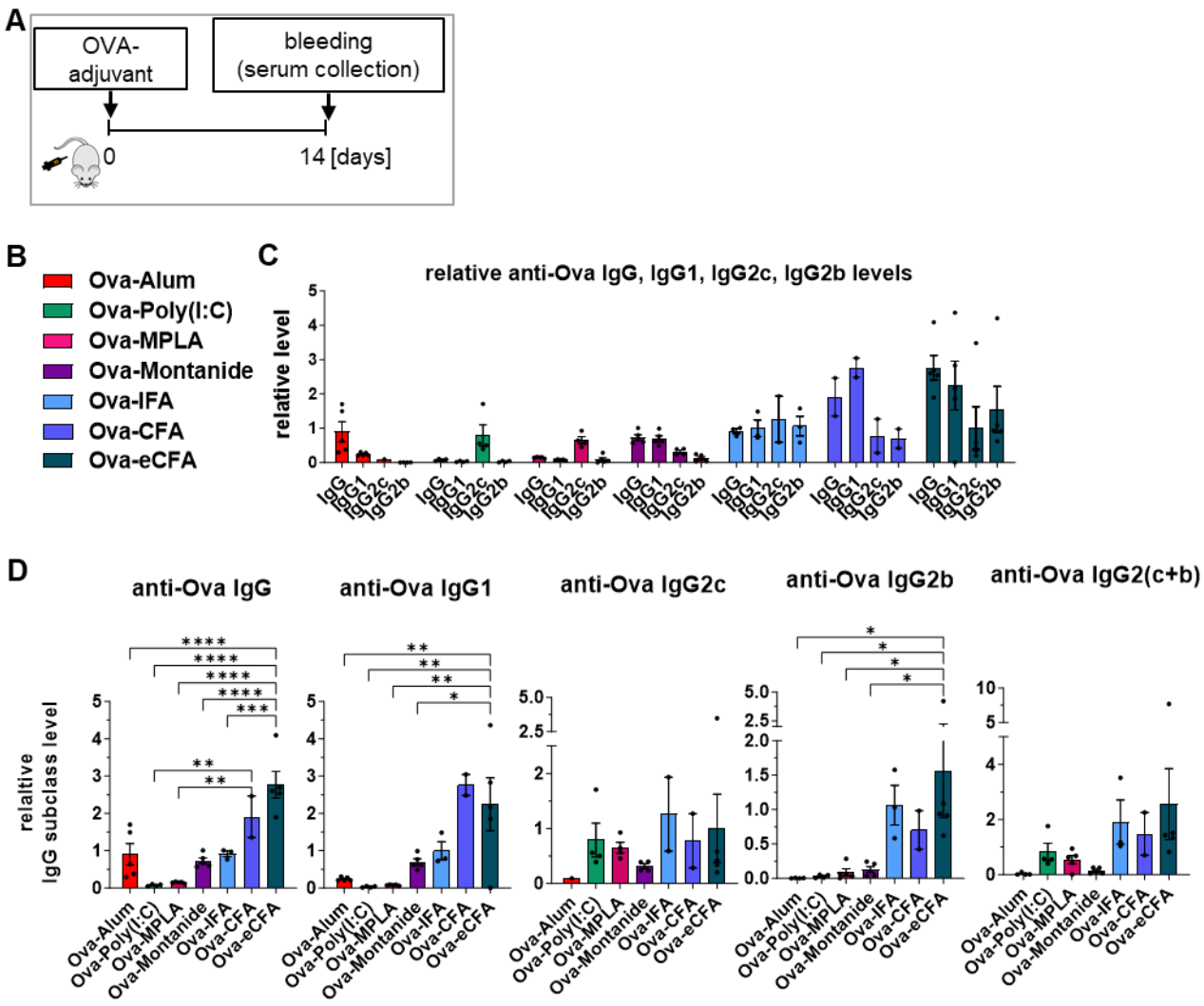

Figure 3.2: IgG subclass titers on day 14 after vaccination with Ova in different adjuvants
(A) Experimental design: C57BL/6 WT mice were immunized with Ova in different adjuvants **(Bartsch et al. 2020)**. On day 14 after immunization, blood was collected, and serum was analyzed for IgG subclass titers. **(B)** Color code of the investigated adjuvants. **(C+D)** Relative serum anti-Ova IgG and IgG subclass levels on day 14 after immunization. All Absorbance values (OD450nm) were normalized to the mean of the absorbance values of anti-Ova IgG1 in the Ova-IFA group using dilution series curves (**Figure S 1**) Statistics: One-way ANOVA, Tukey's multiple comparison, *p < 0.05, **p < 0.01, ***p < 0.001, ****p < 0.0001.

Comparison of serum anti-Ova IgG (total) showed a higher titer induced by the water-in-oil adjuvants compared to Alum and the TLR agonists Poly(I:C) (TLR-3) and MPLA (TLR-4) and can be ordered as follows: eCFA>CFA>IFA>Alum>Montanide>Poly(I:C)>MPLA. Anti-Ova IgG1 titers followed the same trend as shown for total anti-Ova IgG. Anti-Ova IgG2c and 2b titers were lower than the anti-Ova IgG1 levels (equal for Ova-IFA), but abundant for the water-in-oil adjuvants IFA, CFA and eCFA. Anti-Ova IgG2c levels were also higher with Poly(I:C) and MPLA that were comparable to IFA, CFA and eCFA. Anti-Ova IgG3 levels were too low for data processing.

Taken together, IFA, CFA, eCFA, and Montanide induced all IgG subclasses, whereas Alum mainly induced IgG1, and Poly(I:C) and MPLA mainly induced IgG2c.

Notably, the anti-Ova antibody levels of IFA and CFA were only based on two samples that are far apart (Figure 3.2D).

Since IgG2a/c and IgG2b are the more activating subclasses and important for tumor control mechanisms (Nimmerjahn and Ravetch 2005) while IgG1 has less activation function and may even inhibit IgG2 functions (Lilienthal et al. 2018) the IgG2c/IgG1, IgG2b/IgG1 and IgG2 (IgG2c+IgG2b)/IgG1 ratios were determined (Figure 3.3).

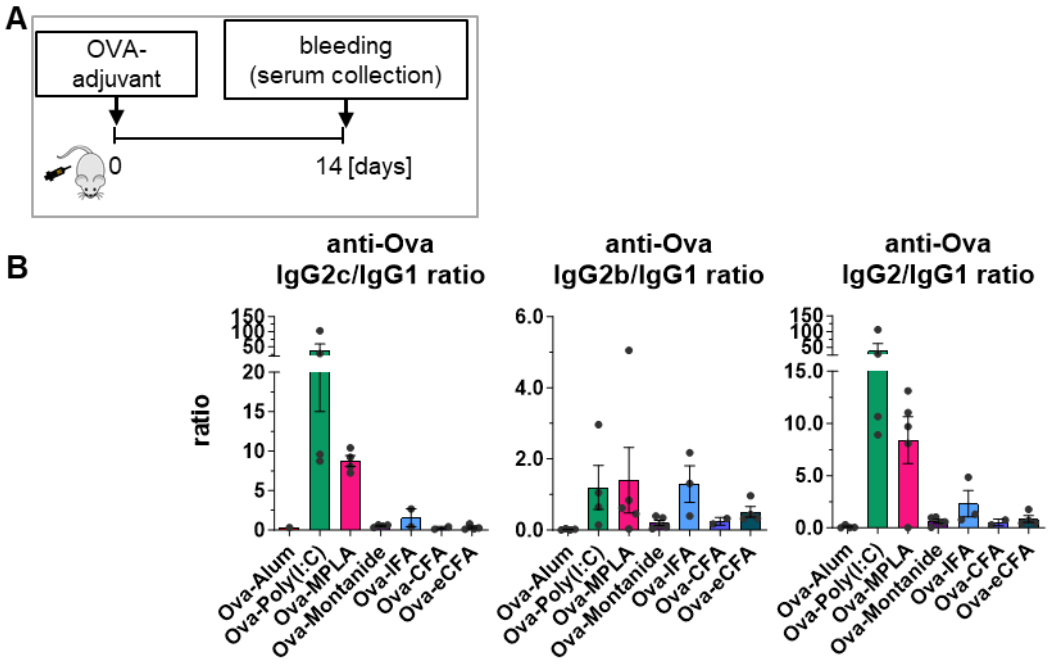

Figure 3.3: Ratios between IgG subclass titers on day 14 after vaccination with Ova in different adjuvants
(A) Experimental design as described in **Figure 3.2**. **(B)** Ratios of relative serum anti-Ova IgG subclass levels on day 14 after immunization as shown in **Figure 3.2**. Relative OD values (**Figure 3.2**) were divided by each other.

The ratio of IgG2c/IgG1 was highest after vaccination with Ova-Poly(I:C), followed by Ova-MPLA, whereas this was not the case with the water-in-oil adjuvants. The IgG2b/IgG1 and IgG2/IgG1 ratio was also >1 for Ova-IFA, as well as for Ova-Poly(I:C) and Ova-MPLA vaccinations.

The data raise the question of whether the relatively high anti-Ova IgG1 levels in the IFA, CFA, eCFA, and Montanide as well as Alum groups may reduce IgG2 functions.

3.1.2.2 Impact of different adjuvants on the IgG subclass glycosylation

Recent murine and human studies have shown that short-term IgG subclass responses after vaccination and booster vaccination are highly galactosylated and sialylated and in human low bisected across all IgG subclasses, whereas long-term IgG responses most likely generated by GC-derived long-live PCs are less galactosylated and sialylated and in human higher bisected across all IgG subclasses (Bartsch et al. 2020; Buhre et al. 2023). It may be possible that differently glycosylated short-term and long-term IgG subclass antibodies have different roles.

In addition, the kind of adjuvant used during vaccination seems to influence the long-term GC-derived long-lived PC response generating IgG antibodies with low galactosylation and sialylation levels. More inflammatory adjuvants seem to more reduce long-term IgG galactosylation and sialylation than less inflammatory adjuvants (Bartsch et al. 2018). The functional consequences are still unclear.

The anti-Ova IgG subclass Fc glycosylation patterns of day 14 serum from mice immunized with Ova and various adjuvants as described above (Figure 1.9, Bartsch et al. 2020) were further re-processed for subsequent correlation with tumor growth.

Anti-Ova IgG subclass levels/summed intensities at day 14 were calculated by summing the areas under the curve of each anti-Ova IgG subclass glycopeptide peak (Figure 3.4C).

The sum intensities of anti-Ova IgG1 and IgG2 (Figure 3.4C) showed comparable levels to the levels analyzed by ELISA.

Anti-Ova IgG subclass glycosylation patterns from day 14 are shown in Figure 3.4D).

No bisected anti-Ova IgG subclass peaks were identified, as mouse IgG generally shows little IgG bisection. In average more than 99% of the anti-Ova IgG1 was fucosylated on day 14 (not described in (Bartsch et al. 2020)). De-fucosylated anti-Ova IgG2 was not detected.

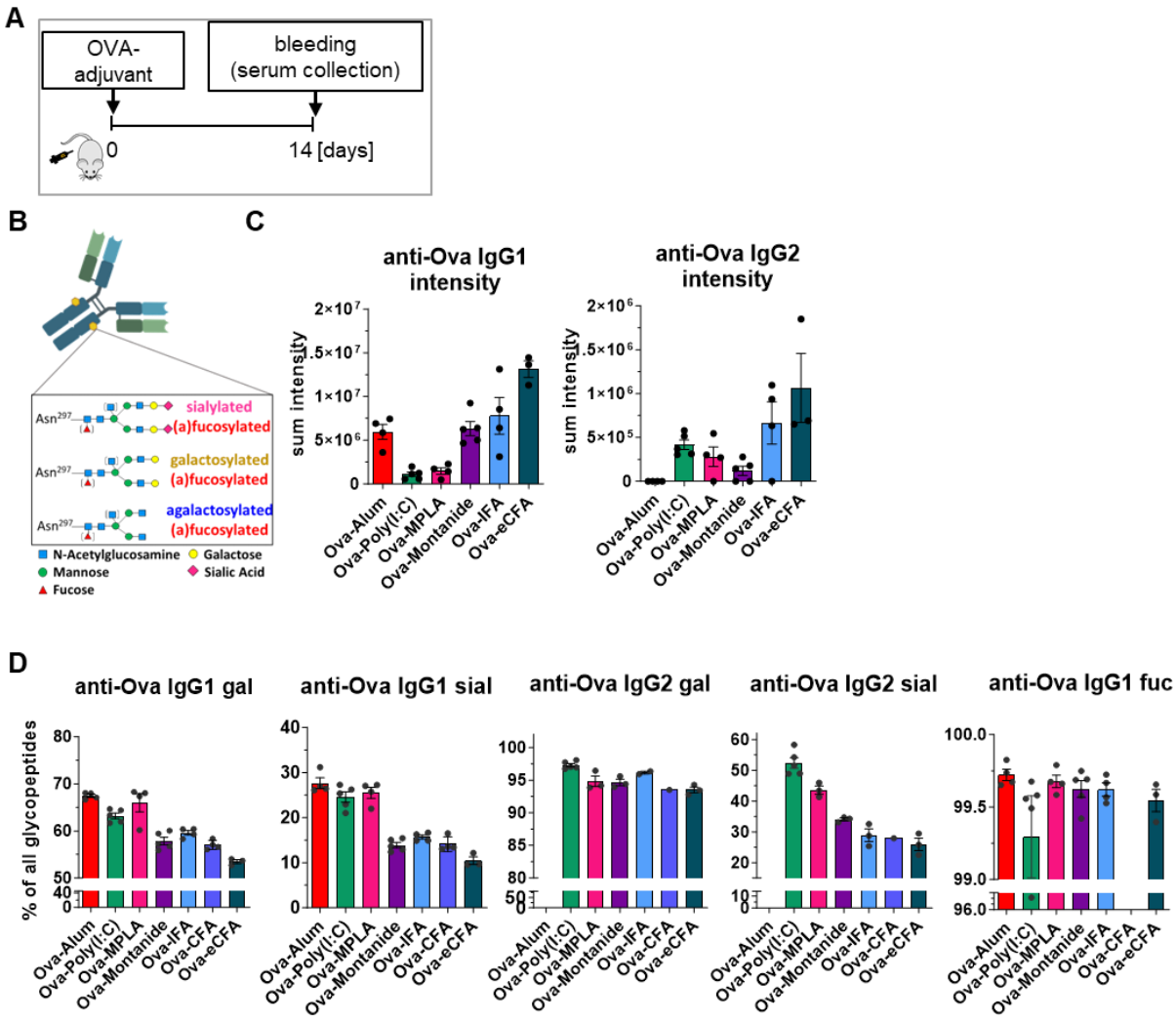

Figure 3.4: IgG Subclass glycosylation patterns on day 14 after vaccination with Ova in different adjuvants.
(A) Experimental design as described in **Figure 3.2**. On day 14 after immunization, blood was collected, and serum was analyzed for IgG subclass patterns **(Bartsch et al. 2020)**. **(B)** Schematic structure of IgG Fc-N glycosylation pattern at Asn-297. **(C)** Sum intensities of anti-Ova IgG1 and IgG2 (IgG2c plus IgG2b; these two subclasses were not distinguished by the analysis) measured by LC-MS. **(D)** Serum anti-Ova IgG1 and IgG2 subclass glycosylation patterns on day 14 after immunization.

Terminal galactosylation (gal) and sialylation (sial) of IgG1 was lower after immunization with the water-in-oil adjuvants IFA, CFA and eCFA as well as Montanide compared to mice immunized with Alum, Poly(I:C) or MPLA. Due to low IgG2 levels after Ova-Alum immunization, no IgG2 glycosylation could be detected in this group. In the other groups the IgG2 galactosylation was quite high with the highest levels after Poly(I:C) and the lowest with CFA and eCFA. However, IgG2 sialylation showed comparable trends as for anti-Ova IgG1.

Beside this, IgG2 galactosylation and sialylation were higher in Ova-Poly(I:C) immunized mice compared to MPLA, Montanide and eCFA. In general, the water-in-oil adjuvants resulted in lower galactosylation and sialylation patterns.

Taken together, the water-in-oil adjuvants induced lower anti-Ova IgG1 galactosylation and sialylation levels compared to the other adjuvants on day 14. Furthermore, on day 14 less than 1% of afucosylated and no bisected anti-Ova IgG subclass antibodies were detected.

3.1.2.3 Relationship between IgG subclass titers and glycosylation patterns and the development of lung metastasis after prophylactic vaccination

It was further investigated whether different anti-Ova IgG subclass levels, ratios and Fc glycosylation patterns correlated with tumor clarence. Therefore, Pearson's correlations were performed between all IgG subclass titers, ratios or glycosylation patterns shown in Figure 3.2, Figure 3.3 and Figure 3.4. and the number of surface lung metastasis shown in Figure 3.1. The mean of each feature of each adjuvant group was used for analysis.

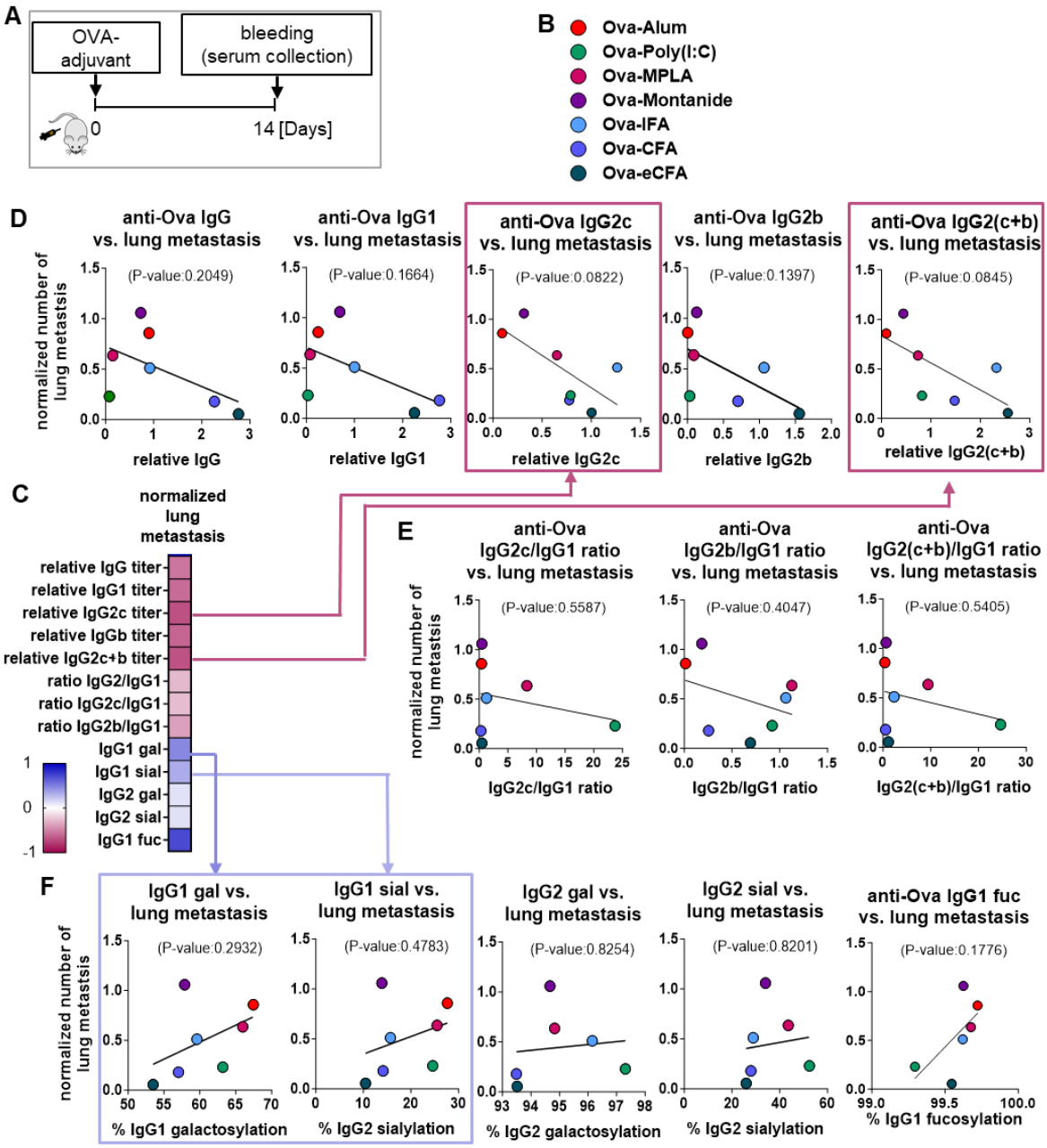

Figure 3.5: Correlation of IgG Subclass titers, ratios and glycosylation pattern on day 14 after vaccination with Ova and different adjuvants and the number of metastasis on day 21 after tumor cell injection (prophylactic vaccination)

(A) Experimental design as described in Figure 3.2. On day 14 after immunization, blood was collected, and serum was analyzed for IgG subclass patterns (Bartsch et al. 2020). **(B)** Color code of the investigated adjuvants. **(C)** Heat map of correlations between normalized number of lung metastasis and IgG subclass titer, ratios and glycosylation patterns. Pearsons's correlation coefficient "R" is shown. **(D-F)** Correlation of serum anti-Ova IgG, IgG1, IgG2c IgG2b, and IgG2(c+b) titers, IgG2c/IgG1, IgG2b/IgG1, IgG2/IgG1 ratios and IgG1 and IgG2 galactosylation and sialylation and IgG1 fucosylation on day 14 after immunization and normalized number of metastasis on day 21 after tumor cell injection (Figure 3.1), representing the prophylactic vaccination. Statistics: Pearsons's correlation *p < 0.05, **p < 0.01, ***p < 0.001, ****p < 0.0001.

The heat map in Figure 3.5C gives an overview about the R values of the Pearsons's correlation between all groups. Reddish boxes indicate negative correlations whereas bluish boxes indicate positive correlations between the number of lung metastasis and the Ova-specific IgG subclass titer, ratios or glycosylation. The strongest trends for correlations are shown for IgG2c and IgG2(c+b) that show a trend towards a negative correlation between metastasis and antibody titer, i.e. the more IgG2c or IgG2(c+b), the fewer lung metastasis developed. Furthermore, IgG, IgG1 and IgG2b also show a trend towards a negative correlation, but not as strong as for IgG2c (Figure 3.5D). Additionally, the IgG2c/IgG1, IgG2b/IgG1, and IgG2/IgG1 ratios (Figure 3.5E) show no significant correlation, but still a trend toward negative associations. The values of the CFA and eCFA groups counteract such a trend.

In addition, the galactosylation and sialylation levels of in particular IgG1 trended to correlate positively, although not significantly, with the number of metastasis (Figure 3.5F). IgG1 fucosylation on day 14 also tended to correlate positively with tumor growth, however, the percentages of IgG1 afucosylation were less than 1%.

Overall, there were tendencies for IgG2c and IgG2c/IgG1 to correlate negatively and IgG1 galactosylation and sialylation to correlate positively with the number of lung metastasis, suggesting that they may play a role in tumor control mechanisms.

To further analyze the correlation between the antibody response of different adjuvants and the tumor growth, Principal component analysis (PCA) was performed (Figure 3.6).

The analysis also showed that the tumor growth tended to negatively correlate with the IgG2c titer, and positively with IgG1 galactosylation and sialylation. Further the effect of Poly(I:C) correlated with the IgG2c/IgG1 ratio, and the effect of CFA correlated with the IgG (subclass) titer and the IgG subclass de-galactosylation and de-sialylation.

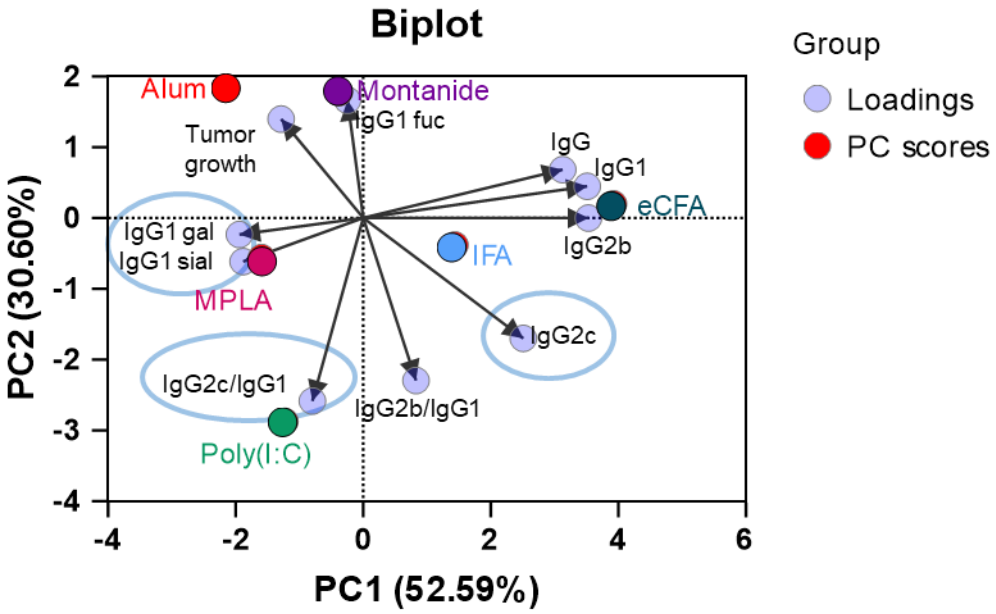

Figure 3.6: Principal component analysis (PCA) of the prophylactic tumor vaccination.
PCA of the data sets from Figure 3.1 - Figure 3.4 containing normalized number of lung metastasis (Figure 3.1), relative anti-Ova IgG titers (Figure 3.2), ratios between anti-Ova IgG subclass titers (Figure 3.3) and anti-Ova IgG subclass glycosylation (Figure 3.4). Loadings and scores of the PCA are shown. (CFA is not shown, due to missing glycosylation values.)

Perhaps different adjuvants induce different effector mechanisms. Poly(I:C) may act via a high IgG2c/IgG1 ratio whereas IFA and eCFA may act via high IgG2c titers and/or low IgG subclass galactosylation and sialylation on injected tumor cells.

3.1.2.4 Development of afucosylated IgG antibodies over time following vaccination

As mentioned above, afucosylated IgG antibodies have a positive effect on tumor control due to increased induction of ADCC in humans probably via human FcγRIIIA or in mice via murine FcγRIV, respectively. It was expected that IgG2 F0 glycosylation forms would correlate with tumor control but no anti-Ova IgG2 F0 could be detected on day 14 after vaccination. So far, the percentage of anti-Ova IgG1 F0 has been analyzed above on day 14 after vaccination showing, however, in average less than 1% anti-Ova IgG1 F0 forms (Figure 3.4).

Next, the appearance of afucosylated anti-Ova IgG subclass antibodies over time was analyzed to gain a better insight into IgG F0 responses after vaccination. To perform this analysis, the previously performed vaccination experiment (Bartsch et al. 2020) also described in the

introduction, was re-analyzed for anti-Ova IgG subclass fucosylation over time (in addition to day 14), which has not been described/published before. As a reminder, WT mice were vaccinated with Ova in different adjuvants (Figure 3.7A) on day 0 and boosted with Ova in PBS without adjuvant on day 28. Blood was collected on day 7, 14, 21, 28, 33 and 42.

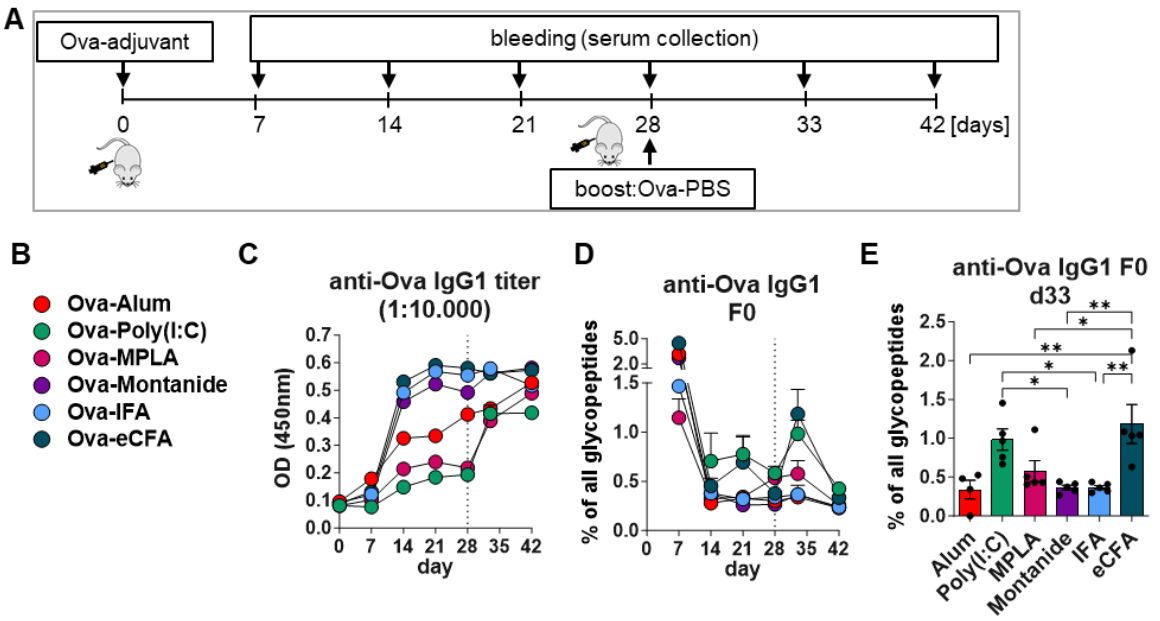

Figure 3.7: Anti-Ova IgG1 levels and non-fucosylation (F0) patterns after vaccination with Ova plus different adjuvants and boosting with Ova.
(A) Experimental design: C57BL/6 WT mice had been immunized with Ova plus different adjuvants on day 0 and boosted with Ova without adjuvant on day 28. On day 7, 14, 28, 33 and 42 after immunization, blood was collected, and serum was analyzed for anti-Ova IgG subclass levels and non-fucosylation (F0) patterns. **(B)** Color code of the investigated adjuvants. **(C)** Serum anti-Ova IgG1 titers on the indicated days after immunization (serum dilution: 1:10,000). **(D)** Serum anti-Ova IgG1 non-fucosylation (F0) after immunization over time. **(E)** Serum anti-Ova IgG1 non-fucosylation (F0) after immunization on day 33. Percentages of anti-Ova IgG1 afucosylated glycopeptides were measured by LC-MS. Statistics: One-way ANOVA (*** P=0.0001), Tukey's multiple comparison, *p < 0.05, **p < 0.01, ***p < 0.001, ****p < 0.0001.

Again, no anti-Ova IgG2 F0 peaks could be detected at any time point. However, as shown in Figure 3.7D, there was a peak of afucosylated anti-Ova IgG1 in all adjuvant groups on day 7 after vaccination, which reached up to 5% in average. At day 14, the percentage of afucosylated anti-Ova IgG1 were decreased to less than 1% and remained approximately at the same level until day 28. The boost on day 28 again resulted in an increase in anti-Ova IgG1 afucosylation levels, but only in the Ova-eCFA and Ova-Poly(I:C) mice, averaging between 1-2%, and moderately in the Ova-MPLA immunized mice on day 33 (Figure 3.7D, E).

Taken together, the time course showed that anti-Ova IgG1 F0 were increased for all adjuvants on day 7, were minimally enhanced for Poly(I:C) and eCFA immunizations on day 14 and 21,

and further increased again after boosting with eCFA and Poly(I:C) and less with MPLA, which may contribute to tumor killing.

3.1.2.5 Effect of different adjuvants used in prophylactic tumor antigen vaccination on T cell responses

T cells play an essential role in the activation of the immune system and in fighting and/or killing of tumorigenic cells (M. S. Paul et al. 2020). $CD4^+$ T helper cells, including T_H1 and T_H17 cells, are responsible for the activation and function of the immune system and the help for $CD8^+$ T cells and B cells. (Schumann et al. 2015). On the other hand, $CD8^+$ cytotoxic T cells, including Tc1 and Tc17 subsets, are more responsible for killing of cancerous cells (Paul 2020). Furthermore, to detect memory and effector T cells, CD44 is the most widely used marker to distinguish memory and effector T cells from their naïve counterparts (Schumann et al. 2015). CD44 is a type 1 transmembrane protein that is expressed on many cell types and is activated upon antigen binding, inducing multiple effector or memory functions in the cell (Schumann et al. 2015; Sckisel et al. 2017). Another cell type that is used as a marker of therapy efficacy or cancer progression/rejection are regulatory T cells (T_{regs}) (Sckisel et al. 2017). T_{regs} downregulate activating and inflammatory immune cell responses to prevent immune tolerance (Seidel, Otsuka, and Kabashima 2018; Zahavi and Weiner 2020). In order to predict the immune status of the prophylactically immunized mice and to find associations between the antibody response and the T cell response, which may be useful to identify processes in the immune system, different T cell subsets were analyzed by flow cytometry. Therefore, the spleens of mice were harvested on day 33 and prepared for flow cytometry staining.

The different cell populations were gated as shown in Figure 3.8.

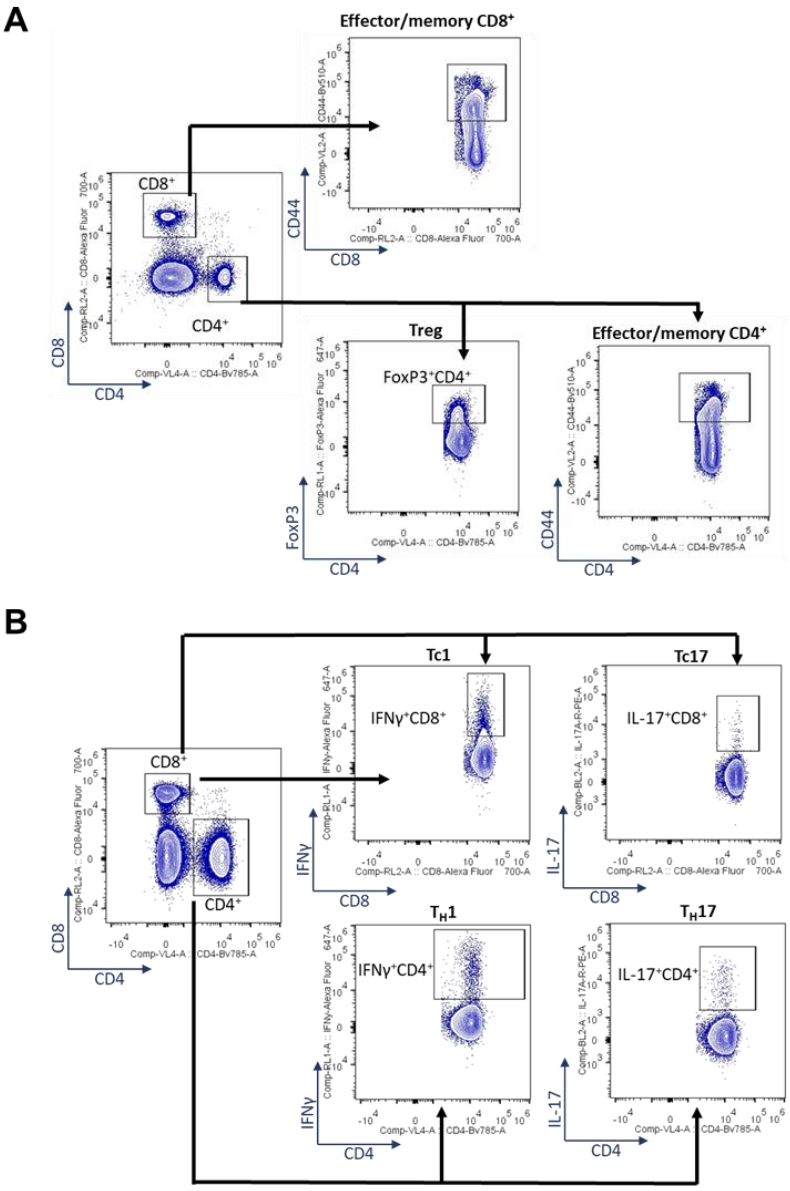

Figure 3.8: Flow cytometry gating strategy for identification of splenic T cells and T cell cytokines
Splenic **(A)** T cells and **(B)** T cell cytokines were stained in separate approaches. T cells were pre-gated on lymphocytes, live cells and B220 negative cells. **(A)** Effector/memory T cells were identified as $CD44^+$ $CD4^+$ and $CD44^+CD8^+$ cells and regulatory T cells (Tregs) as $FoxP3^+CD4^+$ cells. **(B)** For the identification of cytokine expression, $CD4^+$ and $CD8^+$ cells were gated for $IFN\gamma^+$ (T_H1 and Tc1) and $IL\text{-}17^+$ (T_H17 and Tc17) populations.

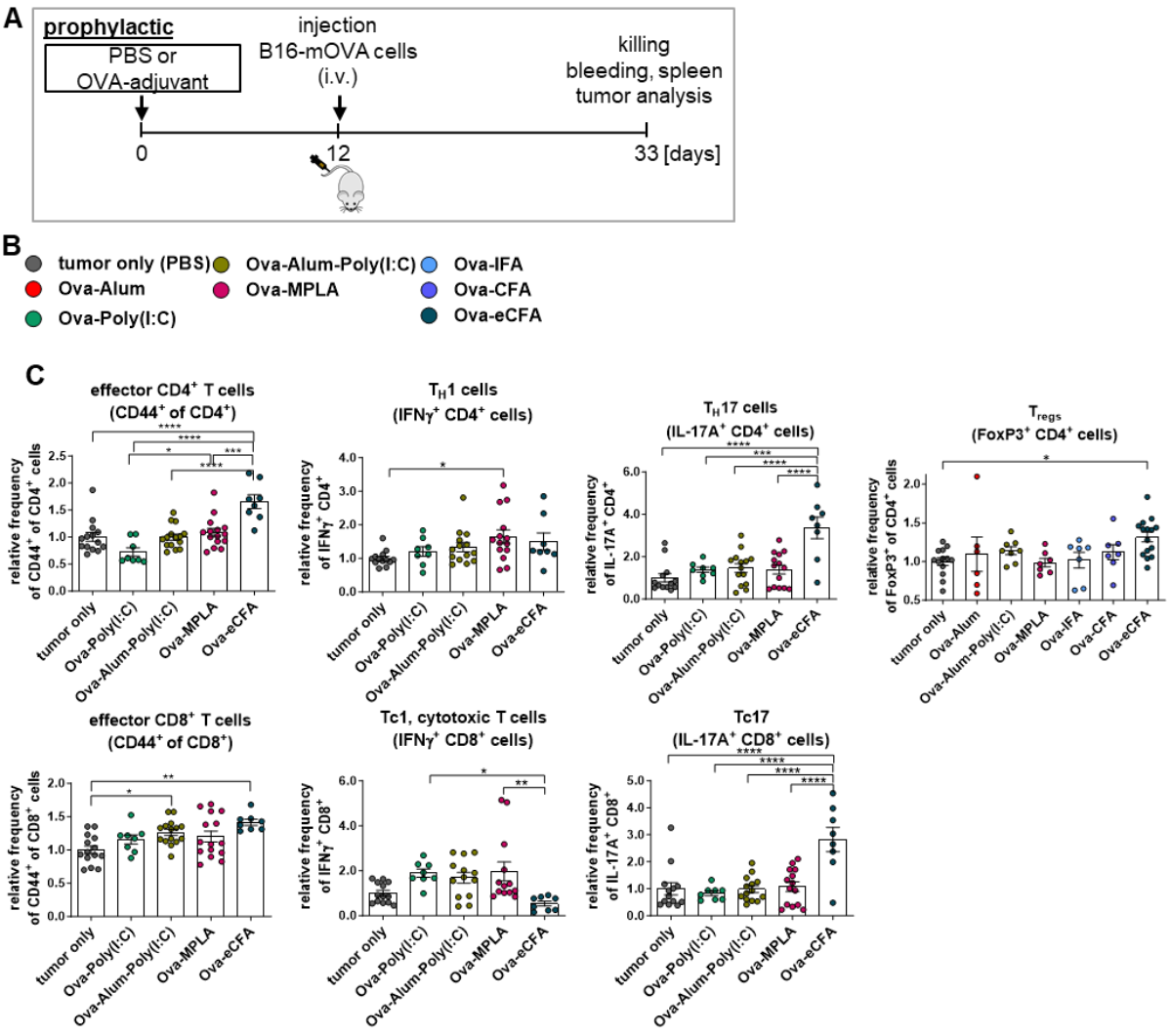

Figure 3.9 Impact of prophylactic vaccination with different adjuvants on the T cell response
(A) Experimental design: C57BL/6 WT mice were prophylactically immunized i.p. with Ova in different adjuvants. 12 days later B16-mOVA cells were injected i.v. 21 days after tumor cell injection, spleens were collected and prepared for flow cytometry. **(B)** Color code of the investigated adjuvants. **(C)** Relative frequencies of different splenic T cell subsets. T cell frequencies of all immunized mice were normalized to the respective mean of the untreated tumor group (tumor only, grey dots) in each single experiment. Graphs show normalized data from different experiments. Statistics: One-way ANOVA, Tukey's multiple comparison, *p < 0.05, **p < 0.01, ***p < 0.001, ****p < 0.0001.

The T cell analysis was not performed in every experiment, so not all adjuvants that were used in the vaccination experiments were analyzed for T cell responses. Therefore, only a selection of some adjuvants was analyzed and normalized to the untreated tumor group (tumor only) to combine different experiments and to get an idea of the effect on the T cell response.

On day 33 after prophylactic immunization, Ova-eCFA immunized mice had a significantly higher frequency of $CD44^+CD4^+$ memory/effector T cells compared to the other adjuvant groups (Figure 3.9C). Poly(I:C), on the other hand, had comparatively fewer. Also, Ova-eCFA,

and Ova-Alum-Poly(I:C) immunized mice had significantly more $CD44^+CD8^+$ effector/memory T cells compared to unimmunized mice. A trend was observed for Poly(I:C) immunizations. No significant differences were observed for T_{regs}.

T_H1 ($IFN\gamma^+$ $CD4^+$) cells were significantly higher in Ova-MPLA immunized mice and a trend was observed for Ova-eCFA immunized mice. T_H17 ($IL\text{-}17^+$ $CD4^+$) were significantly higher in Ova-eCFA immunized mice. Interestingly, T_H17 cells were linked to the induction of IgG antibodies with low levels of galactosylation and sialylation (Pfeifle et al. 2017; Bartsch et al. 2020).

Interestingly, Ova-Poly(I:C), -Alum-Poly(I:C) and -MPLA immunized mice showed a trend towards a higher frequency of $IFN\gamma^+$ cytotoxic $CD8^+$ T cells (Tc1), which have exceptional cytolytic activity to kill tumor cells due to their high secretion of cytokines such as IFNγ as well as perforin and granzyme B, and TNFα (M. S. Paul et al. 2020) and may be very likely involved in the observed reduced tumor growth. In contrast, Ova-eCFA immunized mice had fewer Tc1 cells, which is significant compared to Ova-Poly(I:C) and Ova-MPLA. Instead, Ova-eCFA immunized mice seems to produce significantly more Tc17 cells compared to the other adjuvant immunized mice as described also for the T_H17 cells.

Tc17 cells do not express granzyme B or perforin, and they do not have cytolytic activity against antigen-loaded targets (Hamada et al. 2009; Lopes et al. 2013). Instead, Tc17 as well as T_H17 cells mediate protecting effects e.g. by the recruitment of neutrophils (Hamada et al. 2009; Garcia-Hernandez et al. 2010).

Taken together, both Ova-Poly(I:C) and Ova-CFA/eCFA vaccination protected against tumor growth in the prophylactic vaccination tumor model. However, both may induce different protective T and B cell responses. Poly(I:C) induced Tc1 cells and high IgG2c/IgG1 ratios. eCFA induced T_H17 and Tc17 cells, high IgG (subclass) titers, and low levels of IgG subclass galactosylation and sialylation. In addition, both can at least transiently induce afucosylated IgG1 antibodies, the involvement of which is uncertain due to the low percentages.

3.1.3 Therapeutic vaccination with a "tumor antigen" in combination with different adjuvants leads to differences in tumor growth

Next, the efficacy of different adjuvants in combination with the model "tumor antigen" Ova was investigated in a therapeutic vaccination approach with first application of tumor cells and subsequent vaccination. To investigate this, WT mice were challenged with B16-mOVA cells by i.v. injection and therapeutically vaccinated after 9 days (Figure 3.10A). At 21 days after tumor cell injection or 12 days after vaccination, mice were killed, lungs were examined for metastasis, and blood and spleen were collected for antibody and immune cell analyses.

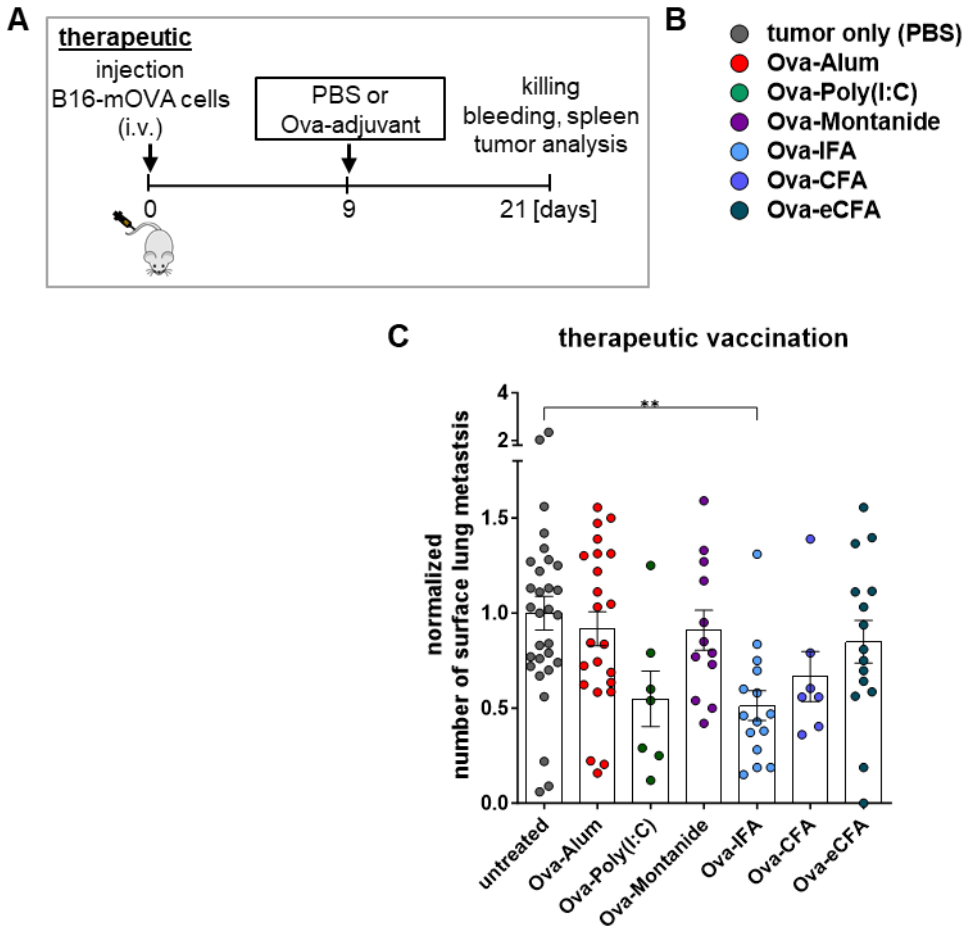

Figure 3.10: Growth of surface lung metastasis in mice after therapeutic vaccination with Ova in different adjuvants.
(A) Experimental design: B16-mOVA cells were injected i.v. into C57BL/6 WT mice on day 0. The mice were therapeutically immunized with Ova plus different adjuvants on day 9 after tumor cell injection. 21 days after tumor cell injection, the number of surface lung metastasis was determined. **(B)** Color code of the investigated adjuvants. **(C)** Normalized number of surface lung metastasis on day 21 after tumor cell injection. The number of metastasis in each mouse was normalized to the mean number of metastasis in the untreated tumor group (tumor only, gray dots) in each individual experiment. The graphs show normalized data from different experiments. Statistics: One-way ANOVA (*** P=0.0001), Tukey's multiple comparison, *p < 0.05, **p < 0.01, ***p < 0.001, ****p < 0.0001.

Ova-Alum and Ova-Montanide vaccination showed no tumor cell reduction (Figure 3.10C). In contrast, Ova-Poly(I:C) had fewer and Ova-IFA vaccinated mice significantly fewer metastasis compared to the Ova-Alum and/or unvaccinated groups. This is consistent with the prophylactic vaccination results described above (Figure 3.1). In contrast to prophylactic vaccination, Ova-CFA and Ova-eCFA did, however, not result in significant reduced tumor growth.

3.1.3.1 Effect of therapeutic vaccination with different adjuvants on IgG subclass distribution

So far, only the induction of IgG antibodies as a result of immunization with the soluble antigen and adjuvants was studied (Bartsch et al. 2020) (Figure 3.2). In this approach, the mice already had a growing tumor on the day of immunization. These circumstances must be considered because the tumor cells express Ova as a membrane-bound “tumor antigen” on their cell surface, indicating that the immune system has already come into contact with this antigen, which could influence the subsequent vaccination-induced immune response, or vice versa. To determine if the tumor induces a distinct antibody subclass or glycosylation patter, and if there are differences in the antibody response in this therapeutic setting compared to the prophylactic setting on day 14, ELISAs and IgG Fc-N glycosylation analysis were performed to measure Ova-specific IgG subclass titers and glycosylation at the end of the experiment on day 21 (Figure 3.11 -Figure 3.13).

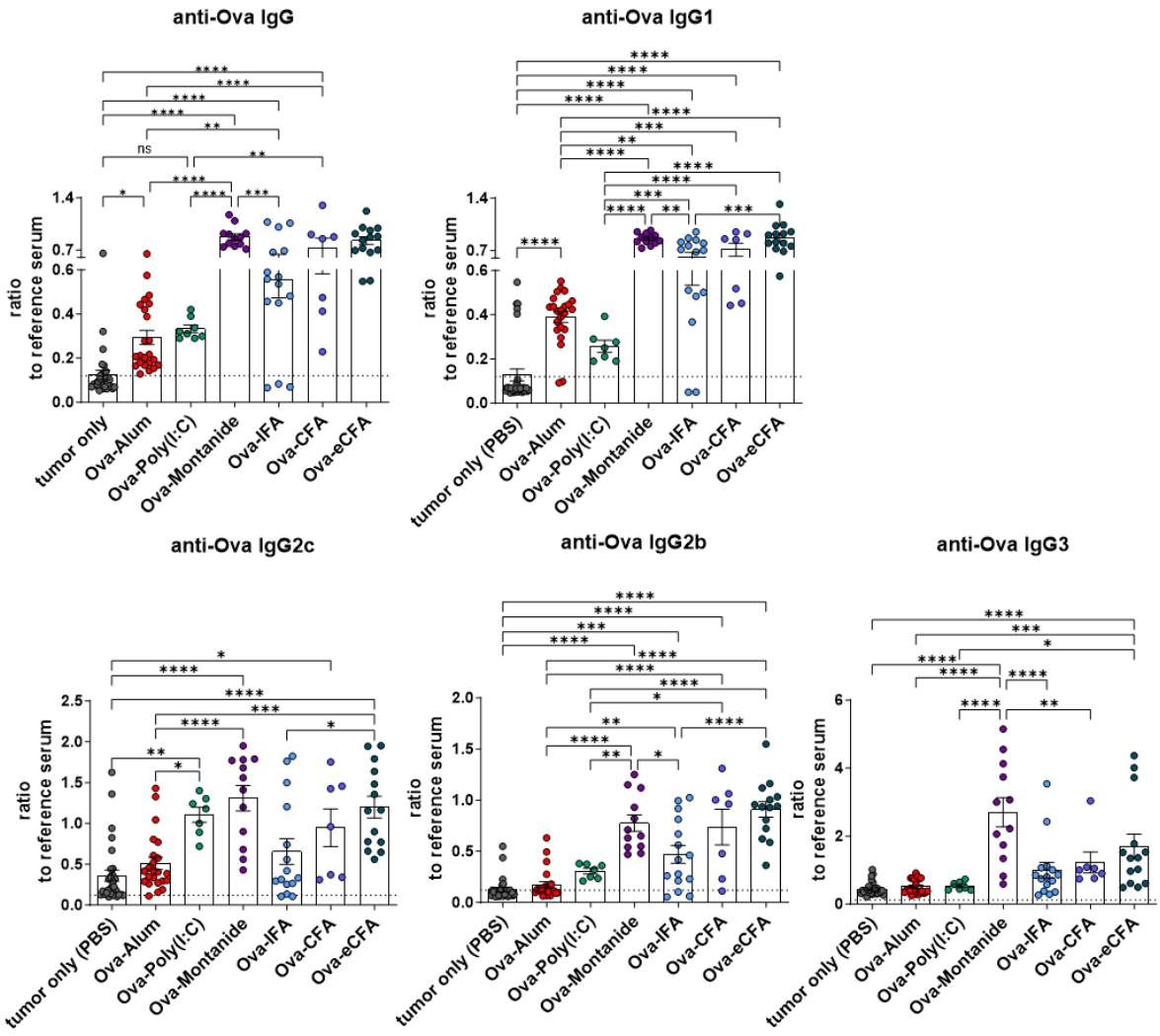

Figure 3.11: Impact of tumor cells and therapeutic vaccination on the generation of anti-Ova IgG subclass levels
Experimental set-up, see Figure 3.10. Relative serum anti-Ova IgG and IgG subclass levels on day 21 (serum dilution 1:100). Absorbance values (OD450nm) were normalized to a reference serum value (pooled serum from Ova-IFA immunized healthy mice on day 12). The dotted line represents serum from healthy untreated (tumor cell- and vaccine-free) mice. Statistics: One-way ANOVA (*** P=0.0001), Tukey's multiple comparison, *p < 0.05, **p < 0.01, ***p < 0.001, ****p < 0.0001.

The unvaccinated tumor-only group tended to express enhanced anti-Ova IgG2c levels compared to untreated control mice (Figure 3.11). Some tumor only mice expressed even higher anti-Ova IgG2b and IgG3 subclass levels.

However, the anti-Ova IgG and IgG subclass titers were significantly higher in all vaccinated groups compared to the unvaccinated tumor-only group, indicating the strong influence of the vaccination. However, in contrast to the prophylactic approach, the Ova-Alum and Ova-Montanide groups showed stronger IgG2c responses, while Montanide also showed stronger IgG responses of all other subclasses (IgG1, IgG2b, IgG3), indicating an influence of the tumor-

specific immune response on at least these vaccination-induced response. Poly(I:C) also seems to induce higher IgG1 and IgG2b titers compared to the prophylactic setting (Figure 3.3).

To further analyze the therapeutic vaccination, the ratio of activating IgG2 to IgG1 antibody levels was analyzed (Figure 3.12).

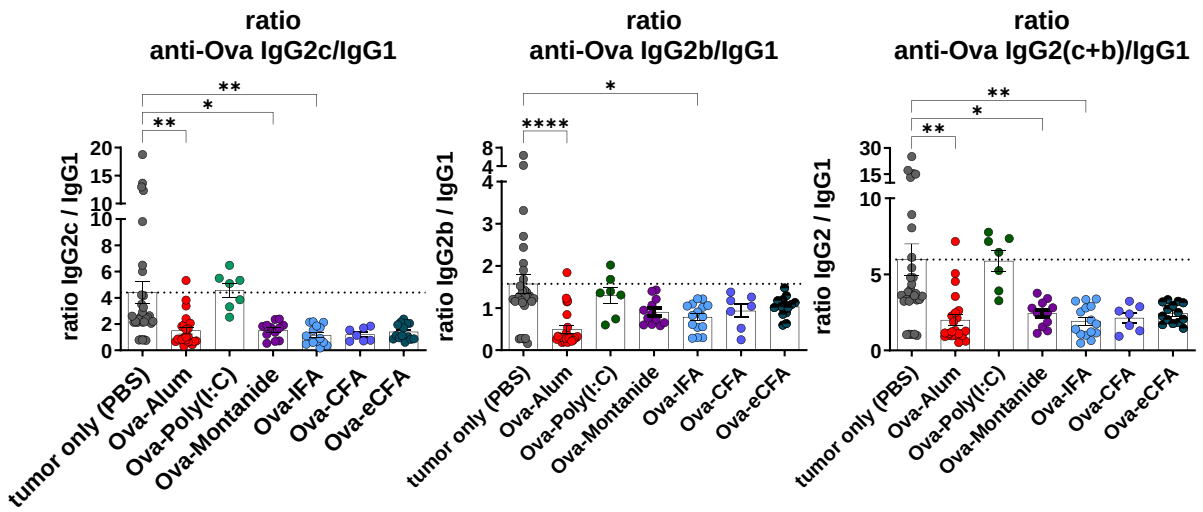

Figure 3.12: Impact of tumor growth and therapeutic vaccination on the anti-Ova IgG subclass ratios
Ratios of serum anti-Ova IgG2c/IgG1, IgG2b/IgG1, and IgG2 (IgG2c+IgG2b)/IgG1 subclass levels on day 21 (Figure 3.11). Absorbance values (OD450nm) were normalized to a reference serum value (pooled serum from Ova-IFA-immunized healthy mice on day 12). Normalized values of the different subclasses were subdivided by each other. The dotted line represents the ratios of the tumor-only group. Statistics: One-way ANOVA (*** P=0.0001), Tukey's multiple comparison, *p < 0.05, **p < 0.01, ***p < 0.001, ****p < 0.0001.

The unvaccinated tumor-only group led to a strong anti-Ova IgG2c/IgG1 ratio, and Alum to a tending increased IgG2c/IgG1 ratio compared to the prophylactic setting (Figure 3.3). However, there was little change in the subclass ratios, indicating a dominance of the vaccine over the tumor. In addition, Alum may be more susceptible to changes due to the generally low antibody titers.

The previously assumption was that tumor cells lead to the induction of a tolerance mechanism that the cells use to evade the immune system (J. Liu et al. 2022). IgG1 antibodies were expected as the tolerogenic antibody subclass, but in the therapeutic vaccination setting, the titer of antigen-specific IgG2c was higher in Ova-Alum and Ova-Montanide immunized mice compared to the prophylactic setting on day 14, contradicting the previous assumption. The induced IgG2c responses in tumor-only mice may be a weak fighting response against the tumor. Accordingly, control tumor cells (B16) without Ova expression grow faster in mice as compared to Ova-expressing tumor cells (B16-mOva) (data not shown).

3.1.3.2 Effect of therapeutic vaccination with different adjuvants on IgG subclass glycosylation

To further characterize the antibody response after therapeutic vaccination on day 9 in the presence of B16-mOVA tumor cells, the IgG subclass level and their Fc N-glycosylation was determined on day 21 by LC-MS as described above (Figure 3.13). Unfortunately, the anti-Ova IgG subclass responses were too low in the unvaccinated tumor-only group for analyzing anti-Ova IgG subclass glycopeptides. Instead, total IgG subclass levels on day 21 were analyzed and are shown in Figure 3.13 and Figure 3.14, to get an idea of the influence of the tumor cells on (at least total) IgG glycosylation.

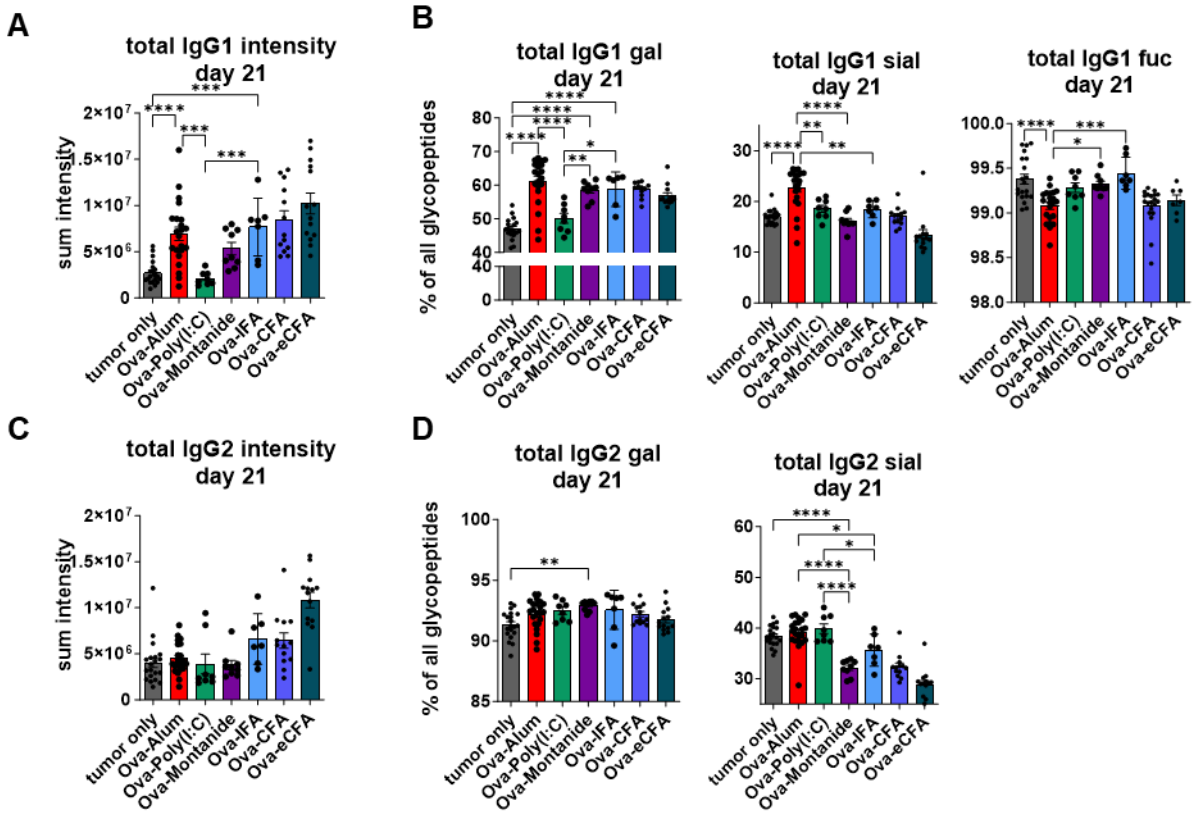

Figure 3.13: Total Serum IgG subclass glycosylation pattern on day 21 after tumor cell injection and therapeutic vaccination on day 9 with Ova in different adjuvants
Experimental design as described in Figure 3.10. On day 12 after immunization, blood was collected, and serum was analyzed for IgG subclass IgG glycosylation patterns. **(A, C)** IgG sum intensities measured by LC-MS. **(B, D)** Serum IgG1 subclass glycosylation patterns on day 12 after immunization. Percentages of galactosylated (gal), sialylated (G1S1+G2S1+G3S1+G2S2) and fucosylated (fuc) glycopeptides were measured by LC-MS. Statistics: One-way ANOVA, Tukey's multiple comparison, *p < 0.05, **p < 0.01, ***p < 0.001, ****p < 0.0001.

The sum intensities of total IgG1 and IgG2 (Figure 3.13A, C) showed similar trends as the ELISA results for anti-Ova IgG (Figure 3.12).

Also, for total IgG1 and IgG2, CFA and eCFA showed lower galactosylation and sialylation levels.

In addition, the glycosylation of total IgG subclasses of unvaccinated tumor bearing mice was compared with that of healthy control mice (Figure 3.14) to make the effects of the tumor cells more visible.

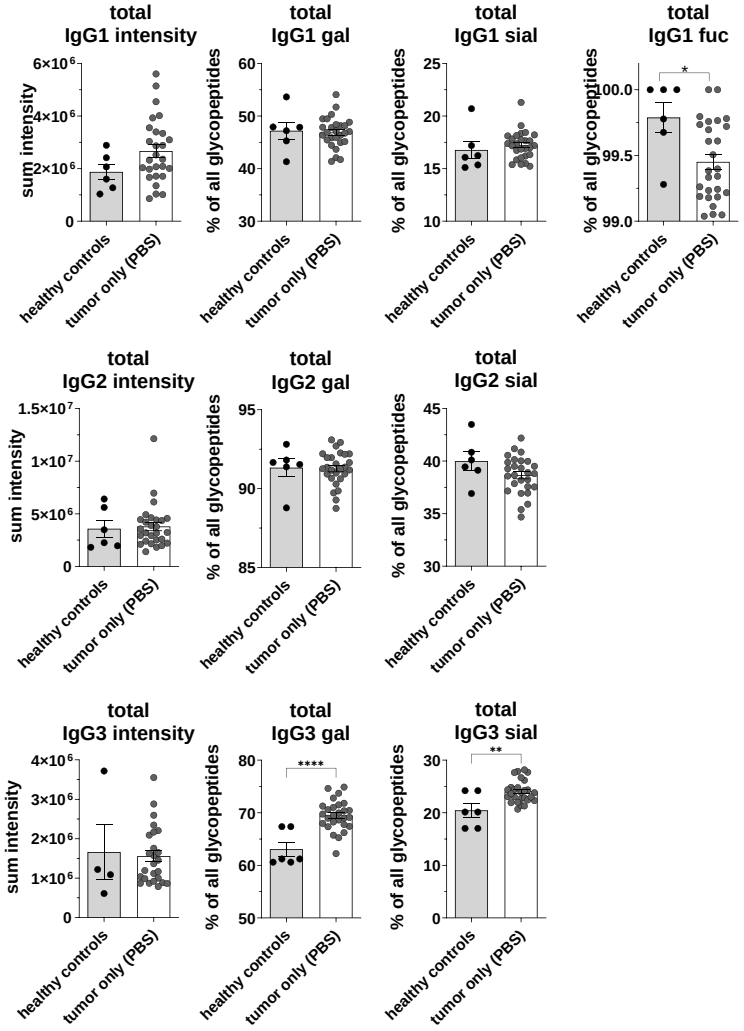

Figure 3.14 Induction of total IgG subclass glycosylation patterns by tumor growth.
Experimental design: B16-mOVA cells were injected i.v. into C57BL/6 WT mice on day 0, and serum was analyzed for total serum IgG sum intensity and glycosylation patterns on day 21. Percentages of anti-Ova IgG glycopeptides were measured by LC-MS. Statistics: Student's t-test *p < 0.05, **p < 0.01, ***p < 0.001, ****p < 0.0001.

IgG glycosylation showed that non-vaccinated tumor-bearing mice induced significantly less IgG1 fucosylation, but significantly more IgG3 galactosylation and sialylation.

Taken together, the effects of pre-existing tumor on IgG response described here may provide some insight into explaining the differences in tumor growth between the prophylactic and therapeutic settings, suggesting that tumor cells may influence the antibody response.

3.1.4 Differences between the prophylactic and therapeutic vaccination on the antibody response

As previously described, the already present tumor in the therapeutic setting impacts the antibody response, compared to the prophylactic setting, where no tumor was present on the day of vaccination. The differences are summed up in Table 15.

Table 15: Differences in the antibody response between the prophylactic and therapeutic vaccination

	Differences of the therapeutic setting compared to the prophylactic setting
Tumor growth	- no tumor reduction with CFA and eCFA
IgG titer	- increased IgG2c in the unvaccinated/tumor only group - higher IgG2c after Ova-Alum immunizations

3.1.5 Verification of the influence of vaccination-induced IgG antibodies on tumor growth by serum transfer experiments

Furthermore, the role of antibodies generated by the vaccination in tumor control was to be verified. Therefore, transfer experiments were performed in which serum from immunized mice was collected on day 12, pooled, and transferred to WT mice and additionally injected with tumor cells. The collected serum was analyzed before for IgG subclass titers by ELISA, which was performed by a master's student (Ilona Zeiser) and showed similar results as described above for Ova-eCFA serum on day 14 (Figure S 2, Figure 3.2). To perform the transfer experiment, mice were injected i.p. with 100 µl of serum in PBS one day before and/or one day after B16-mOVA tumor cell injection (Figure 3.15A). After 22 days, the mice were sacrificed, and the lungs were examined for metastasis.

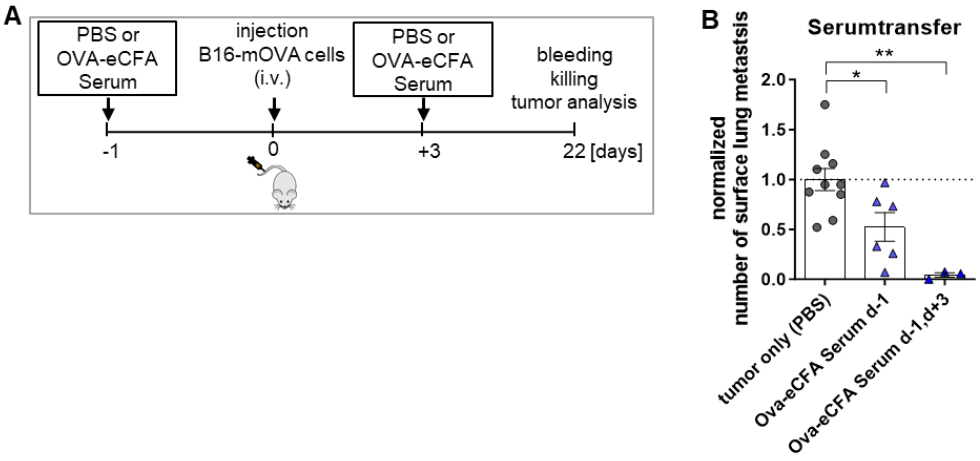

Figure 3.15 Serum transfer from eCFA immunized mice to B16-mOVA-bearing mice
(A) Experimental design: B16-mOVA cells were injected i.v. into C57BL/6 WT mice. Serum was collected from healthy mice 12 days after immunization with Ova-eCFA and injected into the mice on day -1 or -1 and +3 before/after tumor cell injection. At 21 days after tumor cell injection, the number of surface lung metastasis were determined. **(B)** Normalized number of surface lung metastasis on day 21 after tumor cell injection. The number of lung metastasis of all immunized mice was normalized to the mean of the number of lung metastasis of the untreated tumor group (tumor only, grey dots). The dotted line indicates the mean of the untreated tumor group. Statistics: One-way ANOVA, Tukey's multiple comparison, *p < 0.05, **p < 0.01, ***p < 0.001, ****p < 0.0001.

The serum transfer experiment showed that one or two injections of serum from Ova-eCFA-immunized mice significantly protected the mice from lung metastasis (Figure 3.15B), with two injections being more sufficient. However, these results should be verified in the future with sera from different immunized mice.

3.1.1 *In vitro* neutrophil stimulation

To further verify the previously described findings and differences between the adjuvants used during vaccination, a murine ROS release assay was performed to determine whether different sera from immunized mice could activate neutrophils differently. In addition, murine monoclonal IgG subclass antibodies, including different glycosylation forms, were tested to determine whether antibodies of different "quality" affect neutrophil activation differently. The ROS release assays were performed in collaboration with Janina Petry.

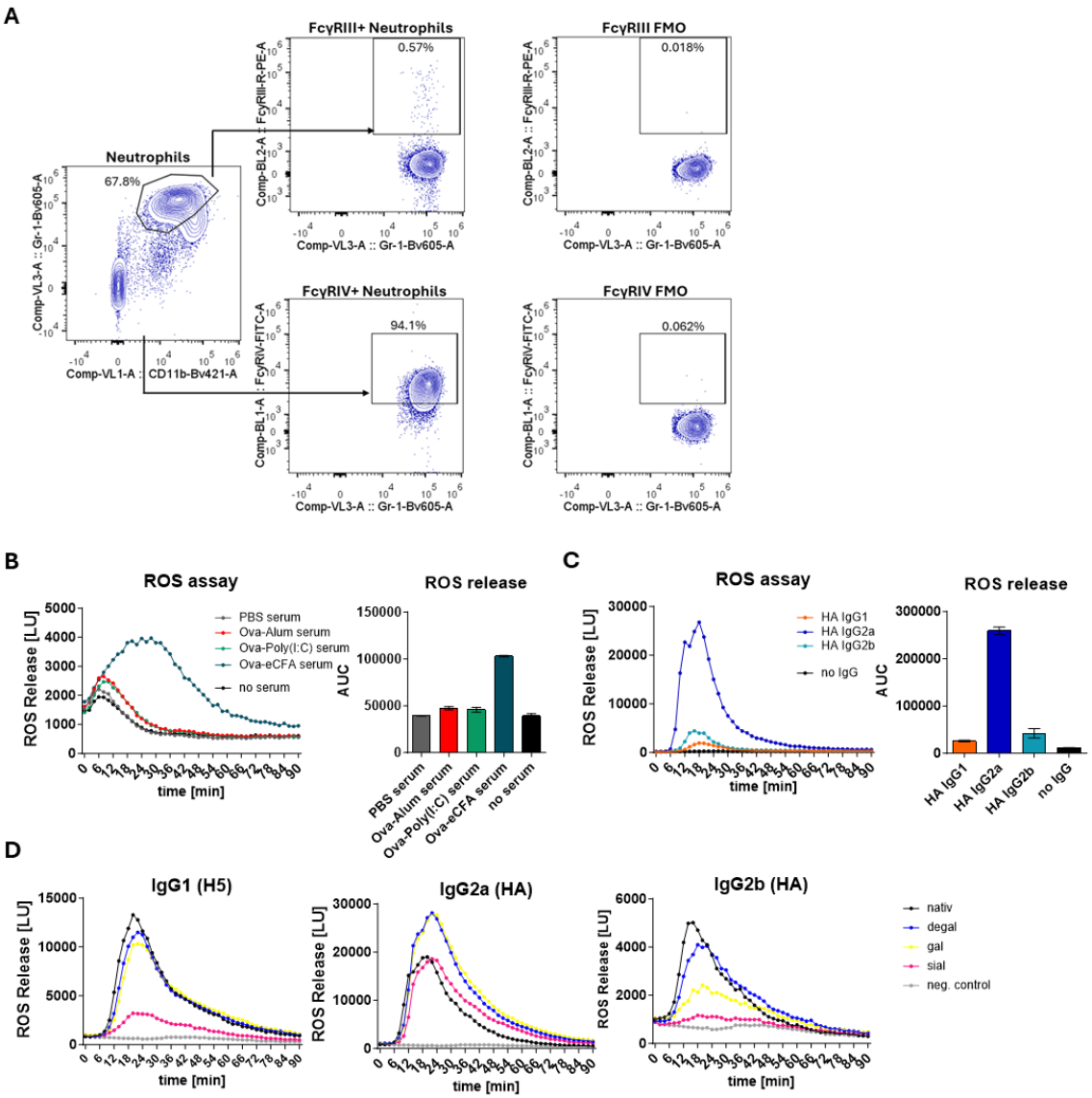

Figure 3.16 ROS release in response to serum and antibody stimulation.
(A) Murine neutrophils were identified in bone marrow cells by flow cytometry as $CD11b^+$ $Gr\text{-}1^+$ cells. Murine FcγRIII and FcγRIV expression was further analyzed (FMO = fluorescence minus one). **(B-D)** ROS release from bone marrow neutrophils of naïve C57BL/6 mice was measured in response to **(B)** serum from immunized mice (serum IgG titer was analyzed in **Figure S 2**) and **(C, D)** monoclonal IgG subclass antibodies and different glycosylation forms (neg. control: no IgG). Measurement was performed in duplicates over 90 min using luminescence. The area under the curve (AUC) was analyzed using GraphPad Prism.

First, the expression of murine FcγRIII and FcγRIV was determined by flow cytometry, showing that more than 90% of neutrophils expressed FcγRIV, while the expression of FcγRIII was quite low (Figure 3.16A). Furthermore, neutrophils activated with serum from Ova-eCFA-immunized mice showed the highest ROS release in this setting, while the stimulation with Ova-Alum and Ova-Poly(I:C) serum was reduced (Figure 3.16B), indicating differences in neutrophil activation between the different adjuvants used. In addition, stimulation was increased with IgG2a subclass antibodies compared to IgG1 and IgG2b antibodies. (Figure 3.16C). The ROS release was further higher with de-galactosylated antibodies compared to sialylated antibodies (Figure 3.16D), indication increased neutrophil activation by IgG2a subclass antibodies and de-galactosylated glycosylation forms, depending on FcγRIV expression (Kaneko, Nimmerjahn, and Ravetch 2006).

3.2 Impact of checkpoint inhibition on the antigen specific immune response

Since certain cancers, especially melanoma, are resistant to chemotherapy or radiotherapy, other therapeutic approaches aim to boost the immune system, to fight against cancer cells (Seidel, Otsuka, and Kabashima 2018). Immune checkpoints are responsible for maintaining immune homeostasis and tolerance mechanisms (Kleffel et al. 2015). Cytotoxic T-lymphocyte associated protein 4 (CTLA-4) and anti-programmed cell death protein 1 (PD-1) are two checkpoint receptors that are targeted by blocking antibodies to stimulate the immune system and anti-tumor immune response (Kleffel et al. 2015; Seidel, Otsuka, and Kabashima 2018; Juneja et al. 2017; Sharma, Vacher, and Allison 2019; Simeone, Grimaldi, and Ascierto 2015; Chen et al. 2018). PD-1 is expressed on T cells and is upregulated after T cell activation and exhaustion, and binding to its ligand (PD-L1) expressed on antigen-presenting cells (dendritic cells, macrophages, and monocytes) leads to inhibition of T cell activation and cytokine secretion (Seidel, Otsuka, and Kabashima 2018; Juneja et al. 2017). In addition, PD-L1 is expressed on tumor cells, which promotes escape from immune surveillance (Chen et al. 2018). CTLA-4 is expressed by T_{regs} and inhibits the immune response by binding the co-stimulatory receptor CD28 on T cells, preventing their activation (Seidel, Otsuka, and Kabashima 2018).

Therefore, it is of interest to investigate how blocking of immune checkpoints affects antigen-specific T and B cell responses, including antibody responses, as well as antigen-unspecific immune responses that may explain inflammatory side effects in such treated cancer patients.

Tumor-specific vaccination in combination with checkpoint inhibitor therapies are also conceivable.

The effect of checkpoint inhibitors on the antibody response and the underlying T and B cell response was investigated in a mouse immunization model using the foreign antigen Ovalbumin (Ova) plus an adjuvant. In addition, the effect of anti-PD-1 was investigated in a murine melanoma model without immunization. This should provide some insight into the specific and unspecific immune response and the impact on antibody subclass distribution and glycosylation.

3.2.1 Impact of anti-PD-1 and anti-CTLA-4 on an antigen-specific antibody and immune cell response

The antigen-specific immune response using anti-PD-1 and anti-CTLA-4 was evaluated by immunizing mice with Ova-Alum to generate Ova-specific immune responses. It was expected that the checkpoint inhibitors would enhance the Ova-specific immune responses. Accordingly, WT mice were immunized with Ova-Alum on day 0 and treated with anti-PD-1 (clone RMP1-14) or anti-CTLA-4 (clone UC10-4F10-11) antibody by i.p. injection one day before immunization and on day 1, 3, 5, 7 and 9 after immunization. As controls, mice were immunized with Ova-Alum or inflammatory Ova-eCFA without checkpoint inhibitors. On day 12 after immunization, blood and spleens were collected from the mice for antibody and immune cell analysis (Figure 3.17A). The experiments were performed in collaboration with Hanna Lunding, a former doctoral student in our laboratory.

The effect of the checkpoint inhibitors on anti-Ova IgG1 Fc glycosylation was analyzed by LC-MS, which was performed by the laboratory of Prof. Manfred Wuhrer (Leiden, the Netherlands).

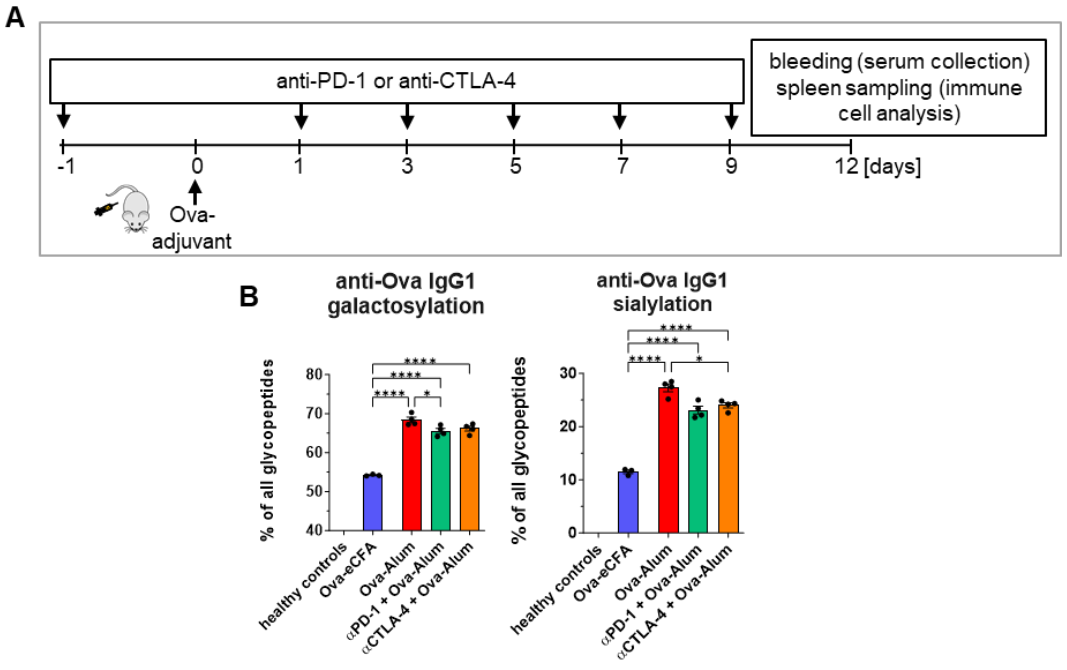

Figure 3.17: Impact of checkpoint inhibition on the Fc glycosylation pattern of anti-Ova IgG1. **(A)** Experimental design: C57BL/6 WT mice were immunized with Ova-Alum or Ova-eCFA on day 0. Ova-Alum treated mice were additionally treated with anti-CTLA-4, anti-PD-1 or PBS on day -1 before immunization and on day 1, 3, 5, 7, 9 after immunization. Ova-eCFA immunized mice were treated with PBS on the same days. **(B)** Anti-Ova serum IgG subclass Fc glycosylation on day 12 after vaccination and treatment with anti-PD-1 or anti-CTLA-4. Percentages of galactosylated (gal) and sialylated (G1S1+G2S1+G3S1+G2S2) glycopeptides were measured by LC-MS. Statistics: One-way ANOVA, Tukey's multiple comparison, *p < 0.05, **p < 0.01, ***p < 0.001, ****p < 0.0001.

The galactosylation level of Ova-specific IgG1 was significantly lower after anti-PD-1 treatment, and the sialylation level tended to be lower after anti-PD-1 treatment and was significantly lower after anti-CTLA-4 treatment (Figure 3.17B) compared to Ova-Alum without antibody treatment, although not as low as with inflammatory Ova-eCFA. Taken together, this indicates that both checkpoint inhibitors result in lower galactosylated and sialylated antigen-specific IgG1 antibodies, which characterize more pro-inflammatory conditions than after Ova-Alum treatment alone, but still less inflammatory than after Ova-eCFA immunization. Furthermore, total IgG1 and IgG2 intensities were plotted to analyze if there is an impact on the total IgG level (Figure S 3), showing an increased IgG1 intensity after checkpoint inhibition compared to Ova-Alum treatment alone.

In addition, the frequency of germinal center (GC) B cells and plasma cells (PC) and the expression of St6gal1 were analyzed by flow cytometry. The gating strategy for the different cell populations was performed as exemplary described in Figure 3.18.

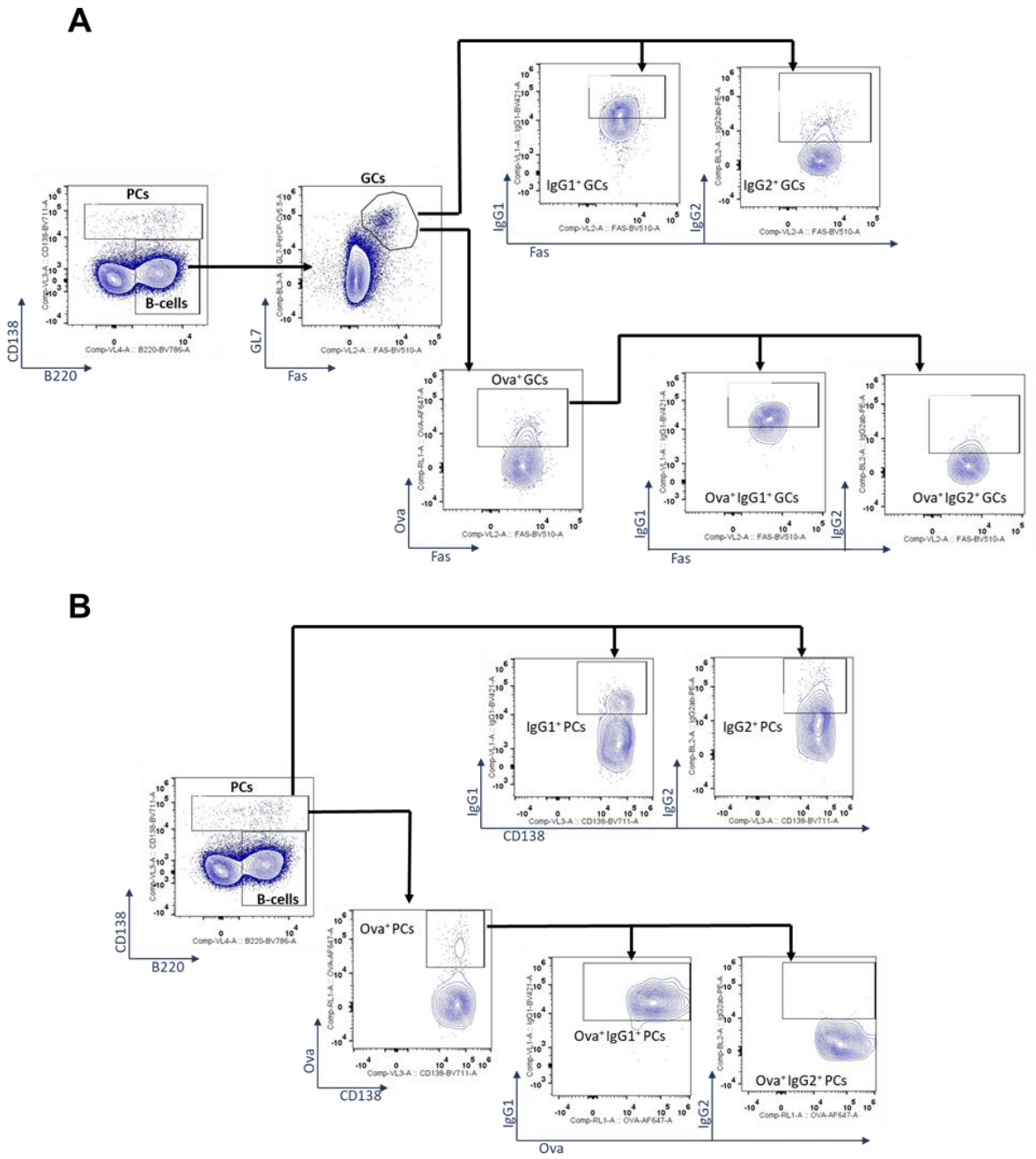

Figure 3.18: Gating strategy of splenic Ova-specific and total IgG subclass+ GCs and PCs
Splenic **(A)** GC B cells and **(B)** plasma cells were analyzed by flow cytometry. Cells were pre-gated on lymphocytes and live cells. **(A)** GCs are characterized by $B220^+$ $CD138^-$ Fas^+ and $GL\text{-}7^+$ and **(B)** PCs as $CD138^+$ cells of live lymphocytes. Ova- and IgG subclass-positive cells were further gated in both populations. Gates were selected with FMO controls.

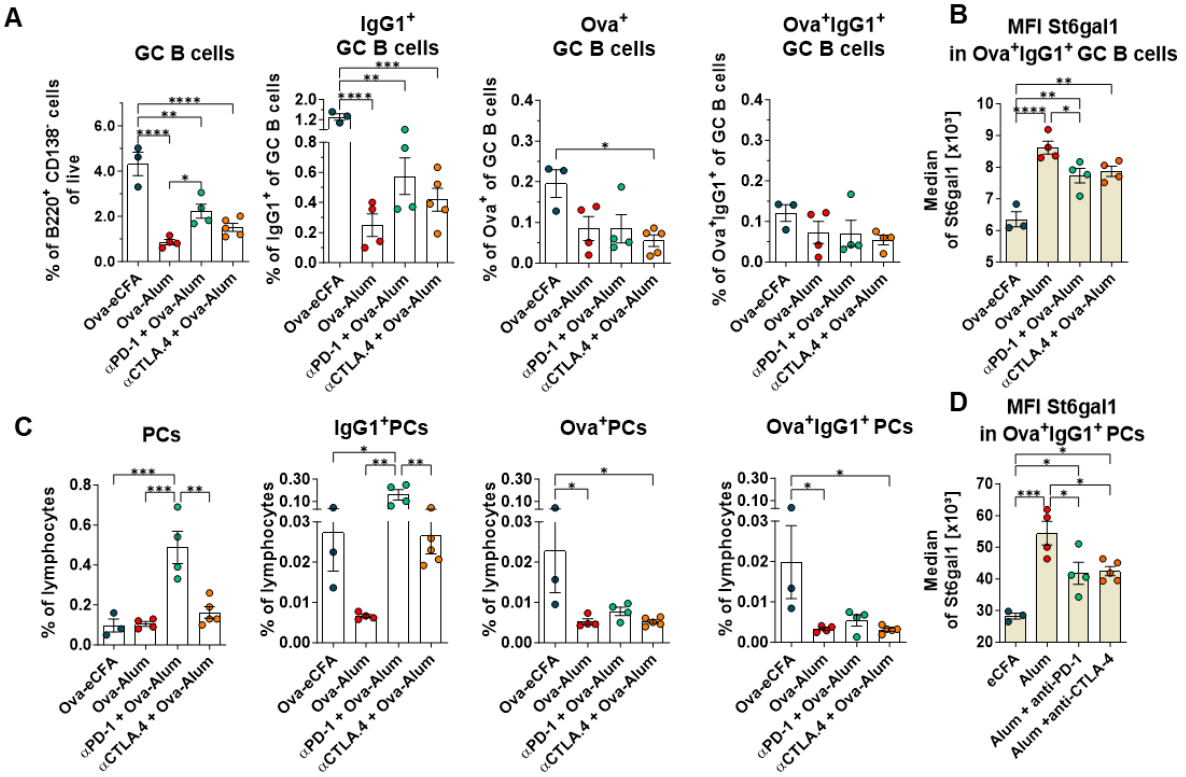

Figure 3.19: Impact of checkpoint inhibition on the B cell response and on the expression level of St6gal1

(A, C) Frequencies of **(A)** germinal center B cells and **(C)** plasma cells on day 12 after vaccination and treatment with anti-PD-1 or anti-CTLA-4. Spleens were collected on day 12 and germinal center B cells and plasma cells were analyzed by flow cytometry. **(B, D)** Intracellular protein expression (mean fluorescence intensity (MFI)) of St6gal1 determined by the median. Statistics: One-way ANOVA, Tukey's multiple comparison, *p < 0.05, **p < 0.01, ***p < 0.001, ****p < 0.0001.

Anti-PD-1 treatment resulted in a significant increase and anti-CTLA-4 treatment resulted in a tending increase in the frequency of GC B cells compared to Ova-Alum treatment alone. Ova-eCFA resulted in the highest frequency of GC B cells (Figure 3.19A). In addition, both checkpoint inhibitor treatments led to a tending increase in the frequency of IgG1 positive, but not in Ova and Ova-IgG1 positive GC B cells (Figure 3.19A). However, the expression level of St6gal1 was significantly lower after anti-PD-1 treatment and tending lower after CTLA-4 treatment, although not as low as after eCFA immunization (Figure 3.19B). Also at the PC level, blocking PD-1 resulted in a significantly higher frequency of PCs and IgG1 positive PCs, and a tending higher frequency after blocking CTLA-4 (Figure 3.19C). However, there was no change in Ova and Ova-IgG1 positive PCs (Figure 3.19C). Nevertheless, the expression level of St6gal1 was significantly lower in Ova^+IgG1^+ PCs after treatment with both checkpoint inhibitors, although still higher than after Ova-eCFA treatment (Figure 3.19D).

This is in consistent with the findings on antibody level. The level of sialylated Ova-specific IgG1 antibodies was lower after anti-PD1 treatment (Figure 3.17D), as was the expression level of St6gal1 in GC B cells and PCs (Figure 3.19D). The data suggest that checkpoint inhibition leads to antigen-unspecific IgG1 responses as well as to antigen-specific GC and PC responses resulting in lower galactosylated and sialylated antigen-specific IgG1 antibodies.

3.2.2 Impact of anti-PD-1 and anti-CTLA-4 on the follicular T- cell response

As mentioned above, both immune checkpoint receptors, PD-1 and CTLA-4, are expressed on T cells and inhibit their downstream activation upon binding of their ligand. Blocking both checkpoint receptors should therefore increase T cell activation. Therefore, the effect of both blocking antibodies on the follicular T cell (including T follicular helper (T_{FH}), T follicular regulatory cells (T_{FR})) response, which affects the germinal center response and subsequently the antibody response, should be investigated. To investigate this, T cell subsets were determined by flow cytometry staining in collaboration with Hanna Lunding, a former doctoral student.

The gating was performed as described Figure 3.20.

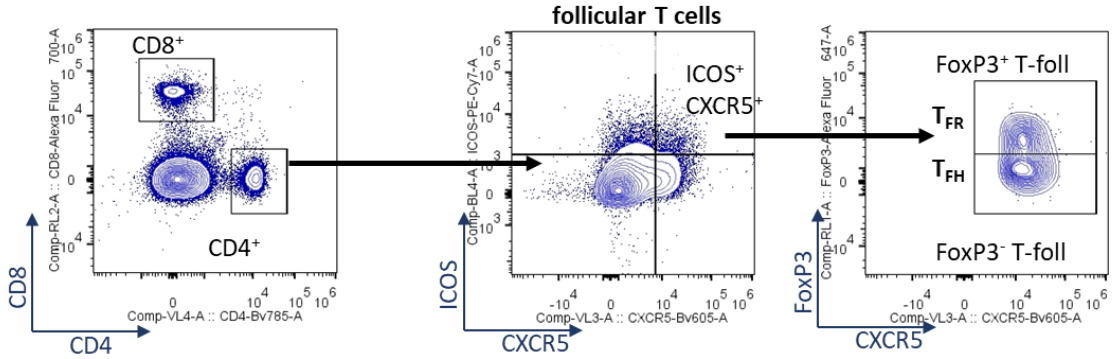

Figure 3.20: Gating strategy follicular T cells
Splenic follicular T cells were investigated by flow cytometry. Cells were pre-gated on lymphocytes and live cells. T-follicular cells are characterized by $CD4^+$, $ICOS^+$ and $CXCR5^+$ cells. T_{FH} cells are characterized as $Foxp3^-$ and T_{FR} cells as $Foxp3^+$.

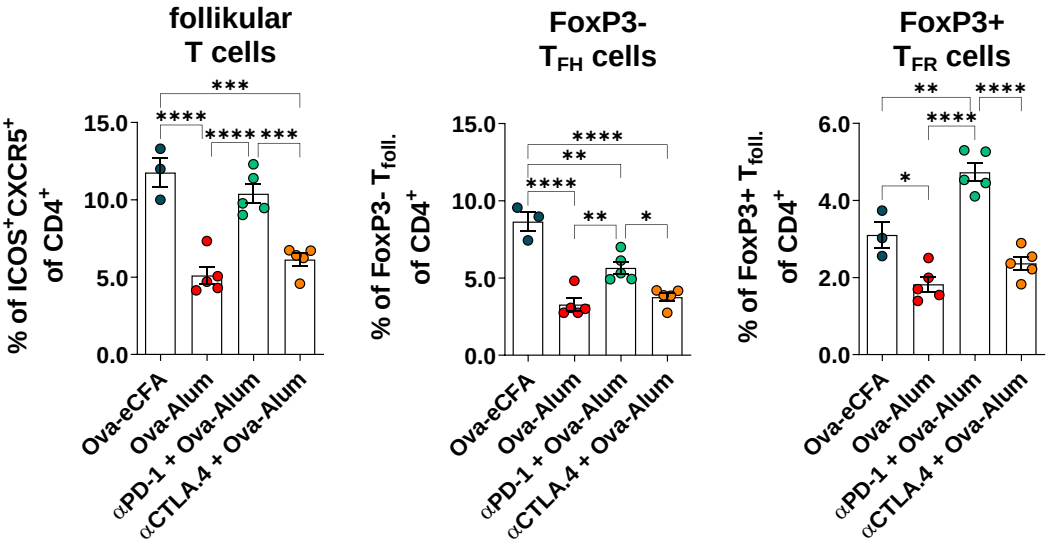

Figure 3.21: Impact of checkpoint inhibition on the follicular T cell response
Frequency of T-follicular, T-follicular helper (T_{FH}), and T-follicular regulatory (T_{FR}) cells on day 12 after vaccination and treatment with anti-PD-1 or anti-CTLA-4 (see Figure 3.17A). Spleens were collected on day 12 and T-cells were analyzed by flow cytometry. Statistics: One-way ANOVA, Tukey's multiple comparison, *p < 0.05, **p < 0.01, ***p < 0.001, ****p < 0.0001.

Blocking PD-1 resulted in a significant increase in the frequency of follicular T cells and blocking CTLA-4 resulted in a tending increase compared to Ova-Alum treatment alone (Figure 3.21). Similar trends were observed for T_{FH} and T_{FR} cells (Figure 3.21).

3.3 Effect of checkpoint inhibition on subcutaneous melanoma growth and immune response

Finally, the effect of the checkpoint inhibitor anti-PD-1 was investigated in a subcutaneous melanoma model.

In this mouse model, B16-F10 melanoma cells, which do not express a model antigen, were used to generate a subcutaneous tumor. Therefore, mice were injected subcutaneously with the melanoma cells in the right flank and treated with anti-PD-1 (clone RMP1-14) on days 7, 9, 11, 13, 15, and 17 after tumor cell injection (Figure 3.22). Subcutaneous tumor growth was monitored over time by measuring the diagonal diameter. After 21 days, the mice were sacrificed, and the final tumor size was determined. Blood and spleen were also collected for antibody and immune cell analysis.

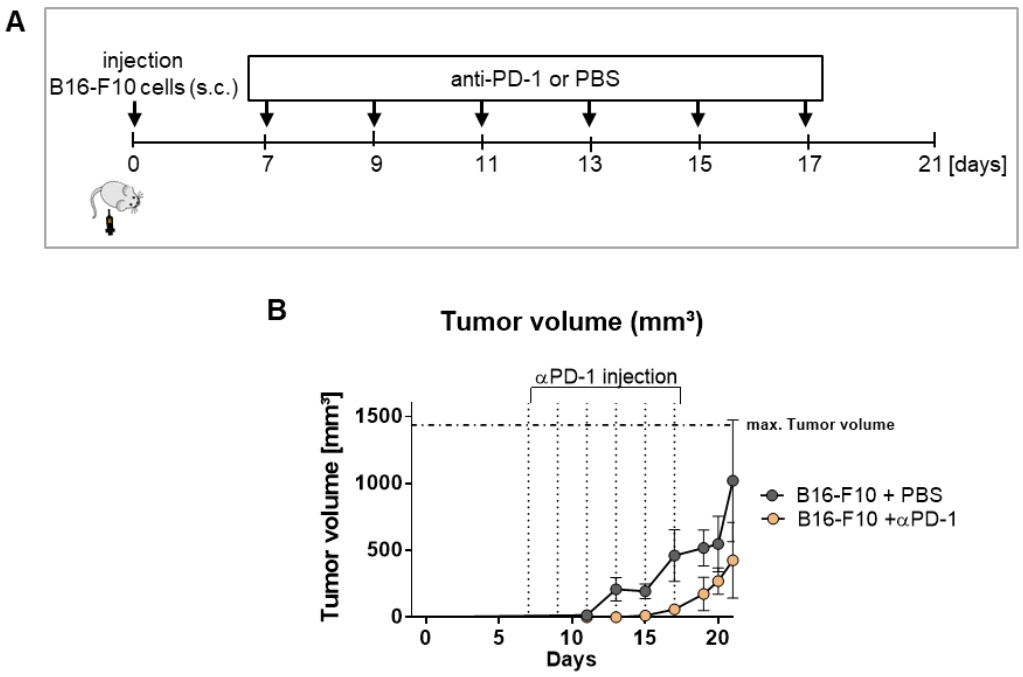

Figure 3.22: Treatment of B16-F10 subcutaneous tumor model with anti-PD-1
(A) Experimental design: B16-F10 cells were s.c. injected into the right flank of C57BL/6 WT mice. Mice were treated with anti-PD-1 (RMP1-14) on days 7, 9, 11, 13, 15 and 17 after tumor cell injection. S.c. tumor growth was determined by measuring the tumor diameter and calculating the tumor volume using the formula: TV (mm3) = a (mm) x b2 (mm2) x 0.5 (a: largest diameter, b: perpendicular diameter of the tumor (idealized ellipsoid)). **(B)** Tumor volume over time in PD-1- and PBS-treated mice. Dotted vertical lines indicate the day of anti-PD-1 injection. Dotted horizontal line indicates the maximum tumor volume, which is 14x14mm in diameter.

Blocking PD-1 resulted in slower and reduced tumor growth in the mice compared to mice injected with PBS. This confirms the function of the blocking antibody in enhancing anti-tumor immunity.

Furthermore, the immune cell response was analyzed to gain insight into the mechanisms of the treatment. Therefore, T and B cells were characterized by flow cytometry. Gating was performed as previously described (Figure 3.18, Figure 3.20).

3.3.1 T cell response during checkpoint inhibition-dependent tumor reduction

As shown before, as anti-PD-1 increases the germinal center-related T cell response, the follicular T cells were investigated in this tumor model. The follicular T cells were characterized by flow cytometry staining. Gating was performed as previously described (Figure 3.20).

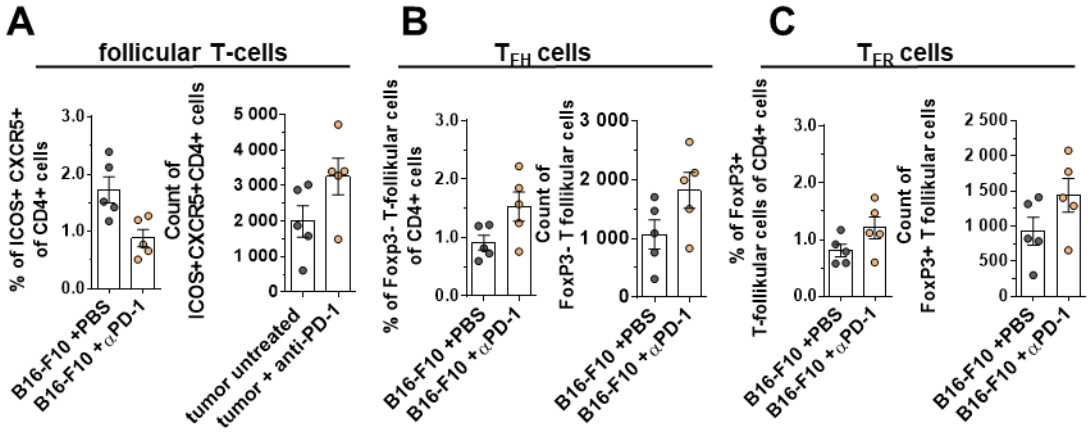

Figure 3.23: Impact of checkpoint inhibition during s.c. tumor growth on the follicular T cell response
(A, B, C) Frequency of **(A)** T-follicular, **(B)** T-follicular helper (T_{FH}), and **(C)** T-follicular regulatory (T_{FR}) cells on day 21 after tumor cell injection and treatment with anti-PD-1. Spleens were collected on day 21 and T cells were analyzed by flow cytometry.

The anti-PD-1 treatment resulted in a tending higher number of follicular T_{FH} cells compared to the control group. In addition, the frequency and number of T_{FH} cells tended to be increased after PD-1 blockade (Figure 3.23B), although the frequency and number of T_{FR} cells also tended to be increased. Further investigations have to be done in the future to identify e.g. differences in cytokine expression of the follicular T cells between the two groups to find further explanations for opposing immune responses.

3.3.1 B cell response during checkpoint inhibition-dependent tumor reduction

To further clarify the mechanism behind the reduced tumor growth, and follicular T cell response, the associated B cell response was analyzed to determine whether the treatment had an effect on the germinal center and/or plasma cells. The B cells were also characterized by flow cytometry. Gating was performed as previously described (Figure 3.18).

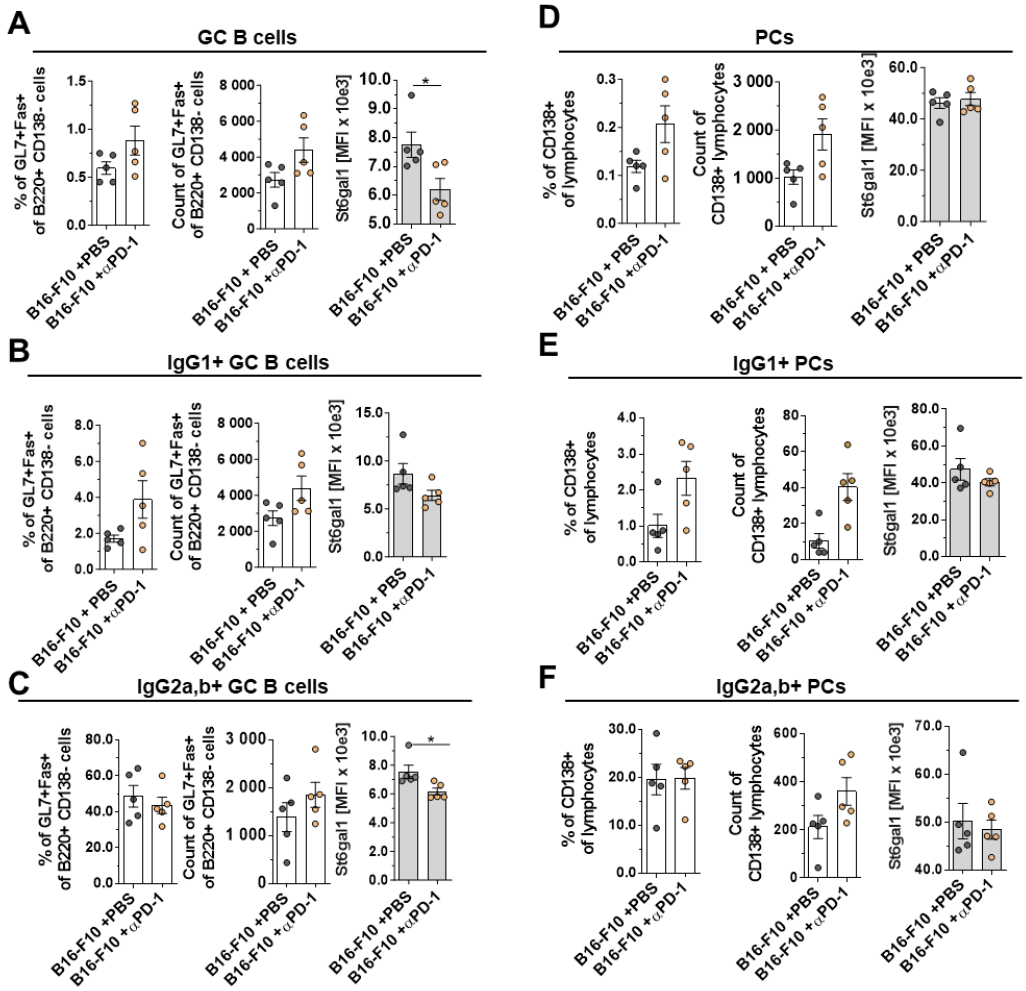

Figure 3.24: Impact of checkpoint inhibition during s.c. tumor growth on the B cell response and on the expression level of St6gal1
(A,B,C) Frequency, count and St6gal1 expression level of **(A)** germinal center (GC) **(B)** IgG1$^+$ GC and **(C)** IgG2a,b$^+$ GC B cells on day 21 after tumor cell injection and treatment with anti-PD-1. **(D,E,F)** Frequency, count and St6gal1 expression level of **(D)** plasma cells (PCs), **(E)** IgG1$^+$ PCs and **(F)** IgG2a,b$^+$ PCs on day 21 after tumor cell injection and treatment with anti-PD-1. Spleens were collected on day 21 and germinal center B cells and plasma cells were analyzed by flow cytometry. Intracellular protein expression (mean fluorescence intensity (MFI)) of St6gal1 was determined by the median. Statistics: Student's t-test, *p < 0.05, **p < 0.01, ***p < 0.001, ****p < 0.0001.

The frequency and count of GC B cells were tending increased after PD-1 blockade, whereas the expression level of St6gal1 was significantly decreased (Figure 3.24A). This was consistent with the non-tumor experiments described above (Figure 3.19). Similar trends were observed in IgG1 positive GC B cells in this (Figure 3.24B) and in a previous experiment (Figure 3.19). In addition, the expression level of St6gal1 was significantly reduced in IgG2a/b positive GC B cells after PD-1 blockade (Figure 3.24C). However, only a trend for an increased count of IgG2a/b positive GC B cells was observed (Figure 3.24C).

In addition, the frequency and count of in particular IgG1 positive PCs were increased after anti-PD-1 treatment (Figure 3.24D,E), which is also consistent with the previous experiments showing in particular an increase of antigen-unspecific $IgG1^+$ PCs (Figure 3.19). In contrast to the previous experiments, the expression level of St6gal1 in $IgG1^+$ PCs did not show a difference between the two groups (Figure 3.24D-F). This could be due to the fact that the increased antigen-unspecific $IgG1^+$ PCs originate from extrafollicular reactions with high St6gal1 expression (Bartsch et al. 2020), so that GC-derived $IgG1^+$ PCs with potentially lower St6gal1 expression could be hidden among the large antigen-unspecific $IgG1^+$ PCs.

Taken together, the data suggest that checkpoint inhibition may reduce the galactosylation and sialylation of GC-derived IgG antibodies, potentially enhancing neutrophil-mediated tumor cell killing.

4. Discussion

Effective cancer treatment is still rare and does not result in complete remission in most cases. Although treatment options have improved in recent years, there are still no suitable therapies for many types of cancer, in part because they are usually discovered late. There is also a lack of suitable biomarkers that can predict the effectiveness of treatment or the development of cancer (Baxter 2014; RKI 2019; Zahavi and Weiner 2020; Cuzzubbo et al. 2021).

Antibodies have become widely used markers of vaccine-induced immunity and are also used as therapeutics for inflammatory autoimmune diseases, allergies or cancer (Anthony et al. 2011; Collin and Ehlers 2013; Hess et al. 2013; Zahavi and Weiner 2020; Delgado and Garcia-Sanz 2023; Zinn et al. 2023). In particular, the "quality" of antibodies, which is characterized by their isotype, subclass and Fc-N glycosylation, determines their effector function.

Therefore, anti-tumor therapies should consider directing the immune response in a specific direction that targets the tumor cells and does not induce tolerogenic conditions. Adjuvants are used in several vaccines to enhance the immune response and, depending on the type of adjuvant, can induce different immune responses (Bartsch et al. 2020). In context of anti-cancer vaccines, the vaccine-induced immune response should be skewed toward a T_H1 and Tc1 immune response, resulting in the induction of cytotoxic $CD8^+$ T cells and the production of IgG2a/IgG2b antibodies in mice and IgG1/IgG3 antibodies in humans, which are known to be the most efficient IgG antibodies in anti-cancer responses (Nimmerjahn and Ravetch 2005; Nimmerjahn et al. 2010; Shibuya et al. 2020; Zhao et al. 2023). Beside this, Tc17 cells have no direct cytotoxic effect, but appears to correlate with T_H17 cells that induce IgG antibodies with low galactosylation and sialylation levels (Pfeifle et al. 2017; Bartsch et al. 2020; Paul and Ohashi 2020).

As already reported in Bartsch et al. 2020 and Hanna Lunding's thesis, different adjuvants induce different T_H cell immune responses, resulting in the generation of different IgG subclasses and Fc-N glycosylation patterns, mediated by different GC responses (Bartsch et al. 2020; Lunding 2021)

Therefore, the aim of this thesis was to identify suitable adjuvants or adjuvant types for anti-tumor vaccines that can reduce tumor growth and whether this is associated with distinct IgG subclass and IgG Fc-N glycosylation patterns that can be used as biomarkers for predicting therapy efficacy or for selecting the right adjuvant depending on the underlying immune response.

To investigate this, a murine melanoma model with tumor cells expressing Ova as “tumor” antigen on their surface was established and used for vaccination experiments with soluble “tumor” antigen (Ova) in combination with different adjuvants. This was done in prophylactic and therapeutic settings.

In addition, the effect of checkpoint inhibition on antibody responses and tumor growth was investigated.

4.1 Prophylactic vaccination reduces tumor growth depending on the kind of adjuvant

After prophylactic vaccination, the number of surface lung metastasis was significantly reduced when the TLR-3 agonist Poly(I:C), the combination of Alum and Poly(I:C), and the two water-in-oil adjuvants CFA and eCFA were used in the vaccine. IFA and the TLR-4 agonist MPLA also moderately reduced tumor growth. TLR-4 activation is known to induce both T_H2 and T_H1 immune responses, whereas TLR-3 activation induces only T_H1 immune response (Zhao et al. 2023). In this study, the TLR-4 agonist MPLA also induced T_H1 cells as well as cytotoxic $CD8^+$ Tc1 cells, confirming the expectations for this adjuvant. The TLR-agonist Poly(I:C) and its mixture with Alum induced slightly more cytotoxic $CD8^+$ Tc1 cells, indicating an activation of an anti-tumor response. Furthermore, Alum-Poly(I:C) and low Poly(I:C) increased effector/memory $CD8^+$ T cells indicating activation of the tumor-specific immune response. CFA and in particular eCFA containing M.tb., which binds MINCLE, induces T_H2, T_H1 and T_H17 immune responses (Bartsch et al, 2020). T_H1 and Tc1 immune responses are important for tumor control mechanisms, which may explain the tumor reduction with the corresponding adjuvants (Coffman, Sher, and Seder 2010; Zhao et al. 2023). The induction of T_H17 cells by CFA and eCFA correlated with the induction of Tc17 cells.

To further test an adjuvant already used in cancer vaccines, Montanide ISA51 was included in the study. However, contrary to expectations, Montanide did not lead to tumor shrinkage, instead the number of metastases was as high as in the unvaccinated group in the model used. In addition, a T_H2 response was observed in the mice.

As reported by Rammensee’s group, “a single injection of a peptide together with a high dose of Montanide led to local sequestration and dysfunction of effector T cells” in mice, while “in patients, repeated injections of peptides in Montanide induced the formation of organized

lymphoid aggregates resembling tertiary lymphoid structures; however, infiltrating T cells were found to be dysfunctional" (Gouttefangeas and Rammensee 2018). The idea behind this was that patients were found to have increased circulating tumor-specific T cells, while the tumor was not reduced after vaccination (Gouttefangeas and Rammensee 2018). Hailemichael et al. 2013 found in a mouse melanoma model vaccinated with gp100 peptide and IFA or Montanide that tumor-specific $CD8^+$ T cells accumulate at the vaccination site and induce inflammatory conditions, but only partially reach the tumor site. However, the T cells at the vaccination site become dysfunctional and tumor regression does not occur. They therefore recommended the use of non-persistent adjuvants to prevent this highly inflammatory state at the injection site (Hailemichael et al. 2013). In addition, no anti-tumor effects were observed for Alum as an adjuvant, but Alum was already known to be T_H2-based and unsuitable for tumor vaccination in mice, although it has been mentioned that Alum induces not only T_H2 but also T_H1 immune responses in humans (J. Liu et al. 2022).

4.2 Different adjuvants induce different IgG subclasses and glycosylation patterns

In addition, the IgG subclass composition and Fc-N glycosylation resulting from these vaccinations were differentiated. To investigate how this looks like on the day of tumor challenge, when no tumor is yet present, the serum of vaccinated mice was analyzed on day 14 after vaccination. As previously reported by Bartsch et al. 2020, **antigen-specific IgG** levels were highest after vaccination with the water-in-oil adjuvants CFA and eCFA, followed by IFA, Montanide, Alum and then the TLR-agonists Poly(I:C) and MPLA (Bartsch et al. 2020).

The same trends were observed for anti-Ova IgG1. IgG1 is mainly induced by T_H2 immune responses and is therefore high for the mentioned adjuvants (Alum, Montanide, IFA, CFA, eCFA) (Zhao et al. 2023). Activation of TLRs mainly induces the production of IgG2a and IgG2b subclasses in mice, which explains the low IgG1 levels but high IgG2c levels (the equivalent of IgG2a in C57BL/6 mice) for Poly(I:C) and MPLA observed in this study (Zhang, Goldschmidt, and Salter 2012; Zhao et al. 2023). In addition, the **ratio of activating IgG2 to IgG1 (A/I (activation/inhibition))** was particularly high after vaccination with Poly(I:C) and MPLA, may be indicating higher potential tumor control efficacy depending on antibody "quality" (subclass).

The water-in-oil adjuvants, which also led to reduced tumor growth, had low A/I (IgG2/IgG1) ratios, because they induce high titers of all IgG subclasses, which might influence each other.

In this case, the reduced tumor growth may depend on the very high “quantity” (amount) of IgG.

To further characterize the antibody response, the Fc-N glycosylation was examined. Lower levels of **galactosylation** and **sialylation** are associated with more inflammatory immune conditions, such as in autoimmune diseases, while high levels of galactosylation, especially sialylation, of IgG are associated with autoimmune disease remission or steady state conditions (Oefner et al. 2012; Collin and Ehlers 2013; Bartsch et al. 2020).

Nevertheless, after vaccination, the initial, most likely extrafollicular plasma cell responses lead to the production of IgG subclass antibodies with increased levels of galactosylation and sialylation. Over time, these responses disappear and it is likely that GC-dependent IgG subclass plasma cell responses will develop with lower levels of galactosylation and sialylation (Bartsch et al. 2020; Buhre et al. 2024) . The adjuvant effects are observable in the GC-dependent PC response, wherein the lowest IgG galactosylation and sialylation levels are induced as follows: Montanide = IFA < CFA < eCFA (lowest gal/sial level) (Bartsch et al. 2020). The data have indicated that the short-term and long-term IgG responses after vaccination may mediate different functions (Buhre et al. 2024).

The level of galactosylation and sialylation of Ova-specific IgG1 on day 14 after vaccination was highest after vaccination with Alum as adjuvant, slightly further decreased with the TLR agonists and was lowest with water-in-oil adjuvants, Montanide, IFA, and especially M.tb. containing CFA and eCFA. Similar effects were observed for Ova-specific IgG2, especially for the sialylation levels. However, IgG2 glycosylation could not be detected in Alum-immunized mice due to low serum IgG2 levels. These results were already reported by Bartsch et al. 2020, who explained that the sialylation levels on day 14 depend on different GC responses and correlates with the expression level of St6gal1, which is decreased after vaccination with water-in-oil adjuvants (Bartsch et al. 2020). eCFA mainly induces IL-17-dependent signaling pathways. These pathways are induced by its cord factor M.tb., which activates IL-6/IL-23 signaling and in turn IL-17, which further influences the GC response to downregulate St6gal1 expression (Bartsch et al. 2020). Accordingly, the immune response results in high IgG titers with low levels of galactosylation and sialylation and inflammatory immune conditions (Bartsch et al. 2020; Lunding 2021).

In this study, the decreased levels of galactosylation and sialylation of the anti-Ova IgG1 and IgG2 subclass antibodies after vaccination with IFA, CFA, and eCFA may be successive associated with reduced tumor growth

However, it was still unclear how IgG agalactosylation may affect tumor growth. Noteworthy, in most cancers, low levels of galactosylation and sialylation of total IgG have been associated with inflammatory conditions (W. Wang et al. 2021). However, several murine studies have reported that low galactosylated and sialylated IgG antibodies enhance antibody-dependent neutrophil activation mediated by the activating FcγRIII and FcγRIV expressed on murine neutrophils (Albanesi et al. 2013; Epp et al. 2018; Lin et al. 2015; Clauder et al. 2021; Johnson et al. 2021). For example, Albanesi and colleagues demonstrated in a murine B16 melanoma model that monoclonal anti-gp-75 IgG2a antibody therapy depends on neutrophil-mediated tumor cell killing (Albanesi et al. 2013). Therefore, the effect of CFA and eCFA in this study could be expected to be dependent on antibody-dependent neutrophil activation. According to this expectation, the *in vitro* activation of neutrophils (ROS assay) by different sera collected from immunized mice was analyzed and showed that serum from eCFA-immunized mice induced higher ROS release from neutrophils compared to serum from Alum and Poly(I:C) immunized mice. In addition, IgG2a and agalactosylated IgG subclass antibodies induced increased neutrophil activation compared to IgG1 and sialylated IgG subclasses. Agalactosylated IgG2 may thereby be even more potent than agalactosylated IgG1.

Accordingly, the protecting functions induced by Poly(I:C) or CFA/eCFA may be different (Figure 4.1). The tumor control capacity of the TLR-3 agonist Poly(I:C) is associated with T_H1 and Tc1 induction and a high A/I ratio characterized by IgG2c/IgG1. IgG2c was previously reported to have the ability to activate ADCC and kill tumor cells in a murine melanoma model, while IgG1 was insufficient to kill tumor cells (Nimmerjahn and Ravetch 2005).The TLR-4 agonist MPLA also showed similar trends to Poly(I:C), but less pronounced. Instead, CFA and eCFA induces T_H17 and Tc17 immune responses, but low A/I ratios (IgG2/IgG1) due to high levels of both subclasses, IgG1 and IgG2. Thus, IgG1 may negatively influence the immune response, which needs to be considered. However, CFA and eCFA induced low levels of galactosylation and sialylation of IgG, which may enhance neutrophil-dependent tumor cell killing (Albanesi et al. 2013). However, the validity of these observations and correlations must be investigated in the future. Nevertheless, eCFA is only used in preclinical models because of its enormous side effects in human (Facciolà et al. 2022).

In addition, the level of **fucosylation** of IgG is very important for tumor control, because afucosylated murine IgG2a and IgG2b antibodies have a higher affinity for FcγRIV in mice (functional correspondent in humans: FcγRIIIA), triggering ADCC activity, an important mechanism for direct killing of tumor cells (Nimmerjahn and Ravetch 2005; Vidarsson, Dekkers, and Rispens 2014; Larsen et al. 2021; W. Wang et al. 2021). In this study, in general, high levels of murine IgG1 fucosylation were observed on day 14, which were highest with Ova-Alum immunization, but showed a slight reduction by using Poly(I:C) or eCFA as adjuvant. However, it should be noted, that the percentage differences in murine IgG1 fucosylation levels on day 14 were quite low (<1%) and could only be detected for IgG1, not for IgG2 (low IgG2 serum titers). However, no differences in IgG fucosylation have been described in previous studies probably because of high fucosylation levels and only small differences in mice (Braster et al. 2021).

Also, because distinct adjuvant effects may have a stronger influence in humans on IgG fucosylation, we further analyzed the effect of different adjuvants over time. Furthermore, soluble protein immunizations have been described to induce only low levels of afucosylated IgG and different application forms, in particular membrane-associated proteins, may induce higher afucosylation IgG1 levels (Larsen et al. 2021), which might then also be dependent on the adjuvant.

Accordingly, the time course of the fucosylation level of murine IgG subclasses was examined following vaccination with Ova and distinct adjuvants, as well as a boost of Ova without an adjuvant on day 28. All adjuvant groups exhibited an early murine IgG1 afucosylation peak at day 7 after vaccination. It is noteworthy that such an early afucosylation peak was also observed in human IgG following vaccination against SARS-CoV-2, which likely represents a very early extrafollicular response (van Coillie et al, 2023; Buhre et al. 2023). Subsequently, the afucosylation levels of murine IgG1 decreased as mentioned above by day 14 but were still higher when Poly(I:C) or eCFA was used as adjuvant. Interestingly, IgG1 afucosylation slightly temporarily increased again on day 33 after the immunized mice were boosted with Ova without adjuvant on day 28, but only with Poly(I:C) and eCFA. In addition, the TLR-4 agonist MPLA induces increased IgG1 afucosylation only after booster vaccination. Noteworthy, the boost with adenovirus-based or mRNA vaccines against SARS-CoV-2 did not temporarily increase IgG afucosylation (van Coillie et al, 2023; Buhre et al. 2023). Subsequently on day 42, the murine IgG1 afucosylation level of Ova-Poly(I:C) and Ova-eCFA immunized groups decreased again. Whether these temporarily increased murine IgG1 afucosylation level may also be

induced and be protective in the prophylactic model after tumor cell injection in the Ova-Poly(I:C) and Ova-eCFA groups is unclear and has to be investigated in the future.

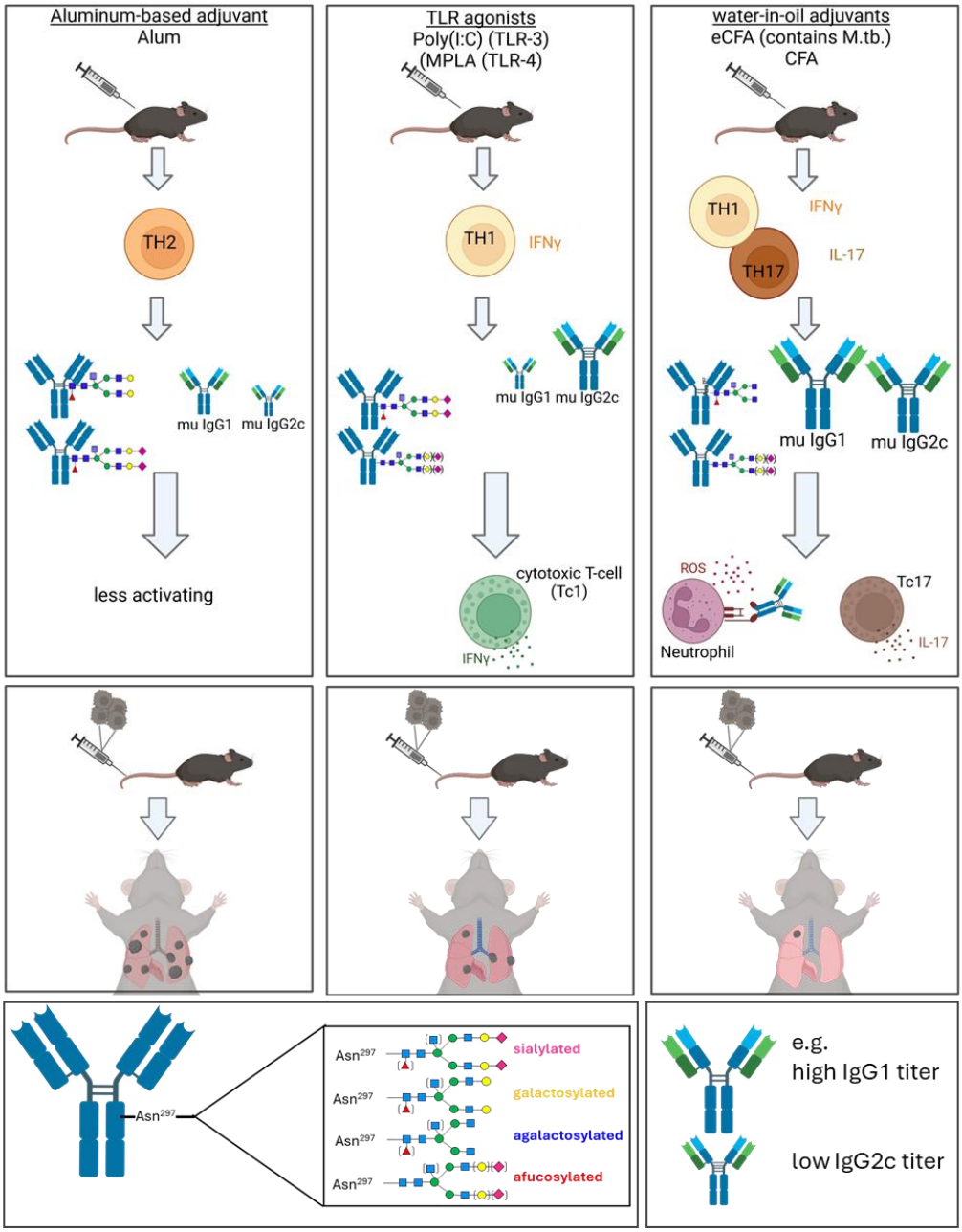

Figure 4.1: Graphical representation of the suggested effects of the various adjuvants used in the prophylactic tumor vaccination.
Depending on the type of adjuvant used, different immune cells and IgGs of different "quality" and "quantity" are induced. **Alum** induces less activating T_H2-dependent immune responses, resulting in low titers of IgG antibodies that are also highly glycosylated. **TLR agonists** induce T_H1-dependent immune responses resulting in high IgG2c to IgG1 antibody ratios and increased sialylated and/or afucosylated glycostructures. This could presumably trigger tumor killing mediated by cytotoxic T cells (or other immune cells (not shown)). **Water-in-oil** adjuvants induce T_H1 and T_H17 dependent immune responses resulting in high IgG1 and IgG2c antibody titers and low galactosylated and sialylated glycans. Some afucosylated glycans were also induced. These antibodies induced increased neutrophil activation (and IL-17 producing T cells), which may lead to increased tumor cell killing. The size of the antibodies shown represents the relative antibody titer (large antibody: high titer, small antibody: low titer).

4.3 Effect of therapeutic vaccination with different adjuvants on tumor growth

Furthermore, the effect of the different adjuvants was also investigated in a therapeutic setting where mice were vaccinated on day 9 after tumor challenge. Tumor growth showed similar results to the prophylactic setting, being reduced after vaccination with Poly(I:C) or IFA as adjuvant and not reduced when Alum or Montanide was used as adjuvant. However, in contrast to the prophylactic setting, CFA and eCFA did not induce tumor reduction, suggesting that the tumor cell-induced immune response may have influenced the vaccination-induced immune response and/or that the therapeutic vaccination induces a different, transient immune response, particularly in these two groups. Furthermore, the impact of the tumor cell-induced immune response on the vaccination-induced immune response in the context of therapeutic vaccination was a subject of interest. Accordingly, an analysis was conducted to compare the IgG responses between the prophylactic and therapeutic settings.

Interestingly, some mice in the unvaccinated tumor bearing group produced **anti-Ova IgG antibodies**, especially IgG2c, indicating an immune response against the tumor cells themselves or the membrane-bound Ova antigen. The ratio of IgG2c/IgG1was also high in the unvaccinated group. This could be explained by the high IgG2c titer induced by the tumor cells themselves. In general, tumor cells induce tolerance mechanisms to perform immune escape, for which an induction of tolerogenic IgG1 would be assumed (Oefner et al. 2012; Walters et al. 2023). In this case, however, an increased IgG2c titer was found, which would be associated with improved tumor control. In fact, this is consistent with the observation that Ova-bearing tumor cells in mice grow more slowly than non-Ova-bearing tumor cells (own observation, not shown here).

Furthermore, in the therapeutic setting, Alum resulted in increased anti-Ova IgG2c titers, which were almost as high as in IFA-immunized mice. The same effect was observed for Montanide, but it induced the highest IgG2c and IgG2b titers, together with eCFA, of the groups studied. This was not seen in the prophylactic setting. Interestingly, Montanide was the only adjuvant that induced IgG3 subclass titers. Nevertheless, the levels of IgG2c were elevated in the Poly(I:C) treated group. However, these levels did not appear to be sufficient to reduce tumor growth in the Ova-Alum and Ova-Montanide groups.

In addition, **Fc-N glycosylation** was analyzed in this setting and showed no obvious differences between day 12/14 of the prophylactic setting and day 21 of the therapeutic setting, also not for CFA and eCFA.

In general, the tumor cell-induced immune response appears to have some, but small, influence on the vaccine-induced immune response, but the vaccine-induced immune response was dominant for all adjuvant groups in the therapeutic setting.

However, the comparable immune responses observed after Ova-CFA or Ova-eCFA vaccination in the therapeutic and prophylactic tumor settings could not explain the observed differences in tumor growth in these two groups between the two settings. However, the observations described here, were only assumptions.

4.4 Effects of vaccination on tumor clearance depend on the type of adjuvant and the timing of vaccination

The results show that vaccination with a soluble "tumor" protein antigen together with different adjuvants induces different immune responses and differences in tumor reduction.

The TLR-agonists showed tumor clearance, especially Poly(I:C). Poly(I:C) activates TLR-3, which leads to the induction of IFNγ-producing cytotoxic Tc1 $CD8^+$ T cells, which are important for tumor cell killing. The study also found an increased ratio of activating to inhibitory IgG subclasses, characterized by increased IgG2c and IgG2b subclass titers and low IgG1 titers. IgG2c/b have been reported to have higher Fc-mediated effector functions compared to IgG1 in mice (Nimmerjahn and Ravetch 2005; Nimmerjahn et al. 2010; Shibuya et al. 2020). The high IgG2c/b to IgG1 ratio may also contribute e.g. to complement activation and complement-enhancing immune cell activation (Peschke et al. 2017; Lilienthal et al. 2018). Poly(I:C) leads to a temporary reduction in IgG1 fucosylation after vaccination. This may indicate decreased binding to FcγRIIB and thus an increased activation ratio (Nimmerjahn and Ravetch 2005). IgG2 afucosylation could not be detected in this study. However IgG2 induction would be preferable, and afucosylated IgG2 would further enhances ADCC activity through increased binding to FcγRIV (Nimmerjahn and Ravetch 2005). Similar trends in IgG1 afucosylation were observed with MPLA, but to a lesser extent. This further suggests that the injection of tumor cells after vaccination may also act as a "boost" and thus contribute to tumor reduction.

Alum and Montanide probably failed to protect from tumor growth because of the dominant IgG1 response. The function of IgG1 may overcome the function of IgG2c by blocking IgG2c function. Shibuya et al. 2020 have shown that antigen-specific IgG1 can inhibit ADCC by antigen-specific IgG2 by competitively disrupting IgG2 binding to the antigen (Shibuya et al. 2020). Similar effects have been shown in humans, where IgG4 (functional homologous to murine IgG1) interferes with Fc-mediated effector functions (Irrgang et al. 2022).

The water-in-oil adjuvants also led to reduced tumor growth in the prophylactic setting, except for Montanide. IFA, CFA and eCFA induced high IgG subclass level with the highest IgG2/IgG1 ratio for IFA. The IgG response of Montanide was dominated by IgG1.

eCFA induced higher frequencies of effector $CD4^+$ and $CD8^+$ T cells, as well as high T_H17 and Tc17 cells. The highest levels of T_H17 and Tc17 cells, which were associated with the induction of low IgG subclass galactosylation and sialylation levels on day 14 after vaccination, indicating that eCFA mainly induces IL-17-dependent signaling pathways (Bartsch et al. 2020; Lunding 2021). Accordingly, the immune response in this study results in high IgG titers with low levels of galactosylation and sialylation and inflammatory immune conditions.

In particular low galactosylated IgG2c levels may have the power to activate neutrophils for enhancing ADCC and tumor clearance in the prophylactic tumor-vaccination setting (Albanesi et al. 2013; Epp et al. 2018; Lin et al. 2015; Clauder et al. 2021; Johnson et al. 2021). However, these underlying mechanisms remain to be verified.

As mentioned in the introduction, vaccination-induced IgG subclass glycosylation patterns follow a certain repeating curve (Figure 1.9). Initial IgG responses from extrafollicular plasma cells or plasma cells differentiated from reactivated memory B cells (after boosting) produce highly galactosylated and sialylated IgG subclass antibodies (Bartsch et al. 2020; Buhre et al. 2024). Over time, when GC-dependent PCs dominate, the galactosylation and sialylation levels of IgG subclasses decrease, especially with water-in-oil adjuvants particularly with CFA and eCFA (Bartsch et al. 2020; Buhre et al. 2024).

However, on day 7 after immunization (day 16 after tumor cell injection) in the therapeutic setting (which was not analyzed in this work) galactosylation and sialylation levels could be high according to the time course of glycosylation (Figure 1.9). Therefore, after immunization with CFA or eCFA in the therapeutic setting, there would be no formation of IgG with low galactosylation and sialylation that could contribute to tumor control in the given time frame.

Subsequently, neutrophil-mediated tumor killing might not occur. IFA may still show protective effects associated with the high IgG2/IgG1 ratio as with Poly(I:C).

However, the time frame used in this melanoma models was quite limited, due to rapid tumor growth and the resulting predetermined end of the experiments. However, repeated vaccinations (boosters) would limit the success, as the galactosylation and sialylation of the IgG subclasses would increase again after each booster vaccination.

In addition, Ova was used in this study as soluble "tumor" antigen, which may have inhibited the induction of higher levels of afucosylated IgG subclass antibodies. Larsen et al. 2021 observed that an antigen must be membrane-associated to induce afucosylated antibodies, because afucosylated antibodies were found only against enveloped viruses (e.g. HIV, SARS-Cov-2, CMV), but not against non-enveloped viruses (e.g. Parvovirus B19) (Larsen et al. 2021).

Therefore, we would expect a higher degree of afucosylation when using a membrane-bound antigen.

Accordingly, the TLR agonists and the water-in-oil adjuvants, IFA, CFA and eCFA, may be acting through different mechanisms (Figure 4.1).

Therefore, the selection of the correct adjuvant and the characteristics of the antigen used in vaccines should be considered, and the induced IgG subclass composition may provide insights into the underlying immune response and disease outcome (Vidarsson, Dekkers, and Rispens 2014; Cobb 2019; Bartsch et al. 2020).

In addition, specific antibody responses induced by different adjuvants can be used as biomarkers to characterize the underlying T cell response, such as the induction of T_H17 and Tc17 cells, which would be important in predicting therapeutic efficacy.

4.5 Immune checkpoint inhibitors influence the vaccine-induced immune response and the tumor-related immune response

One of the most commonly used immunotherapies for cancer, including melanoma, are checkpoint inhibition, such as anti-PD-1 and anti-CTLA-4 therapies, which aim to boost the T cell response against the tumor (Seidel, Otsuka, and Kabashima 2018; Zahavi and Weiner 2020). However underlying mechanisms are still unclear.

Therefore, a further aim of this study was to investigate the effect of checkpoint inhibition on the antigen-specific immune response. In addition, the underlying immune response during anti-PD-1 therapy was investigated in a melanoma model.

Anti-PD-1 therapy resulted in increased proportions of anti-Ova $IgG1^+$ GCs and PCs, while a trend was observed for $IgG2^+$ GCs and PCs in the immunization model. Similar trends were observed with anti-CTLA-4 treatment, but to a lesser extent. In addition, St6gal1 expression was significantly reduced by blocking PD-1 and CTLA-4 in Ova^+IgG1^+ PCs and GCs (no significance for CTLA-4 in GCs) in the immunization experiment.

Similar trends were observed in the tumor model, where St6gal1 expression was significantly reduced in all GCs and $IgG2a,b^+$ GCs after PD-1 blockade. This suggest that both blocking antibodies induce GCs and PCs with reduced St6gal1 expression and IgG antibodies with reduced levels of galactosylation and sialylation.

These results suggest that PD-1 blockade induces pro-inflammatory immune responses, while similar trends were observed when CTLA-4 was blocked. The explanation for the lesser effect of anti-CTLA-4 compared to anti-PD-1 may be that anti-CTLA-4 mainly blocks T_{regs} and their inhibitory function, whereas anti-PD-1 blocks inhibitory signaling in activated T cells, B cells, NK cells and T_{regs}, leading to greater activation of immune cells, especially anti-tumor T cells (Juneja et al. 2017; Seidel, Otsuka, and Kabashima 2018; Zahavi and Weiner 2020). In addition, some tumor cells express PD-1, which they use to evade from the immune system.

The reduced galactosylation and sialylation may also increase neutrophil-mediated tumor killing (Albanesi et al. 2013; Epp et al. 2018; Lin et al. 2015; Clauder et al. 2021; Johnson et al. 2021) as suggested for the vaccinations with CFA and eCFA.

The results of these experiments may also be used to find suitable combination therapies with checkpoint inhibitors and tumor-specific vaccinations for the treatment of melanoma.

4.6 Outlook

This study has shown that the efficacy of cancer vaccination depends on the type of adjuvant and additionally on the timing of vaccination. Different adjuvants appear to be able to induce different protecting mechanisms. One possible might be to select adjuvants that elicit T_H1 and Tc1 immune responses and induce high IgG2c/b subclass titers but low IgG1 subclass titers (in humans: high IgG1 and IgG3 and low IgG2 and IgG4). Poly(I:C) has already been identified as a suitable adjuvant, but its derivative Poly(ICLC), which has a higher stability, was also found to be beneficial for tumor control (De Waele et al. 2021). Results of another study showed that the MyD88 signaling pathway induced by TLRs (except TLR3) is required for early GC formation and enhanced antibody class switch recombination (CSR) to IgG2c, and is important for IFNγ production (Lee et al. 2019). This knowledge can be used to select the appropriate adjuvant.

Another possibility might be the additional induction of low galactosylation and sialylation levels of murine IgG2c/IgG2b (human IgG1 and IgG3). This would enhance effector functions such as ADCC by neutrophils to kill tumor cells.

Furthermore, membrane-associated “tumor” antigens may be used to enhance the induction of afucosylated IgG subclasses.

Such vaccination therapies may be combined with checkpoint inhibitors.

In addition, different adjuvants can be combined to target different innate immune responses or additionally include cytokines such as IL-2, which supports the proliferation and effector function of immune cells (Aranda et al. 2011; Moynihan et al. 2016). It would also be interesting to analyze tumor-infiltrating lymphocytes (TILs) in addition to splenic lymphocytes to learn more about tumor-specific immune responses. Furthermore, additional *vitro* assays can provide information on the effector functions of the induced antibodies, e.g. by NK cells, neutrophils or other immune cells. Furthermore, immunotherapies can be combined with dietary interventions to increase the effectiveness of the therapy by altering the gut microbiome.

5. References

Ada, Gordon. 2005. "Overview of Vaccines and Vaccination." *Molecular Biotechnology* 29 (3): 255–71. https://doi.org/10.1385/MB:29:3:255.

Ai, Wenchao, Haishan Li, Naining Song, Lei Li, and Huiming Chen. 2013. "Optimal Method to Stimulate Cytokine Production and Its Use in Immunotoxicity Assessment." *International Journal of Environmental Research and Public Health* 10 (9): 3834–42. https://doi.org/10.3390/ijerph10093834.

Albanesi, Marcello, David A. Mancardi, Friederike Jönsson, Bruno Iannascoli, Laurence Fiette, James P. Di Santo, Clifford A. Lowell, and Pierre Bruhns. 2013. "Neutrophils Mediate Antibody-Induced Antitumor Effects in Mice." *Blood* 122 (18): 3160–64. https://doi.org/10.1182/blood-2013-04-497446.

Albanesi, Marcello, David A. Mancardi, Lynn E. Macdonald, Bruno Iannascoli, Laurence Zitvogel, Andrew J. Murphy, Jeanette H. Leusen, and Pierre Bruhns. 2012. "Cutting Edge: FcγRIII (CD16) and FcγRI (CD64) Are Responsible for Anti-Glycoprotein 75 Monoclonal Antibody TA99 Therapy for Experimental Metastatic B16 Melanoma." *The Journal of Immunology* 189 (12): 5513–17. https://doi.org/10.4049/jimmunol.1201511.

Alter, Galit, Tom H. M. Ottenhoff, and Simone A. Joosten. 2018. "Antibody Glycosylation in Inflammation, Disease and Vaccination." *Seminars in Immunology*, Immune Correlates of Vaccine Adjuvanticity, Immunogenicity and Efficacy in Infectious Diseases and Cancer., 39 (October):102–10. https://doi.org/10.1016/j.smim.2018.05.003.

Anthony, Robert M., Toshihiko Kobayashi, Fredrik Wermeling, and Jeffrey V. Ravetch. 2011. "Intravenous Gammaglobulin Suppresses Inflammation through a Novel TH2 Pathway." *Nature* 475 (7354): 110–13. https://doi.org/10.1038/nature10134.

Aranda, Fernando, Diana Llopiz, Nancy Díaz-Valdés, José Ignacio Riezu-Boj, Jaione Bezunartea, Marta Ruiz, Marta Martínez, et al. 2011. "Adjuvant Combination and Antigen Targeting as a Strategy to Induce Polyfunctional and High-Avidity T-Cell Responses against Poorly Immunogenic Tumors." *Cancer Research* 71 (9): 3214–24. https://doi.org/10.1158/0008-5472.CAN-10-3259.

Bartsch, Yannic C. 2019. "The Role of IL-6 in Vaccine-Induced IgG Fc Glycosylation." Lübeck: University of Lübeck.

Bartsch, Yannic C., Simon Eschweiler, Alexei Leliavski, Hanna B. Lunding, Sander Wagt, Janina Petry, Gina-Maria Lilienthal, et al. 2020. "IgG Fc Sialylation Is Regulated during the Germinal Center Reaction Following Immunization with Different Adjuvants." *Journal of Allergy and Clinical Immunology* 146 (3): 652-666.e11. https://doi.org/10.1016/j.jaci.2020.04.059.

Bartsch, Yannic C., Johann Rahmöller, Maria M. M. Mertes, Susanne Eiglmeier, Felix K. M. Lorenz, Alexander D. Stoehr, Dominique Braumann, et al. 2018. "Sialylated Autoantigen-Reactive IgG Antibodies Attenuate Disease Development in Autoimmune

Mouse Models of Lupus Nephritis and Rheumatoid Arthritis." *Frontiers in Immunology* 9. https://doi.org/10.3389/fimmu.2018.01183.

Bastian, Kayla, Emma Scott, David J. Elliott, and Jennifer Munkley. 2021. "FUT8 Alpha-(1,6)-Fucosyltransferase in Cancer." *International Journal of Molecular Sciences* 22 (1): 455. https://doi.org/10.3390/ijms22010455.

Baxter, David. 2014. "Active and Passive Immunization for Cancer." *Human Vaccines & Immunotherapeutics* 10 (7): 2123–29. https://doi.org/10.4161/hv.29604.

Beck, Alain, and Janice M. Reichert. 2012. "Marketing Approval of Mogamulizumab: A Triumph for Glyco-Engineering." *mAbs* 4 (4): 419–25. https://doi.org/10.4161/mabs.20996.

Bevaart, Lisette, Marco J.H. Jansen, Martine J. van Vugt, J. Sjef Verbeek, Jan G.J. van de Winkel, and Jeanette H.W. Leusen. 2006. "The High-Affinity IgG Receptor, FcγRI, Plays a Central Role in Antibody Therapy of Experimental Melanoma." *Cancer Research* 66 (3): 1261–64. https://doi.org/10.1158/0008-5472.CAN-05-2856.

Braster, Rens, Marijn Bögels, Hreinn Benonisson, Manfred Wuhrer, Rosina Plomp, Arthur E. H. Bentlage, Rianne Korthouwer, et al. 2021. "Afucosylated IgG Targets FcγRIV for Enhanced Tumor Therapy in Mice." *Cancers* 13 (10): 2372. https://doi.org/10.3390/cancers13102372.

Bruhns, Pierre. 2012. "Properties of Mouse and Human IgG Receptors and Their Contribution to Disease Models." *Blood* 119 (24): 5640–49. https://doi.org/10.1182/blood-2012-01-380121.

Buhre, Jana Sophia, Tamas Pongracz, Ulf Martin Geisen, Mareike Schubert, Wenjun Wang, Jan Nouta, Maureen Obara, et al. 2024. "Anti-TNF Therapy Impairs Both Short- and Long-Term IgG Responses after Repeated Vaccination." *Allergy*, July. https://doi.org/10.1111/all.16241.

Buhre, Jana Sophia, Tamas Pongracz, Inga Künsting, Anne S. Lixenfeld, Franziska Schmelter, Janina Petry, Bandik Föh, et al. 2023. "mRNA Vaccines against SARS-CoV-2 Induce Comparably Low Long-Term IgG Fc Galactosylation and Sialylation Levels but Increasing Long-Term IgG4 Responses Compared to an Adenovirus-Based Vaccine." *Frontiers in Immunology* 13 (January). https://doi.org/10.3389/fimmu.2022.1020844.

Caracciolo, Daniele, Caterina Riillo, Andrea Ballerini, Giuseppe Gaipa, Ludovic Lhermitte, Marco Rossi, Cirino Botta, et al. 2021. "Therapeutic Afucosylated Monoclonal Antibody and Bispecific T-Cell Engagers for T-Cell Acute Lymphoblastic Leukemia." *Journal for ImmunoTherapy of Cancer* 9 (2): e002026. https://doi.org/10.1136/jitc-2020-002026.

Carreno, Beatriz M., Vincent Magrini, Michelle Becker-Hapak, Saghar Kaabinejadian, Jasreet Hundal, Allegra A. Petti, Amy Ly, et al. 2015. "A Dendritic Cell Vaccine Increases the Breadth and Diversity of Melanoma Neoantigen-Specific T Cells." *Science* 348 (6236): 803–8. https://doi.org/10.1126/science.aaa3828.

Chae, Young Kwang, Ayush Arya, Wade Iams, Marcelo R. Cruz, Sunandana Chandra, Jaehyuk Choi, and Francis Giles. 2018. "Current Landscape and Future of Dual Anti-CTLA4

and PD-1/PD-L1 Blockade Immunotherapy in Cancer; Lessons Learned from Clinical Trials with Melanoma and Non-Small Cell Lung Cancer (NSCLC)." *Journal for ImmunoTherapy of Cancer* 6 (1): 39. https://doi.org/10.1186/s40425-018-0349-3.

Chen, Gang, Alexander C. Huang, Wei Zhang, Gao Zhang, Min Wu, Wei Xu, Zili Yu, et al. 2018. "Exosomal PD-L1 Contributes to Immunosuppression and Is Associated with Anti-PD-1 Response." *Nature* 560 (7718): 382–86. https://doi.org/10.1038/s41586-018-0392-8.

Christensen, Dennis. 2016. "Vaccine Adjuvants: Why and How." *Human Vaccines & Immunotherapeutics* 12 (10): 2709–11. https://doi.org/10.1080/21645515.2016.1219003.

Ciccimarra, F., F. S. Rosen, E. Schneeberger, and E. Merler. 1976. "Failure of Heavy Chain Glycosylation of IgG in Some Patients with Common, Variable Agammaglobulinemia." *The Journal of Clinical Investigation* 57 (5): 1386–90. https://doi.org/10.1172/JCI108407.

Clauder, Ann-Katrin, Anna Kordowski, Yannic C. Bartsch, Gabriele Köhl, Gina-Maria Lilienthal, Larissa N. Almeida, Timo Lindemann, et al. 2021. "IgG Fc N-Glycosylation Translates MHCII Haplotype into Autoimmune Skin Disease." *Journal of Investigative Dermatology* 141 (2): 285–94. https://doi.org/10.1016/j.jid.2020.06.022.

Cobb, Brian A. 2019. "The History of IgG Glycosylation and Where We Are Now." *Glycobiology* 30 (4): 202–13. https://doi.org/10.1093/glycob/cwz065.

Coffman, Robert L., Alan Sher, and Robert A. Seder. 2010. "Vaccine Adjuvants: Putting Innate Immunity to Work." *Immunity* 33 (4): 492–503. https://doi.org/10.1016/j.immuni.2010.10.002.

Cohen Saban, Noy, Adam Yalin, Tomer Landsberger, Ran Salomon, Ajjai Alva, Tali Feferman, Ido Amit, and Rony Dahan. 2023. "Fc Glycoengineering of a PD-L1 Antibody Harnesses Fcγ Receptors for Increased Antitumor Efficacy." *Science Immunology* 8 (81): eadd8005. https://doi.org/10.1126/sciimmunol.add8005.

Coillie, Julie Van, Tamas Pongracz, Johann Rahmöller, Hung-Jen Chen, Chiara Elisabeth Geyer, Lonneke A. van Vught, Jana Sophia Buhre, et al. 2023. "The BNT162b2 mRNA SARS-CoV-2 Vaccine Induces Transient Afucosylated IgG1 in Naive but Not in Antigen-Experienced Vaccinees." *eBioMedicine* 87 (January). https://doi.org/10.1016/j.ebiom.2022.104408.

Collin, Mattias, and Marc Ehlers. 2013. "The Carbohydrate Switch between Pathogenic and Immunosuppressive Antigen-Specific Antibodies." *Experimental Dermatology* 22 (8): 511–14. https://doi.org/10.1111/exd.12171.

Coudeville, Laurent, Fabrice Bailleux, Benjamin Riche, Françoise Megas, Philippe Andre, and René Ecochard. 2010. "Relationship between Haemagglutination-Inhibiting Antibody Titres and Clinical Protection against Influenza: Development and Application of a Bayesian Random-Effects Model." *BMC Medical Research Methodology* 10 (1): 18. https://doi.org/10.1186/1471-2288-10-18.

Cuzzubbo, Stefania, Sara Mangsbo, Divya Nagarajan, Kinana Habra, Alan Graham Pockley, and Stephanie E. B. McArdle. 2021. “Cancer Vaccines: Adjuvant Potency, Importance of Age, Lifestyle, and Treatments.” *Frontiers in Immunology* 11. https://www.frontiersin.org/articles/10.3389/fimmu.2020.615240.

Cyster, Jason G., and Christopher D. C. Allen. 2019. “B Cell Responses: Cell Interaction Dynamics and Decisions.” *Cell* 177 (3): 524–40. https://doi.org/10.1016/j.cell.2019.03.016.

Dai, Xiaoming, Yang Gao, and Wenyi Wei. 2022. “Post-Translational Regulations of PD-L1 and PD-1: Mechanisms and Opportunities for Combined Immunotherapy.” *Seminars in Cancer Biology*, Targeting Cellular Signaling Pathways, 85 (October):246–52. https://doi.org/10.1016/j.semcancer.2021.04.002.

De Silva, Nilushi S., and Ulf Klein. 2015. “Dynamics of B Cells in Germinal Centres.” *Nature Reviews Immunology* 15 (3): 137–48. https://doi.org/10.1038/nri3804.

De Waele, Jorrit, Tias Verhezen, Sanne van der Heijden, Zwi N. Berneman, Marc Peeters, Filip Lardon, An Wouters, and Evelien L. J. M. Smits. 2021. “A Systematic Review on Poly(I:C) and Poly-ICLC in Glioblastoma: Adjuvants Coordinating the Unlocking of Immunotherapy.” *Journal of Experimental & Clinical Cancer Research* 40 (1): 213. https://doi.org/10.1186/s13046-021-02017-2.

Dekkers, Gillian, Theo Rispens, and Gestur Vidarsson. 2018. “Novel Concepts of Altered Immunoglobulin G Galactosylation in Autoimmune Diseases.” *Frontiers in Immunology* 9. https://www.frontiersin.org/article/10.3389/fimmu.2018.00553.

Dekkers, Gillian, Louise Treffers, Rosina Plomp, Arthur E. H. Bentlage, Marcella de Boer, Carolien A. M. Koeleman, Suzanne N. Lissenberg-Thunnissen, et al. 2017. “Decoding the Human Immunoglobulin G-Glycan Repertoire Reveals a Spectrum of Fc-Receptor- and Complement-Mediated-Effector Activities.” *Frontiers in Immunology* 8 (August). https://doi.org/10.3389/fimmu.2017.00877.

Delgado, Marisa, and Jose A. Garcia-Sanz. 2023. “Therapeutic Monoclonal Antibodies against Cancer: Present and Future.” *Cells* 12 (24): 2837. https://doi.org/10.3390/cells12242837.

DiLillo, David J., Koichi Yanaba, and Thomas F. Tedder. 2010. “B Cells Are Required for Optimal CD4+ and CD8+ T Cell Tumor Immunity: Therapeutic B Cell Depletion Enhances B16 Melanoma Growth in Mice.” *The Journal of Immunology* 184 (7): 4006–16. https://doi.org/10.4049/jimmunol.0903009.

Dühring, Lara, Janina Petry, Gina-Maria Lilienthal, Yannic C. Bartsch, Marie Kubiak, Clarissa Pfeufer, Selina Lehrian, et al. 2023. “Sialylation of IgE Reduces FcεRIα Interaction and Mast Cell and Basophil Activation in Vitro and Increases IgE Half-Life in Vivo.” *Allergy* 78 (8): 2301–5. https://doi.org/10.1111/all.15665.

Ehst, Benjamin D., Elizabeth Ingulli, and Marc K. Jenkins. 2003. “Development of a Novel Transgenic Mouse for the Study of Interactions Between CD4 and CD8 T Cells During Graft Rejection.” *American Journal of Transplantation* 3 (11): 1355–62. https://doi.org/10.1046/j.1600-6135.2003.00246.x.

Epp, Alexandra, Juliane Hobusch, Yannic C. Bartsch, Janina Petry, Gina-Maria Lilienthal, Carolien A. M. Koeleman, Simon Eschweiler, et al. 2018. "Sialylation of IgG Antibodies Inhibits IgG-Mediated Allergic Reactions." *Journal of Allergy and Clinical Immunology* 141 (1): 399-402.e8. https://doi.org/10.1016/j.jaci.2017.06.021.

Facciolà, Alessio, Giuseppa Visalli, Antonio Laganà, and Angela Di Pietro. 2022. "An Overview of Vaccine Adjuvants: Current Evidence and Future Perspectives." *Vaccines* 10 (5): 819. https://doi.org/10.3390/vaccines10050819.

Garcia-Hernandez, Maria de la Luz, Hiromasa Hamada, Joyce B. Reome, Sara K. Misra, Michael P. Tighe, and Richard W. Dutton. 2010. "Adoptive Transfer of Tumor-Specific Tc17 Effector T Cells Controls the Growth of B16 Melanoma in Mice." *The Journal of Immunology* 184 (8): 4215–27. https://doi.org/10.4049/jimmunol.0902995.

Gouttefangeas, Cécile, and Hans-Georg Rammensee. 2018. "Personalized Cancer Vaccines: Adjuvants Are Important, Too." *Cancer Immunology, Immunotherapy* 67 (12): 1911–18. https://doi.org/10.1007/s00262-018-2158-4.

Haan, Noortje de, Karli R. Reiding, Jasminka Krištić, Agnes L. Hipgrave Ederveen, Gordan Lauc, and Manfred Wuhrer. 2017. "The N-Glycosylation of Mouse Immunoglobulin G (IgG)-Fragment Crystallizable Differs Between IgG Subclasses and Strains." *Frontiers in Immunology* 8 (May):273953. https://doi.org/10.3389/fimmu.2017.00608.

Hailemichael, Yared, Zhimin Dai, Nina Jaffarzad, Yang Ye, Miguel A. Medina, Xue-Fei Huang, Stephanie M. Dorta-Estremera, et al. 2013. "Persistent Antigen at Vaccination Sites Induces Tumor-Specific CD8+ T Cell Sequestration, Dysfunction and Deletion." *Nature Medicine* 19 (4): 465–72. https://doi.org/10.1038/nm.3105.

Hamada, Hiromasa, Maria de la Luz Garcia-Hernandez, Joyce B. Reome, Sara K. Misra, Tara M. Strutt, Kai K. McKinstry, Andrea M. Cooper, Susan L. Swain, and Richard W. Dutton. 2009. "Tc17, a Unique Subset of CD8 T Cells That Can Protect against Lethal Influenza Challenge1." *The Journal of Immunology* 182 (6): 3469–81. https://doi.org/10.4049/jimmunol.0801814.

Han, Kai, Jutaek Nam, Jin Xu, Xiaoqi Sun, Xuehui Huang, Olamide Animasahun, Abhinav Achreja, et al. 2021. "Generation of Systemic Antitumour Immunity via the in Situ Modulation of the Gut Microbiome by an Orally Administered Inulin Gel." *Nature Biomedical Engineering* 5 (11): 1377–88. https://doi.org/10.1038/s41551-021-00749-2.

Hernandez, Juana, Tina Nielsen, Christian Klein, and Michael Wenger. n.d. "Obinutuzumab for the Treatment of Non-Hodgkin Lymphomas." Accessed October 17, 2023. https://www.nature.com/articles/d42473-018-00278-8.

Hess, Constanze, André Winkler, Alexandra K. Lorenz, Vivien Holecska, Véronique Blanchard, Susanne Eiglmeier, Anna-Lena Schoen, et al. 2013. "T Cell–Independent B Cell Activation Induces Immunosuppressive Sialylated IgG Antibodies." *The Journal of Clinical Investigation* 123 (9): 3788–96. https://doi.org/10.1172/JCI65938.

Hiltbrunner, Stefanie, Pia Larssen, Maria Eldh, Maria-Jose Martinez-Bravo, Arnika K. Wagner, Mikael C. I. Karlsson, and Susanne Gabrielsson. 2016. "Exosomal Cancer Immunotherapy Is Independent of MHC Molecules on Exosomes." *Oncotarget* 7 (25): 38707–17. https://doi.org/10.18632/oncotarget.9585.

Hoover, H. C., M. G. Surdyke, R. B. Dangel, L. C. Peters, and M. G. Hanna. 1985. "Prospectively Randomized Trial of Adjuvant Active-Specific Immunotherapy for Human Colorectal Cancer." *Cancer* 55 (6): 1236–43. https://doi.org/10.1002/1097-0142(19850315)55:6<1236::aid-cncr2820550616>3.0.co;2-#.

Irrgang, Pascal, Juliane Gerling, Katharina Kocher, Dennis Lapuente, Philipp Steininger, Katharina Habenicht, Monika Wytopil, et al. 2022. "Class Switch toward Noninflammatory, Spike-Specific IgG4 Antibodies after Repeated SARS-CoV-2 mRNA Vaccination." *Science Immunology* 8 (79): eade2798. https://doi.org/10.1126/sciimmunol.ade2798.

Irvine, Edward B, and Galit Alter. 2020. "Understanding the Role of Antibody Glycosylation through the Lens of Severe Viral and Bacterial Diseases." *Glycobiology* 30 (4): 241–53. https://doi.org/10.1093/glycob/cwaa018.

Iwasaki, Akiko, and Saad B. Omer. 2020. "Why and How Vaccines Work." *Cell* 183 (2): 290–95. https://doi.org/10.1016/j.cell.2020.09.040.

Jennewein, Madeleine F., Ilona Goldfarb, Sepideh Dolatshahi, Cormac Cosgrove, Francesca J. Noelette, Marina Krykbaeva, Jishnu Das, et al. 2019. "Fc Glycan-Mediated Regulation of Placental Antibody Transfer." *Cell* 178 (1): 202-215.e14. https://doi.org/10.1016/j.cell.2019.05.044.

Johnson, Mari, Lisa Stockdale, Noortje de Haan, Manfred Wuhrer, Jan Nouta, Carolien A. M. Koeleman, Jenny Clarke, et al. 2021. "Association of Antibody-Dependent Neutrophil Phagocytosis With Distinct Antibody Glycosylation Profiles Following Typhoid Vaccination." *Frontiers in Tropical Diseases* 2 (September). https://doi.org/10.3389/fitd.2021.742804.

Juneja, Vikram R., Kathleen A. McGuire, Robert T. Manguso, Martin W. LaFleur, Natalie Collins, W. Nicholas Haining, Gordon J. Freeman, and Arlene H. Sharpe. 2017. "PD-L1 on Tumor Cells Is Sufficient for Immune Evasion in Immunogenic Tumors and Inhibits CD8 T Cell Cytotoxicity." *Journal of Experimental Medicine* 214 (4): 895–904. https://doi.org/10.1084/jem.20160801.

Kaneko, Yoshikatsu, Falk Nimmerjahn, and Jeffrey V. Ravetch. 2006. "Anti-Inflammatory Activity of Immunoglobulin G Resulting from Fc Sialylation." *Science* 313 (5787): 670–73. https://doi.org/10.1126/science.1129594.

Karsten, Christian M., Manoj K. Pandey, Julia Figge, Regina Kilchenstein, Philip R. Taylor, Marcela Rosas, Jacqueline U. McDonald, et al. 2012. "Anti-Inflammatory Activity of IgG1 Mediated by Fc Galactosylation and Association of FcγRIIB and Dectin-1." *Nature Medicine* 18 (9): 1401–6. https://doi.org/10.1038/nm.2862.

Kleffel, Sonja, Christian Posch, Steven R. Barthel, Hansgeorg Mueller, Christoph Schlapbach, Emmanuella Guenova, Christopher P. Elco, et al. 2015. "Melanoma Cell-Intrinsic PD-1 Receptor Functions Promote Tumor Growth." *Cell* 162 (6): 1242–56. https://doi.org/10.1016/j.cell.2015.08.052.

Klein, Reinhild, Douglas M. Templeton, and Michael Schwenk. 2014. "Applications of Immunochemistry in Human Health: Advances in Vaccinology and Antibody Design

(IUPAC Technical Report)." *Pure and Applied Chemistry* 86 (10): 1573–1617. https://doi.org/10.1515/pac-2013-1028.

Knudsen, Niels Peter H., Anja Olsen, Cecilia Buonsanti, Frank Follmann, Yuan Zhang, Rhea N. Coler, Christopher B. Fox, et al. 2016. "Different Human Vaccine Adjuvants Promote Distinct Antigen-Independent Immunological Signatures Tailored to Different Pathogens." *Scientific Reports* 6 (1): 1–13. https://doi.org/10.1038/srep19570.

Koprowski, H, Z Steplewski, D Herlyn, and M Herlyn. 1978. "Study of Antibodies against Human Melanoma Produced by Somatic Cell Hybrids." *Proceedings of the National Academy of Sciences* 75 (7): 3405–9. https://doi.org/10.1073/pnas.75.7.3405.

Kurosaki, Tomohiro. 2010. "B-Lymphocyte Biology." *Immunological Reviews* 237 (1): 5–9. https://doi.org/10.1111/j.1600-065X.2010.00946.x.

Larsen, Mads Delbo, Erik L. de Graaf, Myrthe E. Sonneveld, H. Rosina Plomp, Jan Nouta, Willianne Hoepel, Hung-Jen Chen, et al. 2021. "Afucosylated IgG Characterizes Enveloped Viral Responses and Correlates with COVID-19 Severity." *Science* 371 (6532): eabc8378. https://doi.org/10.1126/science.abc8378.

LeBien, Tucker W., and Thomas F. Tedder. 2008. "B Lymphocytes: How They Develop and Function." *Blood* 112 (5): 1570–80. https://doi.org/10.1182/blood-2008-02-078071.

Lee, Michelle Sue Jann, Yayoi Natsume-Kitatani, Burcu Temizoz, Yukiko Fujita, Aki Konishi, Kyoko Matsuda, Yoshikatsu Igari, et al. 2019. "B Cell-Intrinsic MyD88 Signaling Controls IFN-γ-Mediated Early IgG2c Class Switching in Mice in Response to a Particulate Adjuvant." *European Journal of Immunology* 49 (9): 1433–40. https://doi.org/10.1002/eji.201848084.

Lei, Qingyang, Dan Wang, Kai Sun, Liping Wang, and Yi Zhang. 2020. "Resistance Mechanisms of Anti-PD1/PDL1 Therapy in Solid Tumors." *Frontiers in Cell and Developmental Biology* 8. https://www.frontiersin.org/articles/10.3389/fcell.2020.00672.

Li, Yan, Lisa Elmén, Igor Segota, Yibo Xian, Roberto Tinoco, Yongmei Feng, Yu Fujita, et al. 2020. "Prebiotic-Induced Anti-Tumor Immunity Attenuates Tumor Growth." *Cell Reports* 30 (6): 1753-1766.e6. https://doi.org/10.1016/j.celrep.2020.01.035.

Lilienthal, Gina-Maria, Johann Rahmöller, Janina Petry, Yannic C. Bartsch, Alexei Leliavski, and Marc Ehlers. 2018. "Potential of Murine IgG1 and Human IgG4 to Inhibit the Classical Complement and Fcγ Receptor Activation Pathways." *Frontiers in Immunology* 9 (May):958. https://doi.org/10.3389/fimmu.2018.00958.

Lin, Chin-Wei, Ming-Hung Tsai, Shiou-Ting Li, Tsung-I Tsai, Kuo-Ching Chu, Ying-Chih Liu, Meng-Yu Lai, et al. 2015. "A Common Glycan Structure on Immunoglobulin G for Enhancement of Effector Functions." *Proceedings of the National Academy of Sciences* 112 (34): 10611–16. https://doi.org/10.1073/pnas.1513456112.

Liu, Jian, Minyang Fu, Manni Wang, Dandan Wan, Yuquan Wei, and Xiawei Wei. 2022. "Cancer Vaccines as Promising Immuno-Therapeutics: Platforms and Current Progress." *Journal of Hematology & Oncology* 15 (1): 28. https://doi.org/10.1186/s13045-022-01247-x.

Liu, Xuerun, Luoyang Wang, Nan Jing, Guoqiang Jiang, and Zheng Liu. 2020. “Biostimulating Gut Microbiome with Bilberry Anthocyanin Combo to Enhance Anti-PD-L1 Efficiency against Murine Colon Cancer.” *Microorganisms* 8 (2): 175. https://doi.org/10.3390/microorganisms8020175.

Lm, Nadler, Stashenko P, Hardy R, Kaplan Wd, Button Ln, Kufe Dw, Antman Kh, and Schlossman Sf. 1980. “Serotherapy of a Patient with a Monoclonal Antibody Directed against a Human Lymphoma-Associated Antigen.” *Cancer Research* 40 (9). https://pubmed.ncbi.nlm.nih.gov/7427932/.

Löffler, Markus W., P. Anoop Chandran, Karoline Laske, Christopher Schroeder, Irina Bonzheim, Mathias Walzer, Franz J. Hilke, et al. 2016. “Personalized Peptide Vaccine-Induced Immune Response Associated with Long-Term Survival of a Metastatic Cholangiocarcinoma Patient.” *Journal of Hepatology* 65 (4): 849–55. https://doi.org/10.1016/j.jhep.2016.06.027.

Lopes, Ana, Daniel Machado, Susana Pedreiro, Ana Henriques, Isabel Silva, Beatriz Tavares, Maria Jesus Inácio, et al. 2013. “Different Frequencies of Tc17/Tc1 and Th17/Th1 Cells in Chronic Spontaneous Urticaria.” *International Archives of Allergy and Immunology* 161 (2): 155–62. https://doi.org/10.1159/000345401.

Lorentzen, Cathrine Lund, Julie Westerlin Kjeldsen, Eva Ehrnrooth, Mads Hald Andersen, and Inge Marie Svane. 2023. “Long-Term Follow-up of Anti-PD-1 Naïve Patients with Metastatic Melanoma Treated with IDO/PD-L1 Targeting Peptide Vaccine and Nivolumab.” *Journal for ImmunoTherapy of Cancer* 11 (5): e006755. https://doi.org/10.1136/jitc-2023-006755.

Lu, Lenette L., Amy W. Chung, Tracy R. Rosebrock, Musie Ghebremichael, Wen Han Yu, Patricia S. Grace, Matthew K. Schoen, et al. 2016. “A Functional Role for Antibodies in Tuberculosis.” *Cell* 167 (2): 433-443.e14. https://doi.org/10.1016/j.cell.2016.08.072.

Lunding, Hanna B. 2021. “Regulation of the Alpha2,6-Sialyltransferase and IgG Fc Glycosylation in Immunization-Induced Germinal Center Reactions.” Lübek: University of Lübeck.

Ma, Weijie, Brian Pham, and Tianhong Li. 2022. “Cancer Neoantigens as Potential Targets for Immunotherapy.” *Clinical & Experimental Metastasis* 39 (1): 51–60. https://doi.org/10.1007/s10585-021-10091-1.

Malkiel, Susan, Ashley N. Barlev, Yemil Atisha-Fregoso, Jolien Suurmond, and Betty Diamond. 2018. “Plasma Cell Differentiation Pathways in Systemic Lupus Erythematosus.” *Frontiers in Immunology* 9. https://www.frontiersin.org/articles/10.3389/fimmu.2018.00427.

Manz, Rudolf A., Andreas Thiel, and Andreas Radbruch. 1997. “Lifetime of Plasma Cells in the Bone Marrow.” *Nature* 388 (6638): 133–34. https://doi.org/10.1038/40540.

Marriott, Morgan, Brittany Post, and Lipika Chablani. 2023. “A Comparison of Cancer Vaccine Adjuvants in Clinical Trials.” *Cancer Treatment and Research Communications* 34 (January):100667. https://doi.org/10.1016/j.ctarc.2022.100667.

Moynihan, Kelly D., Cary F. Opel, Gregory L. Szeto, Alice Tzeng, Eric F. Zhu, Jesse M. Engreitz, Robert T. Williams, et al. 2016. “Eradication of Large Established Tumors in Mice by Combination Immunotherapy That Engages Innate and Adaptive Immune Responses.” *Nature Medicine* 22 (12): 1402–10. https://doi.org/10.1038/nm.4200.

Murphy, Kenneth, and Casey Weaver. 2018. *Janeway Immunologie*. Berlin, Heidelberg: Springer. https://doi.org/10.1007/978-3-662-56004-4.

Nelde, Annika, Hans-Georg Rammensee, and Juliane S. Walz. 2021. “The Peptide Vaccine of the Future.” *Molecular & Cellular Proteomics* 20 (January):100022. https://doi.org/10.1074/mcp.R120.002309.

Nieuwenhuis, P., and D. Opstelten. 1984. “Functional Anatomy of Germinal Centers.” *The American Journal of Anatomy* 170 (3): 421–35. https://doi.org/10.1002/aja.1001700315.

Nigro, Cristiana Lo, Marco Macagno, Dario Sangiolo, Luca Bertolaccini, Massimo Aglietta, and Marco Carlo Merlano. 2019. “NK-Mediated Antibody-Dependent Cell-Mediated Cytotoxicity in Solid Tumors: Biological Evidence and Clinical Perspectives.” *Annals of Translational Medicine* 7 (5): 27. https://doi.org/10.21037/atm.2019.01.42.

Nimmerjahn, Falk, Anja Lux, Heike Albert, Melissa Woigk, Christian Lehmann, Diana Dudziak, Patrick Smith, and Jeffrey V. Ravetch. 2010. “FcγRIV Deletion Reveals Its Central Role for IgG2a and IgG2b Activity in Vivo.” *Proceedings of the National Academy of Sciences* 107 (45): 19396–401. https://doi.org/10.1073/pnas.1014515107.

Nimmerjahn, Falk, and Jeffrey V. Ravetch. 2005. “Divergent Immunoglobulin G Subclass Activity Through Selective Fc Receptor Binding.” *Science* 310 (5753): 1510–12. https://doi.org/10.1126/science.1118948.

Oberli, Matthias A., Andreas M. Reichmuth, J. Robert Dorkin, Michael J. Mitchell, Owen S. Fenton, Ana Jaklenec, Daniel G. Anderson, Robert Langer, and Daniel Blankschtein. 2017. “Lipid Nanoparticle Assisted mRNA Delivery for Potent Cancer Immunotherapy.” *Nano Letters* 17 (3): 1326–35. https://doi.org/10.1021/acs.nanolett.6b03329.

Oefner, Carolin M., André Winkler, Constanze Hess, Alexandra K. Lorenz, Vivien Holecska, Melanie Huxdorf, Tim Schommartz, et al. 2012. “Tolerance Induction with T Cell–Dependent Protein Antigens Induces Regulatory Sialylated IgGs.” *Journal of Allergy and Clinical Immunology* 129 (6): 1647-1655.e13. https://doi.org/10.1016/j.jaci.2012.02.037.

Ollila, Thomas A., Ilyas Sahin, and Adam J. Olszewski. 2019. “<p>Mogamulizumab: A New Tool for Management of Cutaneous T-Cell Lymphoma</P>.” *OncoTargets and Therapy* 12 (February):1085–94. https://doi.org/10.2147/OTT.S165615.

O’Neil-Andersen, Nancy J., and David A. Lawrence. 2002. “Differential Modulation of Surface and Intracellular Protein Expression by T Cells after Stimulation in the Presence of Monensin or Brefeldin A.” *Clinical and Vaccine Immunology* 9 (2): 243–50. https://doi.org/10.1128/CDLI.9.2.243-250.2001.

Ortho Multicenter Transplant Study Group. 1985. “A Randomized Clinical Trial of OKT3 Monoclonal Antibody for Acute Rejection of Cadaveric Renal Transplants.” *The New England Journal of Medicine* 313 (6): 337–42. https://doi.org/10.1056/NEJM198508083130601.

Ott, Patrick A., Zhuting Hu, Derin B. Keskin, Sachet A. Shukla, Jing Sun, David J. Bozym, Wandi Zhang, et al. 2017. “An Immunogenic Personal Neoantigen Vaccine for Patients with Melanoma.” *Nature* 547 (7662): 217–21. https://doi.org/10.1038/nature22991.

Overwijk, Willem W., and Nicholas P. Restifo. 2000. “B16 as a Mouse Model for Human Melanoma.” *Current Protocols in Immunology* 39 (1): 20.1.1-20.1.29. https://doi.org/10.1002/0471142735.im2001s39.

Paul, Michael St, Samuel D. Saibil, Scott C. Lien, SeongJun Han, Azin Sayad, David T. Mulder, Carlos R. Garcia-Batres, et al. 2020. “IL6 Induces an IL22+ CD8+ T-Cell Subset with Potent Antitumor Function.” *Cancer Immunology Research* 8 (3): 321–33. https://doi.org/10.1158/2326-6066.CIR-19-0521.

Paul, Sourav, Neeraja Kulkarni, Shilpi, and Girdhari Lal. 2016. “Intratumoral Natural Killer Cells Show Reduced Effector and Cytolytic Properties and Control the Differentiation of Effector Th1 Cells.” *Oncoimmunology* 5 (12). https://doi.org/10.1080/2162402X.2016.1235106.

Peng, Miao, Yongzhen Mo, Yian Wang, Pan Wu, Yijie Zhang, Fang Xiong, Can Guo, et al. 2019. “Neoantigen Vaccine: An Emerging Tumor Immunotherapy.” *Molecular Cancer* 18 (1): 128. https://doi.org/10.1186/s12943-019-1055-6.

Pereira, Natasha A., Kah Fai Chan, Pao Chun Lin, and Zhiwei Song. 2018. “The ‘Less-Is-More’ in Therapeutic Antibodies: Afucosylated Anti-Cancer Antibodies with Enhanced Antibody-Dependent Cellular Cytotoxicity.” *mAbs* 10 (5): 693–711. https://doi.org/10.1080/19420862.2018.1466767.

Petry, Janina, Johann Rahmöller, Lara Dühring, Gina-Maria Lilienthal, Selina Lehrian, Jana Sophia Buhre, Yannic C. Bartsch, et al. 2021. “Enriched Blood IgG Sialylation Attenuates IgG-Mediated and IgG-Controlled-IgE-Mediated Allergic Reactions.” *Journal of Allergy and Clinical Immunology* 147 (2): 763–67. https://doi.org/10.1016/j.jaci.2020.05.056.

Pfeifle, René, Tobias Rothe, Natacha Ipseiz, Hans U. Scherer, Stephan Culemann, Ulrike Harre, Jochen A. Ackermann, et al. 2017. “Regulation of Autoantibody Activity by the IL-23–TH17 Axis Determines the Onset of Autoimmune Disease.” *Nature Immunology* 18 (1): 104–13. https://doi.org/10.1038/ni.3579.

Rammensee, Hans-Georg, Karl-Heinz Wiesmüller, P. Anoop Chandran, Henning Zelba, Elisa Rusch, Cécile Gouttefangeas, Daniel J. Kowalewski, et al. 2019. “A New Synthetic Toll-like Receptor 1/2 Ligand Is an Efficient Adjuvant for Peptide Vaccination in a Human Volunteer.” *Journal for ImmunoTherapy of Cancer* 7 (1): 307. https://doi.org/10.1186/s40425-019-0796-5.

RKI. 2019. “Krebs - Krebs in Deutschland.” 2020 2019. https://www.krebsdaten.de/Krebs/DE/Content/Publikationen/Krebs_in_Deutschland/krebs_in_deutschland_node.html.

Routy, Bertrand, Emmanuelle Le Chatelier, Lisa Derosa, Connie P. M. Duong, Maryam Tidjani Alou, Romain Daillère, Aurélie Fluckiger, et al. 2018. “Gut Microbiome Influences Efficacy of PD-1–Based Immunotherapy against Epithelial Tumors.” *Science* 359 (6371): 91–97. https://doi.org/10.1126/science.aan3706.

Sage, Peter T., and Arlene H. Sharpe. 2015. “T Follicular Regulatory Cells in the Regulation of B Cell Responses.” *Trends in Immunology* 36 (7): 410–18. https://doi.org/10.1016/j.it.2015.05.005.

Sahin, Ugur, Petra Oehm, Evelyna Derhovanessian, Robert A. Jabulowsky, Mathias Vormehr, Maike Gold, Daniel Maurus, et al. 2020. “An RNA Vaccine Drives Immunity in Checkpoint-Inhibitor-Treated Melanoma.” *Nature* 585 (7823): 107–12. https://doi.org/10.1038/s41586-020-2537-9.

Schumann, Julia, Katarina Stanko, Ulrike Schliesser, Christine Appelt, and Birgit Sawitzki. 2015. “Differences in CD44 Surface Expression Levels and Function Discriminates IL-17 and IFN-γ Producing Helper T Cells.” *PLOS ONE* 10 (7): e0132479. https://doi.org/10.1371/journal.pone.0132479.

Sckisel, Gail D., Annie Mirsoian, Christine M. Minnar, Marka Crittenden, Brendan Curti, Jane Q. Chen, Bruce R. Blazar, Alexander D. Borowsky, Arta M. Monjazeb, and William J. Murphy. 2017. “Differential Phenotypes of Memory CD4 and CD8 T Cells in the Spleen and Peripheral Tissues Following Immunostimulatory Therapy.” *Journal for ImmunoTherapy of Cancer* 5 (1): 33. https://doi.org/10.1186/s40425-017-0235-4.

Seidel, Judith A., Atsushi Otsuka, and Kenji Kabashima. 2018. “Anti-PD-1 and Anti-CTLA-4 Therapies in Cancer: Mechanisms of Action, Efficacy, and Limitations.” *Frontiers in Oncology* 8. https://doi.org/10.3389/fonc.2018.00086.

Seliger, Barbara, Ursula Wollscheid, Frank Momburg, Thomas Blankenstein, and Christoph Huber. 2001. “Characterization of the Major Histocompatibility Complex Class I Deficiencies in B16 Melanoma Cells.” *Cancer Research* 61 (3): 1095–99.

Sharma, Naveen, Jean Vacher, and James P. Allison. 2019. “TLR1/2 Ligand Enhances Antitumor Efficacy of CTLA-4 Blockade by Increasing Intratumoral Treg Depletion.” *Proceedings of the National Academy of Sciences of the United States of America* 116 (21): 10453–62. https://doi.org/10.1073/pnas.1819004116.

Shibuya, Meito, Taiki Aoshi, Etsushi Kuroda, and Yasuo Yoshioka. 2020. “Murine Cross-Reactive Nonneutralizing Polyclonal IgG1 Antibodies Induced by Influenza Vaccine Inhibit the Cross-Protective Effect of IgG2 against Heterologous Virus in Mice.” *Journal of Virology* 94 (12): 10.1128/jvi.00323-20. https://doi.org/10.1128/jvi.00323-20.

Simeone, Ester, Antonio M Grimaldi, and Paolo A Ascierto. 2015. “Anti-PD1 and Anti-PD-L1 in the Treatment of Metastatic Melanoma.” *Melanoma Management* 2 (1): 41–50. https://doi.org/10.2217/mmt.14.30.

Stebegg, Marisa, Saumya D. Kumar, Alyssa Silva-Cayetano, Valter R. Fonseca, Michelle A. Linterman, and Luis Graca. 2018. “Regulation of the Germinal Center Response.” *Frontiers in Immunology* 9. https://doi.org/10.3389/fimmu.2018.02469.

Strait, Richard T., Monica T. Posgai, Ashley Mahler, Nathaniel Barasa, Chaim O. Jacob, Jörg Köhl, Marc Ehlers, et al. 2015. "IgG1 Protects against Renal Disease in a Mouse Model of Cryoglobulinaemia." *Nature* 517 (7535): 501–4. https://doi.org/10.1038/nature13868.

Taeye, Steven W. de, Arthur E. H. Bentlage, Mirjam M. Mebius, Joyce I. Meesters, Suzanne Lissenberg-Thunnissen, David Falck, Thomas Sénard, et al. 2020. "FcγR Binding and ADCC Activity of Human IgG Allotypes." *Frontiers in Immunology* 11. https://www.frontiersin.org/journals/immunology/articles/10.3389/fimmu.2020.00740.

Taranger, John, Birger Trollfors, Teresa Lagergård, Valter Sundh, Dolores A. Bryla, Rachel Schneerson, and John B. Robbins. 2000. "Correlation between Pertussis Toxin IgG Antibodies in Postvaccination Sera and Subsequent Protection against Pertussis." *The Journal of Infectious Diseases* 181 (3): 1010–13. https://doi.org/10.1086/315318.

Vattepu, Ravi, Sunny Lyn Sneed, and Robert M. Anthony. 2022. "Sialylation as an Important Regulator of Antibody Function." *Frontiers in Immunology* 13. https://www.frontiersin.org/journals/immunology/articles/10.3389/fimmu.2022.818736.

Victora, Gabriel D., and Michel C. Nussenzweig. 2012. "Germinal Centers." *Annual Review of Immunology* 30 (1): 429–57. https://doi.org/10.1146/annurev-immunol-020711-075032.

Vidarsson, Gestur, Gillian Dekkers, and Theo Rispens. 2014. "IgG Subclasses and Allotypes: From Structure to Effector Functions." *Frontiers in Immunology* 5:520. https://doi.org/10.3389/fimmu.2014.00520.

Visciano, Maria Luisa, Maria Tagliamonte, Maria Lina Tornesello, Franco M. Buonaguro, and Luigi Buonaguro. 2012. "Effects of Adjuvants on IgG Subclasses Elicited by Virus-like Particles." *Journal of Translational Medicine* 10 (1): 4. https://doi.org/10.1186/1479-5876-10-4.

Wagner, Ralf, and Eberhard Hildt. 2019. "Zusammensetzung und Wirkmechanismen von Adjuvanzien in zugelassenen viralen Impfstoffen." *Bundesgesundheitsblatt - Gesundheitsforschung - Gesundheitsschutz* 62 (4): 462–71. https://doi.org/10.1007/s00103-019-02921-1.

Walters, Adam A., Abrar Ali, Julie Tzu-Wen Wang, and Khuloud T. Al-Jamal. 2023. "Anti-Tumor Antibody Isotype Response Can Be Modified with Locally Administered Immunoadjuvants." *Drug Delivery and Translational Research* 13 (7): 2032–40. https://doi.org/10.1007/s13346-022-01258-8.

Wang, Junyan, Chuncui Huang, Jinyu Zhou, Keli Zhao, and Yan Li. 2021. "Causal Link between Immunoglobulin G Glycosylation and Cancer: A Potential Glycobiomarker for Early Tumor Detection." *Cellular Immunology* 361 (March):104282. https://doi.org/10.1016/j.cellimm.2021.104282.

Wang, Wenjun, Yuan Yu, Hongbo Liu, Hanxue Zheng, Liyuan Jia, Jing Zhang, Xue Wang, Yang Yang, and Fulin Chen. 2021. "Protein Core Fucosylation Regulates Planarian Head Regeneration via Neoblast Proliferation." *Frontiers in Cell and Developmental Biology* 9:1870. https://doi.org/10.3389/fcell.2021.625823.

Xiong, Shumin, Liaoliao Dong, and Lin Cheng. 2021. “Neutrophils in Cancer Carcinogenesis and Metastasis.” *Journal of Hematology & Oncology* 14 (1): 1–17. https://doi.org/10.1186/s13045-021-01187-y.

Zahavi, David, and Louis Weiner. 2020. “Monoclonal Antibodies in Cancer Therapy.” *Antibodies* 9 (3): 34. https://doi.org/10.3390/antib9030034.

Zhang, Zhiping, Tom Goldschmidt, and Hugh Salter. 2012. “Possible Allelic Structure of IgG2a and IgG2c in Mice.” *Molecular Immunology* 50 (3): 169–71. https://doi.org/10.1016/j.molimm.2011.11.006.

Zhao, Tingmei, Yulong Cai, Yujie Jiang, Xuemei He, Yuquan Wei, Yifan Yu, and Xiaohe Tian. 2023. “Vaccine Adjuvants: Mechanisms and Platforms.” *Signal Transduction and Targeted Therapy* 8 (1): 1–24. https://doi.org/10.1038/s41392-023-01557-7.

Zinn, Sacha, Rodrigo Vazquez-Lombardi, Carsten Zimmermann, Puja Sapra, Lutz Jermutus, and Daniel Christ. 2023. “Advances in Antibody-Based Therapy in Oncology.” *Nature Cancer* 4 (2): 165–80. https://doi.org/10.1038/s43018-023-00516-z.

6. Supplement

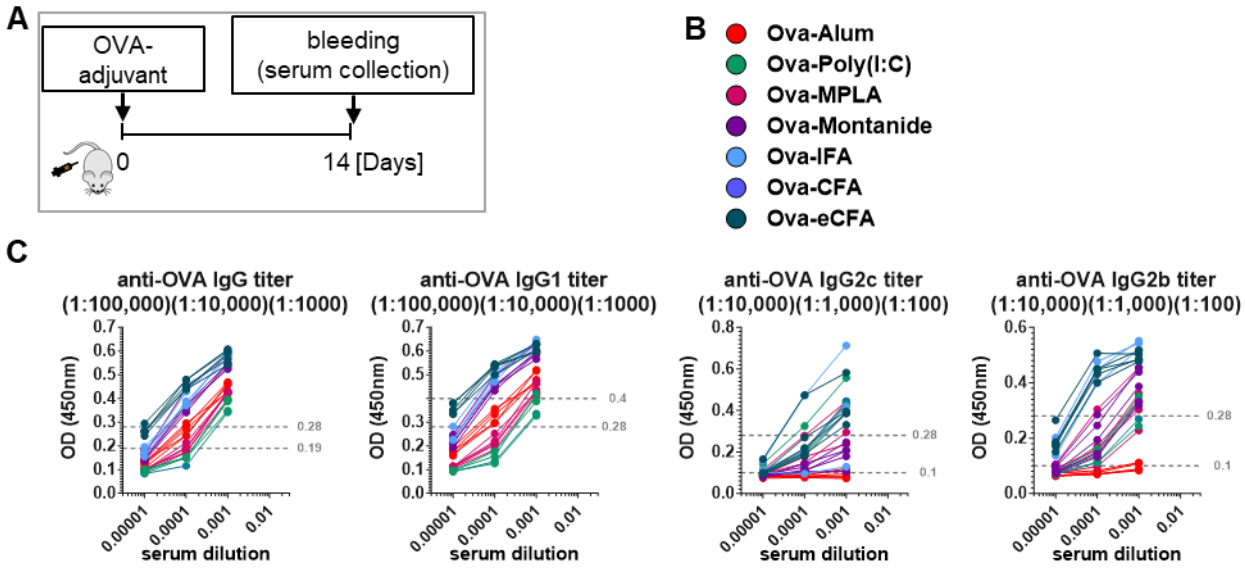

Figure S 1: Serial dilution curves of different serum samples and detection of the different IgG subclasses on day 14 after vaccination with Ova in different adjuvants
(A) Experimental design: C57BL/6 WT mice were immunized with Ova in different adjuvants. On day 14 after immunization, blood was collected, and serum was analyzed for IgG subclass titers and IgG glycosylation patterns. **(B)** Color code of the investigated adjuvants. **(C)** Serum anti-Ova IgG titers of different subclasses on day 14 after immunization. Dilution curves were generated using different serum dilutions as indicated. Relative titers (**Figure 3.2**) were determined using the x-axis intercept of each adjuvant at a defined y-axis intercept. The x-axis intersection of each adjuvant was normalized to the x-axis intersection of Ova-IFA.

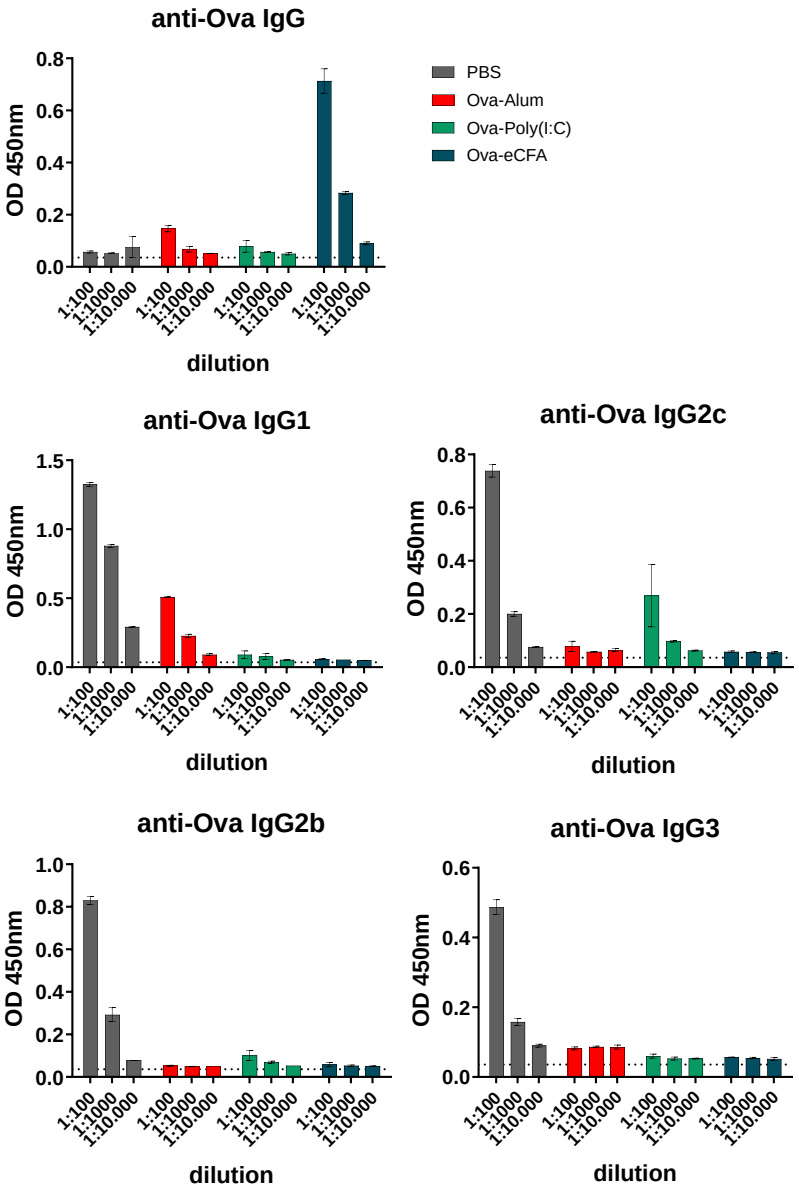

Figure S 2: Anti-Ova IgG subclass levels in pooled serum from Ova-Immunized mice used for transfer experiments

Serum anti-Ova IgG subclass levels on day 12 after immunization. ELISA plates were coated with 10 µg/mL Ova, blocked with 2.5% milk and serum was added in different dilutions as indicated. Detection was performed with HRP-coupled anti-IgG, -IgG1, -IgG2b, -IgG2c and -IgG3. Absorbance values were measured at OD450nm.

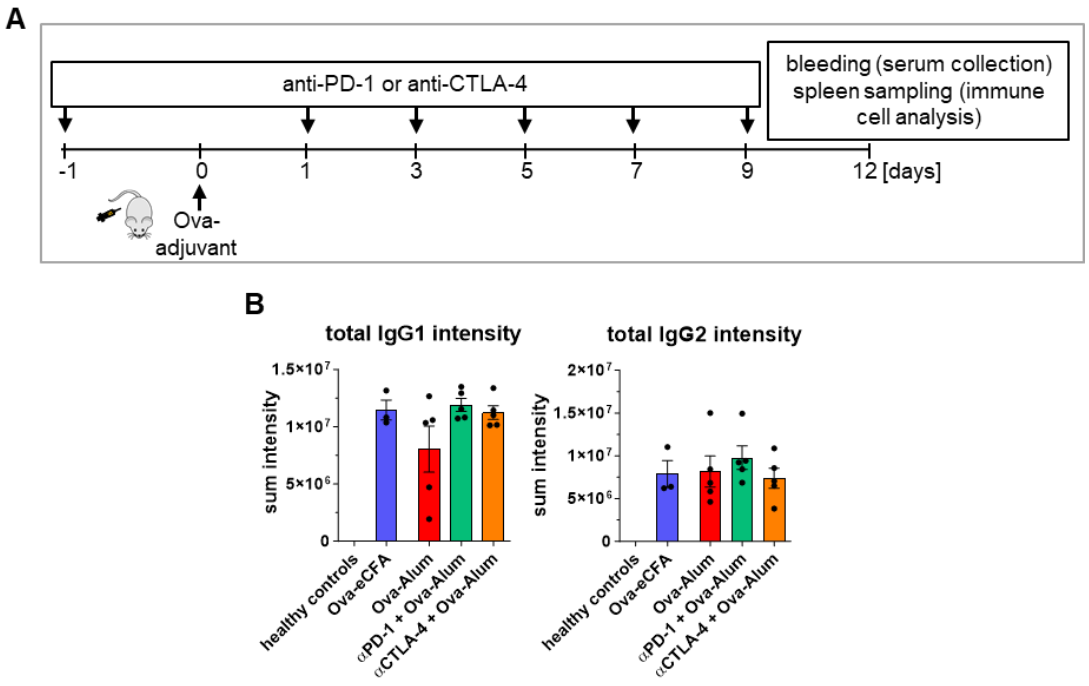

Figure S 3: Impact of checkpoint inhibition on the immune response and on the IgG glycosylation pattern.
(A) Experimental design: C57BL/6 WT mice were immunized with Ova-Alum or Ova-eCFA on day 0. Ova-Alum treated mice were additionally treated with anti-CTLA-4, anti-PD-1 or PBS on day -1 before immunization and on day 1, 3, 5, 7, 9 after immunization. Ova-eCFA immunized mice were treated with PBS on the same days. **(B)** Total **s**erum IgG subclass intensities on day 12 after vaccination and treatment with anti-PD-1 or anti-CTLA-4. IgG intensities were measured by LC-MS.

7. Acknowledgement

First of all, I would like to thank my supervisor Marc Ehlers, who gave me the opportunity to carry out and complete my doctoral thesis in his laboratory. Many thanks also for the many ideas for experiments, discussions and constant challenges that have helped me progress in every respect. Thanks also to Christian Sina for allowing me to carry out my work in his institute.

Next, I would like to thank our cooperation partners from Manfred Wuhrer's working group, who carried out the glycosylation analysis for us.

Many thanks also to AG Sina for the support and help with mouse experiments when I needed a few more hands. Special thanks to Annika Raschdorf, Lea Kubetzko, Larissa Nogueira de Almeida and Mohab Ragab.

Special thanks also to my colleagues Hanna Lunding, Lara Dühring and Jana Buhre, who always supported me in every way and had an open ear. Thank you for the time we spent together in the lab, at lunch and at everything else, where we laughed, discussed and ultimately mastered our time together.

Jana, thank you for the last two years that we have been through together. I owe you so much! Many thanks also to you, Janina Petry, for your help and support over the past year and for the time we spent together in the office! And thank you, Philipp, for your company over the last few months.

Finally, I would like to thank my family and friends who have supported and positively distracted me during this time. Many thanks to my sister Eileen, you has always listened to me and encouraged me. Thank you to my mother for her encouragement and regular visits. Thank you for everything! It wouldn't have been possible without your support.